81-04

NUMERICALLY PREDICTED FIBER ORIENTATIONS IN DILUTE SUSPENSIONS

RICHARD C. GIVLER

CENTER FOR COMPOSITE MATERIALS

College of Engineering
University of Delaware
Newark, Delaware

*MSG DI4 DROLS PROCESSING-LAST INPUT IGNORED

-- 1 OF 1

-- ***DTIC DOES NOT HAVE THIS ITEM***

-- 1 - AD NUMBER: D433440

-- 5 - CORPORATE AUTHOR: DELAWARE UNIV NEWARK CENTER FOR COMPOSITE MATERIALS

-- 6 - UNCLASSIFIED TITLE: NUMERICALLY PREDICTED FIBER ORIENTATIONS IN DILUTE SUSPENSIONS,

-10 - PERSONAL AUTHORS: GIVLER,R. C. ;

-11 - REPORT DATE: FEB , 1981

-12 - PAGINATION: 216P

-14 - REPORT NUMBER: CCM-81-04

-20 - REPORT CLASSIFICATION: UNCLASSIFIED

-22 - LIMITATIONS (ALPHA): APPROVED FOR PUBLIC RELEASE; DISTRIBUTION UNLIMITED. AVAILABILITY: CENTER FOR COMPOSITE MATERIALS, COLLEGE OF ENGINEERING, UNIV. OF DELAWARE, NEWARK, DE 19711.

-33 - LIMITATION CODES: 1

-******

END OF DISPLAY LIST

((ENTER NEXT COMMAND))

NUMERICALLY PREDICTED FIBER ORIENTATIONS IN DILUTE SUSPENSIONS

By

Richard C. Givler

Center for Composite Materials
University of Delaware
Newark, Delaware

Sponsored By The

Industry-University Research Program
Center for Composite Materials
ACMIP 1980-81

February 1981

ACKNOWLEDGEMENTS

Dr. R. Byron Pipes of the University of Delaware Center for Composite Materials is acknowledged for his support and guidance in this research. Also, Dr. Marcel Crochet of the Université Catholique de Louvain and his instruction in finite element methods were integral to this study.

ABSTRACT

Owing to the lack of analytical and/or numerical tools with which to properly investigate the resulting fiber orientations in a filled, low Reynold's number flow field, a numerical model has been developed to predict such phenomena. The motivation for such a study is evident from the fact that the mechanical properties of a molded two-phase component are inherently determined by the fiber orientations. Accurately predicting the orientations of the fibers from the rheological kinematics enhances the feasibility of designing a mold with the aid of the computer.

Fiber orientations in complex geometry flows of dilute suspensions are solved in a two-part fashion. The initial step includes the numerical solution of the steady-state fluid mechanics problem via the finite element method for either Newtonian or power law constitutive assumptions. The application of Jeffery's theory [25] in conjunction with the discretized representation of the velocity field subsequently determines the fiber orientations. Numerically predicted fiber orientations have been verified with

existing analytical solutions of a two-dimensional channel flow for Newtonian and power law fluids. Application of the fiber orientation model to the expansion flow problem has yielded results that correspond qualitatively to those found empirically. A complete set of computer graphics routines has been incorporated with the analysis to provide easy data interpretation.

TABLE OF CONTENTS

Acknowledgements ii

Abstract iii

Nomenclature ix

List of Illustrations. xiii

1. Problem Definition and Motivation. 1

2. Introduction 4

3. Qualitative Orientation Models 7

4. Quantitative Orientation Models. 14

4.1 Jeffery's Orientation Equation. 14

4.2 Solution of the Orientation Equation by Analytical Methods. 18

4.2.1 2-D Poiseuille Flow. 18

4.2.2 Power Law Flow 25

4.3 Application to the Discretized System 32

5. The Numerical Routine "COLINS" 35

5.1 Methodology 35

5.2 Convergence of the Numerical Scheme 38

5.3 Defining an Orientation Parameter 43

6. Selected Numerical Examples. 47

6.1 2-D Poiseuille Flow 47

6.2 2-D Power Law Flow. 50

6.2.1 Solution of the Problem. 50

6.2.1.1 Boundary Conditions 51

6.2.1.2 Numerically Predicted Fiber Orientations. 54

6.3 Expansion Flow. 55

6.3.1 Solution of the Problem. 57

6.3.1.1 Boundary Conditions 57

6.3.1.2 Numerically Predicted Fiber Orientations. 60

7. Extensions to the Theory 69

8. Conclusions. 73

Literature Cited 75

Appendix 1 Fluid Mechanics 78

A1.1 General Concepts. 80

A1.1.1 Conservation of Mass. 80

A1.1.2 Conservation of Linear Momentum . 83

A1.1.3 The Stress Tensor 88

A1.1.4 Conservation of Angular Momentum. 92

A1.1.5 Material Motion 94

A1.1.6 The Stream Function 97

A1.2 Constitutive Relationships. 99

A1.2.1 The Inviscid Fluid. 99

A1.2.2 The Newtonian Fluid 103

A1.2.3 The Generalized Newtonian Fluid . 104

A1.2.4 The Oldroyd-Maxwell Fluid 109

A1.3 Selected Analytical Examples. 113

A1.3.1 Planar Poiseuille Flow. 114

A1.3.2 Planar Power-Law Fluid. 119

Appendix 2 Finite Elements in Fluid Mechanics. . . . 122

A2.1 Introduction. 122

A2.2 The Finite Element Approach 125

A2.2.1 Direct Stiffness Approach 125

A2.2.2 Variational Methods 129

A2.3 Choice of Elements. 140

A2.4 Method of Weighted Residuals. 151

A2.5 Derivation of Stoke's Problem 154

A2.6 Solution by Frontal Elimination 161

A2.7 Calculating the Derived Quantities. . . . 168

A2.7.1 Stream Function 168

A2.7.2 Vorticity 172

A2.8 Numerical Solution of 2-D Poiseuille Flow. 174

Appendix 3 Numerical Code "COLINS" 178

NOMENCLATURE

Roman Symbols

A	Area
a	Acceleration
a	Radius
$a(x_i)$	Position vector
b_i	Axes of an ellipsoid of revolution ($i = 1,3$)
C_1 , C_2 , ...	Constants
D	Measure of the degree of orientation
$\underset{\sim}{d}$	Deformation rate tensor
F_i	Components of the traction vector
f_i	Body force components
f	Force
f	Orientation parameter
$I(y(x))$	Functional
I_{ij}	Moment of inertia tensor
I_d , II_d , III_d	Scalar invariants of the deformation rate tensor
k	Stiffness coefficient
ℓ	Length
M	Constant

m	Mass
n	Power law index
P_o , P_1 , ...	Arbitrary spatial points
P_{ij}	Deviatoric stress tensor
p	Pressure
p	Constant
q	Velocity vector
R	Gas constant
R	Residual
Re	Reynold's number
r_g	Radius of gyration
r_p	Ellipsoidal aspect ratio
T	Temperature
t	Time
t_x , t_y	Components of the surface traction vector
u , v	Two-dimensional velocity components
V	Volume
v_i	Three-dimensional velocity components
v_i	Weighting functions
v	Velocity
W_i	Linear/quadratic interpolation functions
x_1 , x_2 , x_3	Orthogonal coordinates
y_i	Nodal values of the field variable (one dimension)

y	Displacement
Z_k	Vorticity vector

Greek Symbols

α_i	Constants
Γ	Strain rate
Δ	Area of triangle
δ_{ij}	Kronecker delta
ε_{ijk}	Permutation symbol
ε	Infinitesimal change
η	Variable viscosity
$\eta(x)$	Arbitrary function
η , ζ	Local coordinates
μ	Viscosity (constant)
θ	Relaxation time constant
θ , ϕ	Euler angles
π	3.14159...
Σ	Summation symbol
σ_{ij}	Total stress tensor
ρ	Density
T	Torque vector
ϕ	Unknown field variable
ϕ	Velocity potential
ϕ_i	Nodal values of the field variable (two dimensions)

ϕ_i	Linear/quadratic shape functions
ϕ_i	Local angle of orientation
$\overline{\phi}$	Mean angle of orientation
ϕ_{rms}	Root mean square value of orientation
Ψ_i	Linear shape functions
ψ_i	Quadratic shape functions
ψ	Stream function
Ω	Angular velocity
ω_{ij}	Vorticity tensor

Mathematical Operations

$\frac{d}{dt}$	Ordinary total derivative
$\frac{\partial}{\partial t}$	Partial derivative
$\frac{\delta}{\delta t}$	Oldroyd convective derivative
$\cdot$	$\frac{d}{dt}$
∇	Del operator
L( )	Ordinary differential operator
<a,b>	Inner product of a and b
||	Absolute value
O( )	Of the order

LIST OF ILLUSTRATIONS

Figure 3.1	Orientation model for shearing flow. . .	8
Figure 3.2	Experimentally observed fiber orientation in shear flow for the P.E.T. (polyethylene terephthalate) material system	10
Figure 3.3	Orientation model for expansion flow . .	11
Figure 3.4	Experimentally observed fiber orientation in region of diverging flow . . .	13
Figure 3.5	Orientation model for converging flow. .	13
Figure 4.1	Coordinate system used in describing fiber rotations.	16
Figure 4.2	Two-dimensional wall-bounded shearing flow	18
Figure 4.3	Angular orientation of a particle subjected to shearing flow.	21
Figure 4.4a	Variation of the degree of equilibrium orientation for 2-D Poiseuille flow. . .	24
Figure 4.4b	Three-dimensional plot of $D = f(\bar{x}_2, \bar{x}_3)$ for 2-D Poiseuille flow ($n = 1$)	24
Figure 4.5a	Boundary layers of aligned fibers ($D = 5$) for shear thinning flows.	28
Figure 4.5b	Three-dimensional plot of $D = f(\bar{x}_2, \bar{x}_3)$ for power law fluid in wall-bounded shear flow ($n = 0.1$).	28
Figure 4.6	Analytically predicted fiber orientations in 2-D Poiseuille flow. Random orientation introduced at $\bar{x}_3 = 0$.	30

Figure 4.7	Alternative methods of determining fiber orientations in dilute systems . .	33
Figure 5.1	Constructing a path line	37
Figure 5.2	Respective grids for conducting a convergence study	40
Figure 5.3	Results of the convergence study	42
Figure 5.4	Determining local fiber orientations and their relation with the global coordinate system.	45
Figure 6.1	Fiber orientation in two-dimensional Poiseuille flow.	48
Figure 6.2	Finite element solution to the generalized Newtonian fluid between parallel walls with the power law approximation (n = 0.2)	52
Figure 6.3	Representation of the pressure distribution by concentrated nodal forces for quadratic interpolation.	53
Figure 6.4	Fiber orientations in two-dimensional, power law flow	56
Figure 6.5	Finite element grid for a two-dimensional expansion flow of a Newtonian fluid. . .	58
Figure 6.6	Jeffery-Hamel flow in a diverging section.	59
Figure 6.7a	Shear stress contours of the expansion flow problem	61
Figure 6.7b	Contours of axial velocity of the expansion flow problem	62
Figure 6.7c	Contours of the stream function of the expansion flow problem	63
Figure 6.7d	Contours of vorticity of the expansion flow problem	64
Figure 6.8	Fiber orientation in the expansion flow problem	66

Figure 6.9 Orientation parameter in the expansion flow problem. 67

Figure A1.1 Control volume for conservation of mass 80

Figure A1.2 Control volume for conservation of linear momentum. 83

Figure A1.3 Fluid in a long, rotating cylinder . . . 85

Figure A1.4 Control volume for force balance on a fluid element in the x_1-direction. . . 86

Figure A1.5 An illustration of the normal stresses found in egg whites. 91

Figure A1.6 Control volume for moment balance about the x_3 axis. 92

Figure A1.7 Material motion for a fluid continuum. . 94

Figure A1.8 Flow between two streamlines 97

Figure A1.9 Variation of shear stress with deformation rate for a power law fluid. . . . 106

Figure A1.10 Two-dimensional Couette flow 107

Figure A1.11 Normalized velocity profile for two-dimensional Poiseuille flow. 114

Figure A1.12 Velocity profiles for the power law fluid. 121

Figure A2.1 One-dimensional domain, D, for the FEM . 126

Figure A2.2 A one-dimensional element with two degrees of freedom 127

Figure A2.3 The variation of $y(x)$ on the interval $(x_i - x_o)$ 129

Figure A2.4 The function $\eta(x)$. 131

Figure A2.5 Linear shape functions 135

Figure A2.6 Transformation to local coordinates. . . 136

Figure A2.7 Linear triangular element in global coordinates 141

Figure A2.8 Standard triangular element 143

Figure A2.9 Determination of shape functions by inspection. 144

Figure A2.10 Area coordinates. 146

Figure A2.11 Six node (quadratic) triangular element in local coordinates 147

Figure A2.12 Determining ψ_1 by inspection. 147

Figure A2.13 The shape functions ψ_1 and ψ_4 for the six node triangle. 149

Figure A2.14 Pascal's triangle illustrating the degree of interpolation 149

Figure A2.15 Typical element for the u,v,p formulation. 156

Figure A2.16 System of equations governing Stoke's flow. 160

Figure A2.17 Storing a banded, symmetric matrix. . . 162

Figure A2.18 Element and nodal numbering scheme for frontal elimination 163

Figure A2.19 Two-dimensional Poiseuille flow 174

Figure A2.20 Finite-element solution of planar Poiseuille flow 176

1. PROBLEM DEFINITION AND MOTIVATION

Industry is currently producing large quantities of reinforced plastics with application in a wide variety of disciplines. Reinforced plastics apply the same principle known to the Egyptians nearly three thousand years ago; the fibers carry the load whereas the matrix acts as a bonding material to allow the fibers to maintain their orientation. By varying the fiber orientation one may in effect tailor the composite material in such a manner to suit its application. In particular, the automotive industry views the short fiber composite as replacing many structural vehicle components in an effort to reduce weight. It is a feasible solution to the problem in light of recent advances in processing techniques that have shortened production times. The processing techniques referred to are those appropriate to molding short fiber systems; injection molding, transfer molding, and compression molding are the usual methods for producing components in a reasonable time, so important to high production applications.

In the above processing techniques, it is assumed that short fibers are combined with a liquid resin to form

the raw material (frequently referred to as the charge). The newly formed slurry is then forced to flow within the mold either through the application of pressure or by closing the mold. When the material (thermosets) has filled the cavity, it is cured by subjecting it to high pressure and temperature. Note that we have chosen to speak of both a generic fiber and matrix instead of specifying the constituent phases. It is desired to remain as general as possible in the problem formulation to accommodate a broad class of material systems. Questions concerning specific material systems will be undertaken when one views the constitutive relationships for specific systems.

The fiber orientation of composite materials is known to influence both modulus and strength. This fact is especially evident in the continuous, layered systems commonly associated with the aerospace industry. However, unlike the continuous fiber systems where the orientation is known, the fiber orientation of the molded short fiber system is yet to be determined. Its determination will inherently depend upon the rheological behavior of the fibrous suspension. Thus, it seems that if one is able to determine the relative position and orientation of the fibers, it will be possible to utilize existing methodologies to determine: first, the pointwise material properties,

and secondly, the stress state within the molded part. Numerical codes have been developed to achieve the determination of the stress state once the local material properties are known. Without much insight, it is easy to see that what is being suggested is the possibility of a computer-aided mold design. The motivation is one of economics, in that the costly empirical development of optimum part and mold geometry could be eliminated. No longer would a mold designer be obligated to fabricate the mold in order to determine resulting fiber orientation; rather he would have the ability to interact with a mold model and develop a design accordingly.

It was pointed out above that both the fiber position and orientation are sought. Recall that questions of material position are usually connected with homogeneity while those involving orientation or direction are associated with material anisotropy/isotropy. It is assumed that the rheology within the mold will affect the anisotropy/isotropy to a greater extent than that of homogeneity. Most experimental data seem to show that the fiber distribution is relatively uniform throughout a given molded part, but that the orientation is highly dependent upon the flow conditions. Thus, the major emphasis will be placed upon determining the fiber orientation within a given flow regime.

2. INTRODUCTION

The underlying motives for writing this thesis are twofold. Clearly the dominant reason is to present the findings from some original research, as is usually the case. But secondly, it is important that the manuscript be an article of instruction as well. Care has been taken to insure that unfamiliar ideas are developed and useful examples are included.

It is anticipated that many readers may not be familiar with the various methodologies referred to in this text. For that reason, it may be helpful to review certain background material. Appendix A1 provides an introduction to fluid mechanics which is intended to introduce the fundamental concepts that are the basis of all work in rheology and associated fields. While this material may be found in various textbooks, the concepts presented in Appendix A1 are of a concise nature and follow a logical scheme of development pertaining to this research. Also included in this section are the various constitutive equations that are utilized herein as well. Several examples are included to elucidate the

contrasting behavior between the Newtonian and non-Newtonian fluids.

Many of the practical mold geometries found in industry today are complex. This consideration has forced the use of a numerical scheme in order to solve the fluid mechanics problem. The finite element method (FEM) was chosen primarily because of its superior ability to approximate irregular boundaries. The FEM as pertaining to fluid systems is outlined in Appendix A2, making special mention of the key considerations, as well as the similarities that exist with the solid mechanics formulation.

Intuitive orientation models are explained in Chapter 3 for the shear and extensional flow fields. These are especially useful in reconciling the orientations dictated by the analytical expressions in Chapter 4. In Chapter 4 an expression for the motion of a single ellipsoidal particle in a viscous flow is presented. This is the initial consideration in the overall process of determining fiber orientation of a dilute suspension in an arbitrary flow. Building upon this simplified model, one extends the theory to include discretized systems where the flow field is solved via the FEM.

Chapter 5 examines the numerical code COLINS, responsible for determining the fiber orientation within a given mold from the rheological behavior. The detailed program is examined to reveal its nature and the convergence of the scheme is discussed briefly. The numerical code COLINS is then called upon to solve several specific examples in Chapter 6. Examples include simple shearing flow, as well as extensional flows that are found, say, in a 10:1 expansion. The results of the examples show the mold geometry with individual fibers plotted at their respective locations and orientations. The use of an orientation parameter greatly assists in describing the fiber orientations in a qualitative manner. Finally in Chapter 7, several extensions to the theory as motivation for further research are offered.

3. QUALITATIVE ORIENTATION MODELS

Included in the discourse of Appendices A1 and A2, material has been provided to construct the necessary background needed to appreciate the objective of this work. At this point it is our intent to promulgate some of the intuitive ideas concerning the orientation of fiber-like particles in a fluid flow. The models which are discussed are based on the general trends exhibited by suspended particles that have been observed experimentally. This qualitative appeal toward understanding the mechanisms will be useful later, when one endeavors to analyze fiber orientation behavior for geometrically complicated domains.

The last few years have seen numerous experimental studies that have illustrated the orientation trends of fiber-filled systems undergoing characteristic flow patterns. The first such orientation model exists when the suspension is subject to a shearing-type motion. Regions of shearing flow are characterized by a velocity gradient tensor of the following form:

$$\frac{\partial v_i}{\partial x_j} = \Gamma \begin{pmatrix} 0 & 1 & 0 \\ 0 & 0 & 0 \\ 0 & 0 & 0 \end{pmatrix}$$

where Γ is defined as the shear rate. The coordinate system that has been adopted for this discussion finds the x_1 axis parallel to the flow direction while the x_2 axis is aligned with the direction of varying velocity. For completeness, the x_3 axis is so arranged to form a right-handed system of the three coordinate directions. Under steady, two-dimensional flow, the deformation rate may depend upon the spacial coordinate, (x_2), but not upon time.

Common occurrences of shearing flow are found in the vicinity of physical boundaries such as mold walls or inserts. Clearly this is so in light of the "no slip" boundary condition at the wall, which requires the local velocity of the fluid to be zero at the wall surface and yet attain a finite value in the bulk of the flow. Figure 3.1 depicts a single fiber, initially transverse to the flow direction, in a shearing flow. If the local velocity

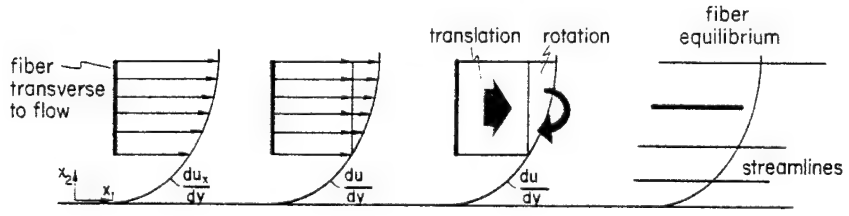

Figure 3.1 Orientation from shearing flow

field surrounding the fiber is separated into two parts, it is seen from the figure that the distinct contributions may be represented as translational and rotational velocity components, respectively. The translational velocity acts only to transport the fiber with the mean, local fluid velocity. Thus, since the particle center moves with the same velocity as the fluid there can be no resultant force acting on it. The only possible action on the particle results from a couple, which consists of two contributions; the first tends to rotate the fiber with the same angular velocity of the surrounding fluid while the second acts to align the particle axes with those of the principal axes of the deformation rate tensor. In view of these considerations it is shown that the equilibrium position for a large aspect ratio ellipsoid is parallel to the fluid streamlines. Figure 3.2 shows experimentally the resultant fiber orientation in regions of steady shearing flow.

Equally important to realize is the mechanism responsible for orienting the fibers where the flow possesses significant dilational components of the deformation rate tensor. For convenience in describing flows of this type, the radial coordinate system (r,θ) as shown in Figure 3.3 is introduced. In terms of this coordinate

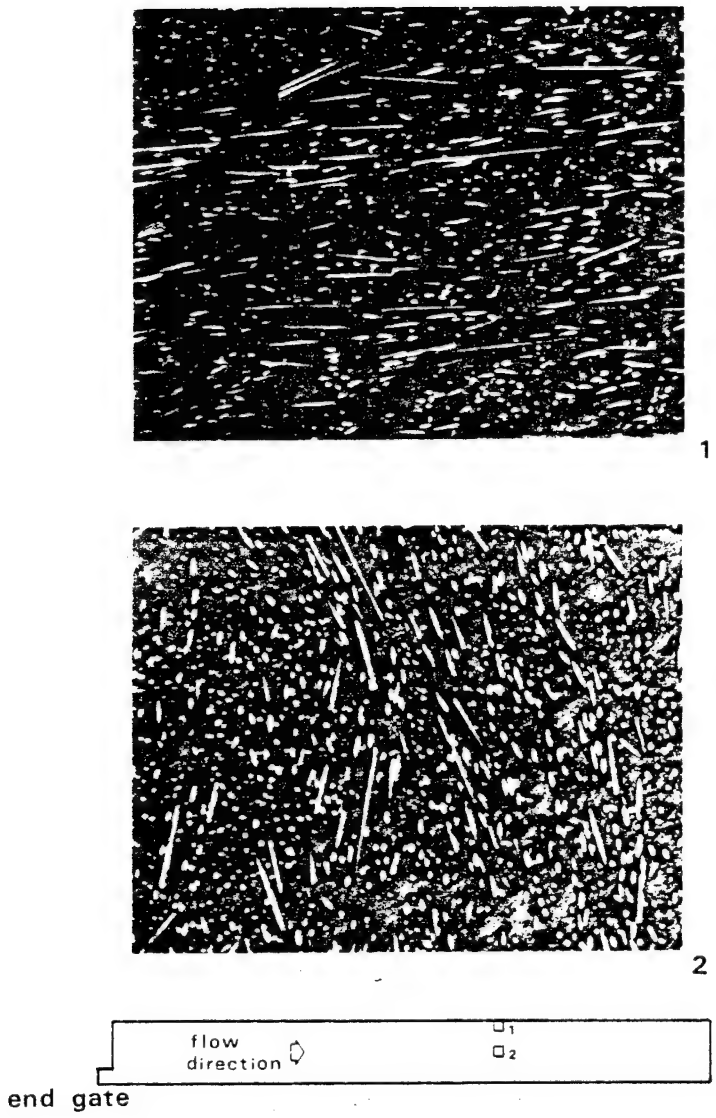

Figure 3.2 Experimentally observed fiber orientation in shear flow for the P.E.T. (polyethylene terephthalate) material system (100×)

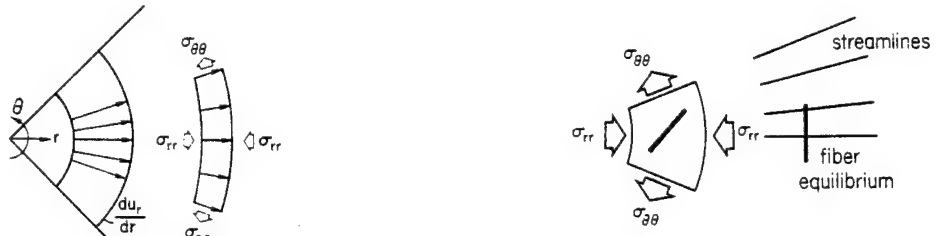

(a) (b)

Figure 3.3 Orientation from elongation

system, then, the deformation rate tensor appears as

$$\underset{\sim}{d} = d_{ij} = \begin{pmatrix} d_{11} & 0 & 0 \\ 0 & d_{22} & 0 \\ 0 & 0 & 0 \end{pmatrix}$$

and the corresponding stresses acting on the fluid element are also shown in Figure 3.3. The radially directed stress decelerates the fluid in that coordinate direction, and from the equations of motion, the tangential component of stress tends to elongate a fluid element in the θ-direction. If one imagines that a fiberlike particle is within a fluid element undergoing such a deformation, then it is not hard to visualize the appropriate motion of the particle. Figure 3.3 depicts the

equilibrium position of a fiber subjected to an elongated flow situation. Experimentally this effect has been observed in the molding of numerous short fiber composites. Figure 3.4 illustrates orientation patterns as the slurry enters a region of expanding flow. Clearly the flow in this region approximates the flow situation of Figure 3.3 and as a result tangential orientation is anticipated.

In contrast with the equilibrium position for expansion flows described above, converging flow will orient a particle parallel to fluid streamlines. To see this, one notes the stresses on a fluid element act in opposite directions to those of Figure 3.3. The intuitive arguments for radially oriented fibers in converging flow are outlined in Figure 3.5.

So far, we have alluded to the equilibrium position of fibers undergoing certain flow criteria. Nothing has been mentioned concerning the transient response of the suspended particles -- i.e. how do they reach their equilibrium state. The next chapter will be concerned with investigating the motion of the particles from a quantitative point of view.

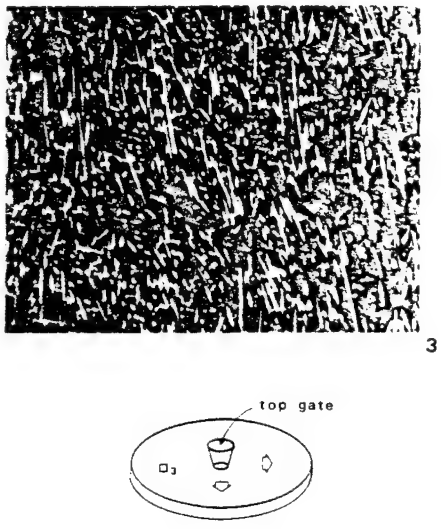

Figure 3.4 Experimentally observed fiber orientation in region of diverging flow (100×)

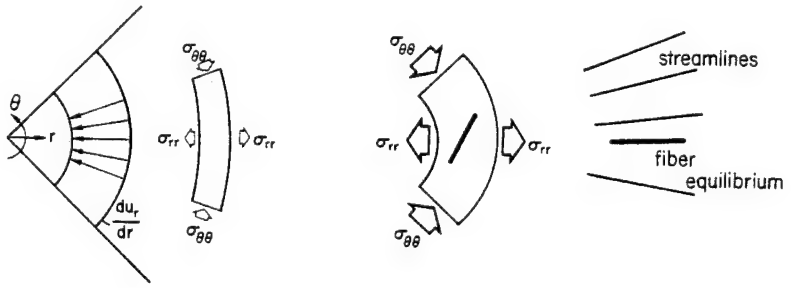

Figure 3.5 Orientation model for convering flow

4. QUANTITATIVE ORIENTATION MODELS

4.1 Jeffery's Orientation Equation

To this point one will have noted certain qualitative trends in particle orientation that have been observed experimentally. Explanations of these trends were offered in the previous section. Within this section the basic equations and assumptions needed to describe the particle motions quantitatively are introduced.

The earliest work addressing the problem of suspended particle motions was by G. B. Jeffery [25]. Here, Jeffery endeavored to solve the linearized Newtonian equations of motion for a single ellipsoidal particle immersed in a viscous flow. The boundary conditions he proposed were the following: i) the fluid shall adopt the same motion as that of the particle at the solid-fluid interface and the fluid shall attain the free stream velocity at sufficient distances away from the particle; ii) the free stream velocity was taken to be a general shearing-type flow with a fully populated deformation rate tensor. In his early development of the problem,

Jeffery assumed that the components of the deformation rate tensor were constant in space on a scale that is large when compared with the particle dimensions. Later this restriction is modified to include flows such that the components of the deformation rate tensor are indeed functions of the spacial coordinates. The original solution is carried out formally in an ellipsoidal coordinate system. Here the axes of the ellipsoid serve to define a local, orthogonal coordinate system x_1^o, x_2^o, x_3^o, translating and rotating with the particle, such that $x_1^{o2}/b_1^2 + x_2^{o2}/b_2^2 + x_3^{o2}/b_3^2 = 1$. Rather than discussing the solution methods here, the reader is referred to the original paper for details [25]. The results of the analysis assert that the resultant force on the particle vanishes as it translates with the local, mean velocity of the fluid. Secondly, the resultant couple acting on the particle consists of two parts: one part is due to the local rotation (vorticity) of the fluid and the other results from the fluid deformation.

It is natural to define the components of the resultant torque in terms of a fixed or inertial coordinate system, since the fluid kinematics will most naturally be defined in the latter reference frame. For this purpose, then, the Euler angles ϕ_1 and θ_1, defined by Figure 4.1, are introduced.

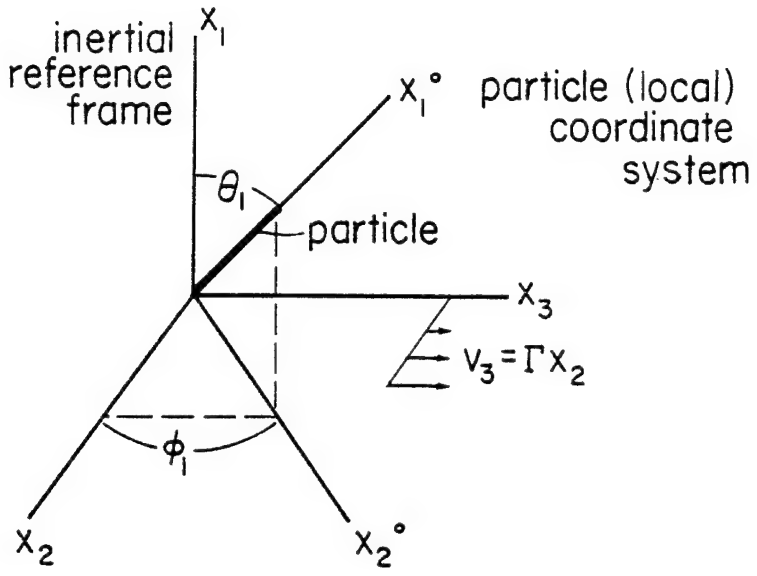

Figure 4.1 Coordinate system used in describing fiber rotation

From the expressions denoting the resultant couple, it may then be shown [18] that the fiber motion may be defined in terms of the Euler angles such that

$$\begin{aligned}\dot{\phi}_1 = {} & Z_1 - Z_2\cos\phi_1\cot\theta_1 - Z_3\sin\phi_1\cot\theta_1 \\ & + B[-d_{12}\sin\phi_1\cot\theta_1 + d_{23}\cos 2\phi_1 \\ & \quad + d_{31}\cos\phi_1\cot\theta_1 - \tfrac{1}{2}(d_{22}-d_{33})\sin 2\phi_1]\end{aligned} \tag{4.1}$$

$$\begin{aligned}\dot{\theta}_1 = {} & -Z_2\sin\phi_1 + Z_3\cos\phi_1 + B[d_{12}\cos\phi_1\cos 2\theta_1 \\ & + \tfrac{1}{2}d_{23}\sin 2\phi_1\sin 2\theta_1 + d_{31}\sin\phi_1\cos 2\theta_1 \\ & + \tfrac{1}{4}(d_{22}-d_{33})\cos 2\phi_1\sin 2\theta_1 \\ & + \tfrac{3}{4}(d_{22}+d_{33})\sin 2\theta_1]\end{aligned} \tag{4.2}$$

where the dot (•) denotes differentiation with respect to time. Also

Z_i = components of the vorticity vector $[Z_i = \frac{1}{2}(u_{j,k}-u_{k,j})\,e_{ijk}]$

d_{ij} = components of the deformation rate tensor $[d_{ij} = \frac{1}{2}(u_{i,j}+u_{j,i})]$

$B = (r_p^2 - 1)/(r_p^2 + 1)$

and $r_p = b_1/b_2$ defines the particle aspect ratio.

If one confines the analysis to two-dimensional fluid flows, such that variations in the third coordinate direction may be ignored, then the vorticity vector will be perpendicular to the plane of the flow. In light of this limitation eq.(4.1) may be simplified to

$$\dot{\phi}_1 = Z_1 + B[d_{23}\cos 2\phi_1 - \tfrac{1}{2}(d_{22}-d_{33})\sin 2\phi_1] \qquad (4.3)$$

Eq.(4.2) is no longer needed to describe the in-plane fiber orientation thus it shall be disregarded in further discussion.

To reiterate, eq.(4.3) describes the in-plane orientation response of a single-ellipsoidal particle in a general Newtonian shearing flow. Within the previous statement lie the bulk of the assumptions and limitations of the quantitative descriptive ability of eq.(4.3). Even in its simplified form eq.(4.3) is

difficult to solve except for situations where the vorticity and deformation rates are easily expressible in terms of the flow field. The following sections provide examples of two such flow fields that allow analytical expressions to be found for the components of $\underset{\sim}{d}$ and Z_i. In these particular cases, eq.(4.3) may be integrated directly to yield analytical expressions for the fiber orientation as a function of time.

4.2 Solution of the Orientation Equation by Analytical Methods

4.2.1 2-D Poiseuille Flow

Consider a pressure-driven, wall-bounded shear flow to exist such that the velocity variation occurs in the x_2-x_3 plane. Figure 4.2 illustrates the nomenclature that will be utilized for the subsequent discussion.

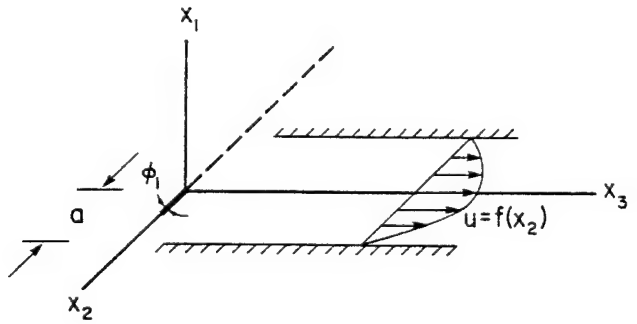

Figure 4.2 Two-dimensional wall-bounded shearing flow

For a unit flow, the normalized velocity profile has been shown in eq.(A1.65) to be

$$u = \tfrac{3}{2}\left(1 - \frac{x_2^2}{a^2}\right) \tag{4.4}$$

and the components of the vorticity vector and deformation rate tensor are respectively calculated to be

$$z_i = \begin{Bmatrix} \tfrac{1}{2}\Gamma \\ 0 \\ 0 \end{Bmatrix} \tag{4.5}$$

$$d_{ij} = \begin{bmatrix} 0 & 0 & 0 \\ 0 & 0 & \tfrac{1}{2}\Gamma \\ 0 & \tfrac{1}{2}\Gamma & 0 \end{bmatrix} \tag{4.6}$$

where $\Gamma \equiv \frac{du}{dx_2} = -3x_2/a^2$.

Inserting eqs.(4.5) and (4.6) into eq.(4.3), the expression for the angular orientation of the particle becomes

$$\dot{\phi}_1 = \frac{\Gamma}{r_p^2 + 1}\left(r_p^2 \cos^2\phi_1 + \sin^2\phi_1\right) \quad . \tag{4.7}$$

Recall that r_p was defined as the aspect ratio of the particle (b_1/b_2). One nominally chooses $r_p = 50$ for the discussion of fiber-like particles. Integration of

eq.(4.7) with respect to time admits the solution

$$\tan\phi_1 = r_p \tan\left(\frac{\Gamma t}{r_p + \frac{1}{r_p}}\right) \quad . \tag{4.8}$$

If one designates that the initial fiber orientation is perpendicular to the flow (i.e. $\phi_1 = 0$, $t = 0$) then the corresponding particle response is shown in Figure 4.3. The abscissa is a product of the shear rate and the time; for a constant shear rate Figure 4.3 shows the variation of ϕ_1 as a function of time. However, for a non-uniform shear rate some explanation is needed to interpret the particle response in flows of this type. In general, particles will assume orientations that depend upon their relative position in the flow, as well as the duration of time.

First and foremost, it was previously pointed out that Jeffery's original assumptions included a deformation rate tensor whose components were spacially independent. Now this restriction is removed in light of the work of Goldsmith and Mason [18] who showed quantitative agreement with the rotational motions of particles between Couette flow and Poiseuille flow. Provided that the particles are small when compared to the channel half-width, the rotations proved identical between the two flows

despite the linear variation of shear rate for Poiseuille flow. Hence, Figure 4.3 may also be interpreted as providing high degrees of orientation for particles subjected to high shear rates for short durations of time, as it is the product Γt that determines the orientation.

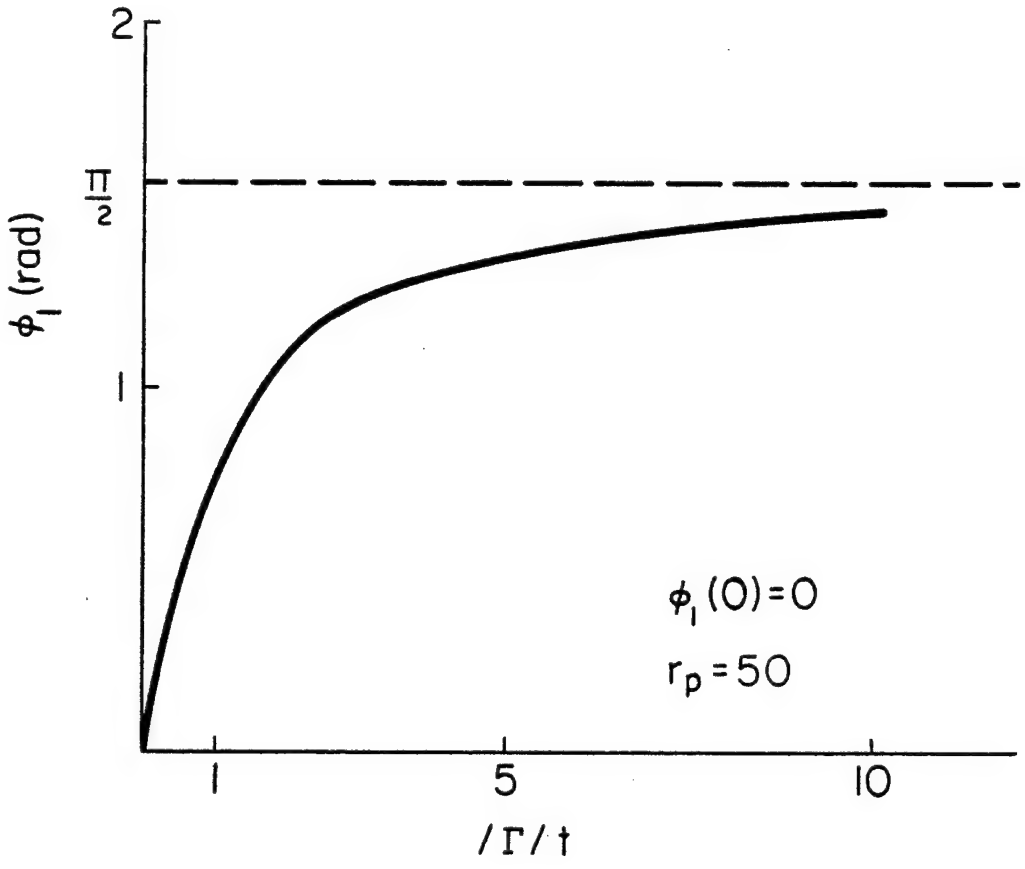

Figure 4.3 Angular orientation of a particle subjected to shearing flow

If one considers an alternative method of interpreting Figure 4.3 we define the quantity

$$D = |\Gamma| t \tag{4.9}$$

that may be regarded as a measure of the degree of equilibrium particle orientation for shearing flows. We shall endeavor to illustrate the behavior of D throughout a flow regime to isolate the regions of various degrees of orientation. Toward this end, it is advantageous to recast the right-hand side of eq.(4.9) in terms of the coordinate positions within the domain. Suppose that the local velocity is given by

$$u = \frac{dx_3}{dt} = \frac{x_3}{t} \qquad \text{(for steady flow)} \tag{4.10a}$$

$$t = \frac{x_3}{u} \tag{4.10b}$$

where one disallows velocity variations with x_3. Utilizing eq.(4.10b) and substituting for the local velocity from eq.(4.4), the expression for D (eq.(4.9)) becomes

$$D = \frac{|\Gamma| x_3}{\tfrac{3}{2}[1 - (x_2^2/a^2)]} = \frac{2x_2x_3}{a^2 - x_2^2} \tag{4.11}$$

or alternatively,

$$x_3 = \frac{D(a^2 - x_2^2)}{2x_2} \quad . \tag{4.12}$$

For convenience, the dimensionless channel coordinates are introduced in the form of eqs.(4.13a) and (4.13b)

$$\bar{x}_3 = \frac{x_3}{a} \tag{4.13a}$$

$$\bar{x}_2 = \frac{x_2}{a} \tag{4.13b}$$

When these modifications are added to eq.(4.12) the resulting expression becomes

$$\bar{x}_3 = \frac{D(1 - \bar{x}_2^{\,2})}{2\bar{x}_2} \tag{4.14}$$

The consequence of eqs.(4.9) to (4.14) has been to remove the time dependence from the orientation equation (eq.(4.8)) in exchange for a spacial dependence. This was accomplished explicitly in eq.(4.10b). If one plots the behavior of $\bar{x}_3$ as a function of $\bar{x}_2$ with D as a parameter, the results are given in Figure 4.4a. To interpret the figure, the reader is reminded that the value D is a measure of the degree of equilibrium orientation (see Figure 4.3). The flow regime consists of half a channel with an aspect ratio ($\bar{x}_3/\bar{x}_2$) of 10 . Regions bounded by contour lines indicate the respective areas of orientation that result from the flow conditions.

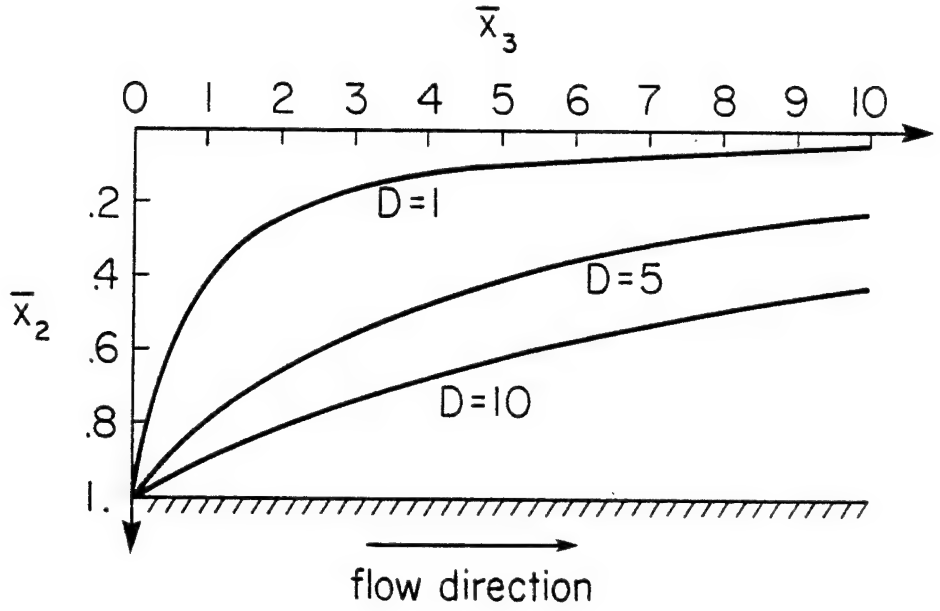

Figure 4.4a Variation of the degree of equilibrium orientation for 2-D Poiseuille flow

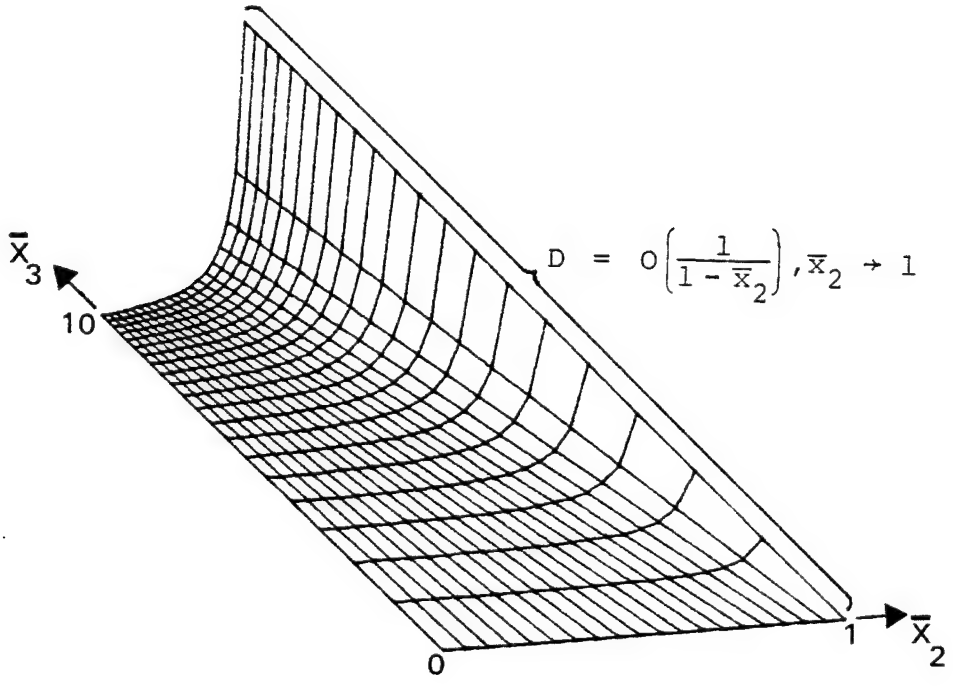

Figure 4.4b Three-dimensional plot of $D = f(x_2, x_3)$ for 2-D Poiseuille flow ($n = 1$)

Another way to summarize the above discussion is to recognize that eq.(4.14) may be solved explicitly for D .

$$D = \frac{2\bar{x}_2\bar{x}_3}{(1-\bar{x}_2^2)} \tag{4.15}$$

From eq.(4.15) one may note that D is a function of both x_2 and x_3 , and may by represented as a surface in three-dimensional space. This surface is plotted in perspective in Figure 4.4b, with the variation of D being plotted out of the $\bar{x}_2$-$\bar{x}_3$ plane. From eq.(4.15), the singular behavior of the function at $\bar{x}_2 = 1$ may easily be seen. Factoring the denominator, the strength of the singularity is recognized to be of the first order for the case of Newtonian flow. The singularity at the wall ($\bar{x}_2 = 1$) may be attributed to the fact that the velocity vanishes there resulting in a division by zero in eq.(4.11). The extreme values of the parameter D near the wall reiterate the notion of highly aligned fibers parallel to the flow adjacent to the boundary of the domain.

4.2.2 Power Law Flow

If one considers the same domain as shown in Figure 4.2, but changes the constitutive behavior of the

fluid in the channel, the effect of a shear thinning (pseudoplastic) flow on particle behavior can be investigated. The flow remains steady in the x_3 direction and possesses a nonuniform velocity gradient in the x_2 direction (see Figure A1.11 for n<1). This problem is governed by the same assumptions of the previous section, where nonuniform velocity gradients were shown to correctly predict the particle orientation.

The normalized velocity profile for a unit flow of a power law fluid can be shown to be (see Appendix A1.3)

$$u = \frac{1 + 2n}{1 + n}\left[1 - (x_2/a)^{\frac{n+1}{n}}\right] \tag{4.16}$$

where n ≡ power law index. Straightforward differention yields the particular component of the deformation rate tensor, namely

$$|\Gamma| = \frac{(1 + 2n)}{n} \frac{x_2^{\frac{1}{n}}}{a^{\frac{n+1}{n}}} . \tag{4.17}$$

Following the identical sequence of events of the previous section, one finds the degree of orientation to be

$$D \equiv |\Gamma|t = \frac{(1 + n)}{n} x_3 x_2^{\frac{1}{n}} \frac{1}{a^{\frac{n+1}{n}} - x_2^{\frac{n+1}{n}}} \tag{4.18}$$

Introducing the normalized coordinates of eqs.(4.13), the desired expression analogous to eq.(4.14) becomes

$$\bar{x}_3 = D\left(\frac{n}{1+n}\right)\frac{(1-\bar{x}_2^{\left(\frac{n+1}{n}\right)})}{\bar{x}_2^{\frac{1}{n}}} \qquad (4.19)$$

Since it is of interest to discern the effect of the pseudoplasticity of the fluid on particle orientations, the value of D is taken as constant and n is the parameter. In Figure 4.5a, a plot of eq.(4.19) is shown where the effect of the power law constitutive equation may be seen upon the fiber orientation. This result can be explained if one recalls the associated velocity profile for shear thinning flows in a channel (see Figure A1.11). For these types of flow conditions there exists a region where the velocity profile is flat, originating at the tube centerline and extending radially outward. Corresponding to this flat velocity profile region is a random core of fibers. Oriented regions of fibers are found only in a boundary layer near the wall whose thickness varies according to the index n . These distributions of fibers are characteristic of shear thinning flows and have been observed experimentally.

For purposes of comparison, Figure 4.5b illustrates the continuous variation of D throughout the x_2 , x_3 domain of Figure 4.5a. The discrete value for the

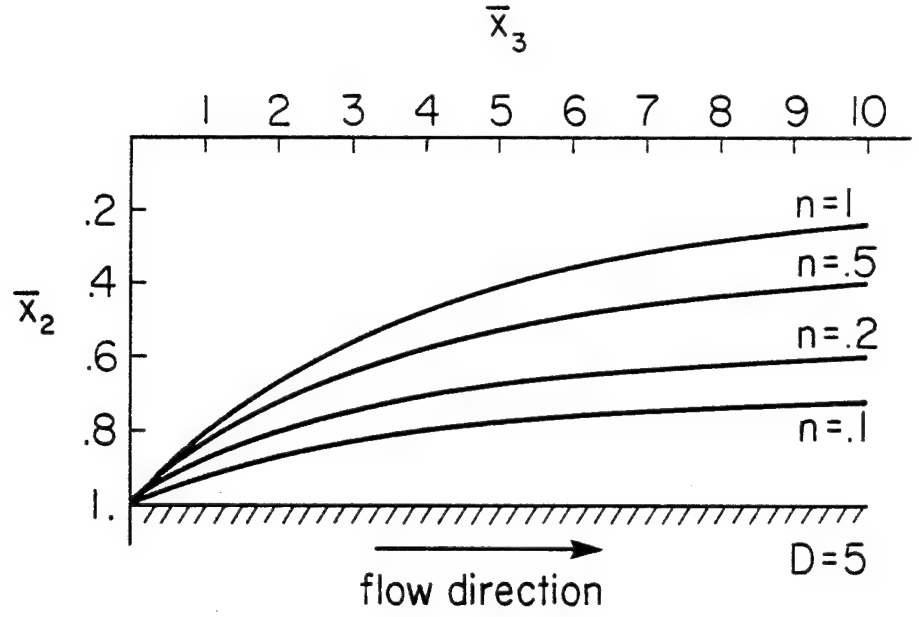

Figure 4.5a Boundary layers of aligned fibers (D = 5) for shear thinning flows

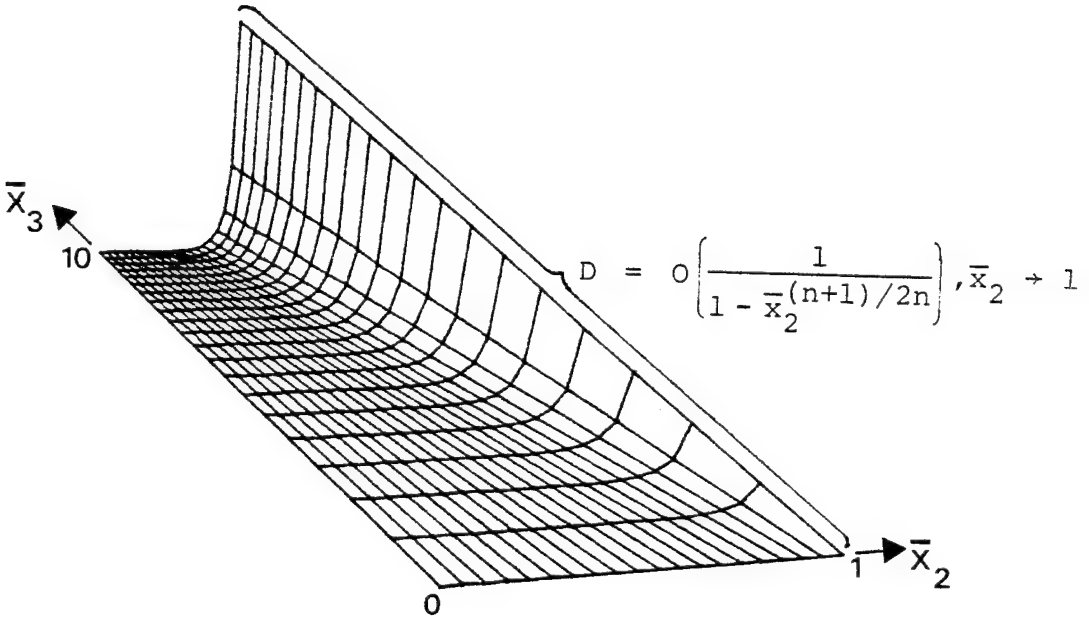

Figure 4.5b Three-dimensional plot of $D = f(\bar{x}_2, \bar{x}_3)$ for power law fluid in wall-bounded shear flow (n = 0.1)

power law index was chosen to be 0.1, which approximates a highly shear thinning flow. The important comparison to note arises from the variation of D close to the wall. Here, it may be shown that for a general power law fluid, the singularity occurring at $\bar{x}_2 = 1$ is of the order

$$O(1/(1 - \bar{x}_2^{\left(\frac{n+1}{2n}\right)})) \quad . \tag{4.20}$$

This gives rise to a distinct boundary layer and identifiable core region.

So far, it has been assumed that the initial fiber orientations have been perpendicular to the fluid streamlines. Suppose that the initial fiber distribution is assumed to be random in nature. What will the resulting fiber distribution be within the half channel? A plot of this situation is shown in Figures 4.6a - d, for decreasing values of the power law index. Clearly, these illustrations of fiber orientation display the aligned regions of fibers and enhance the notion of a distinct boundary layer for small values of n. This close agreement among Figures 4.5a and 4.6a - d indicates that the initial conditions have a negligible effect on the downstream part of the solution. It is the flow kinematics that exercise a major role in the resulting orientation of the particles for these dilute systems.

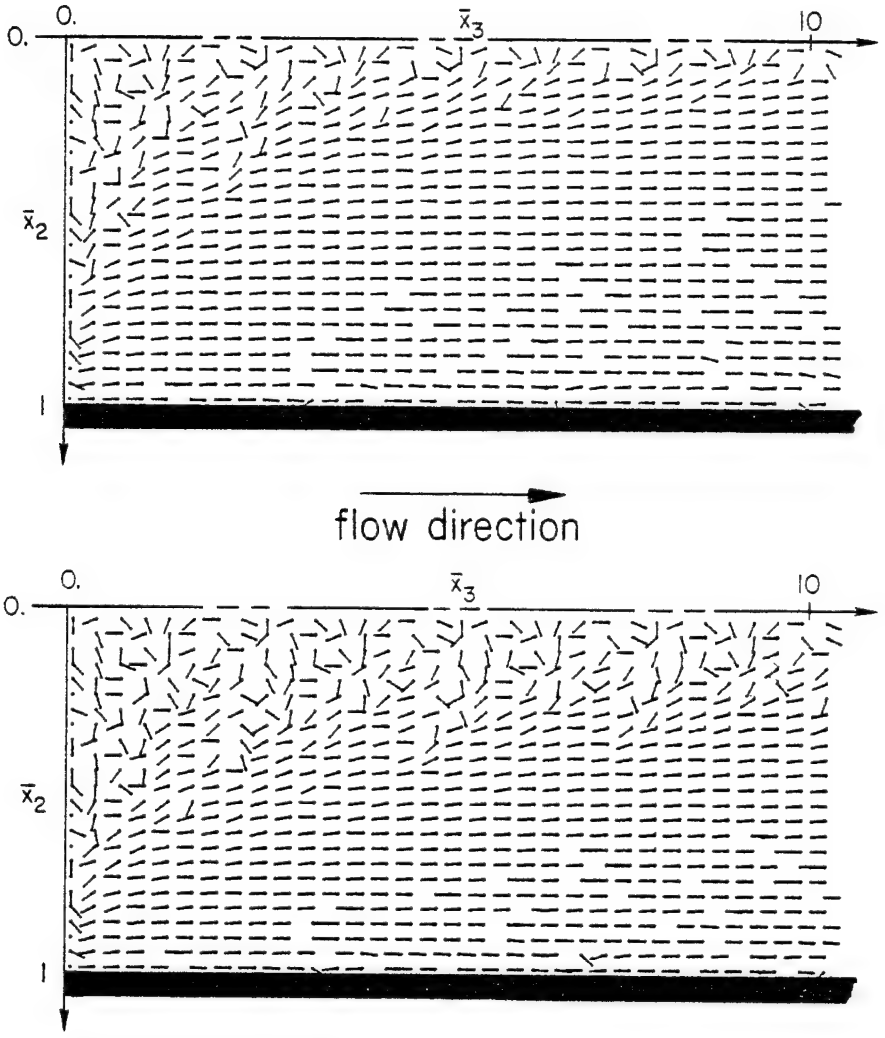

Figure 4.6 Analytically predicted fiber orientations in 2-D Poiseuille flow. Random orientation introduced at $\bar{x}_3 = 0$. (Figure continued next page.)

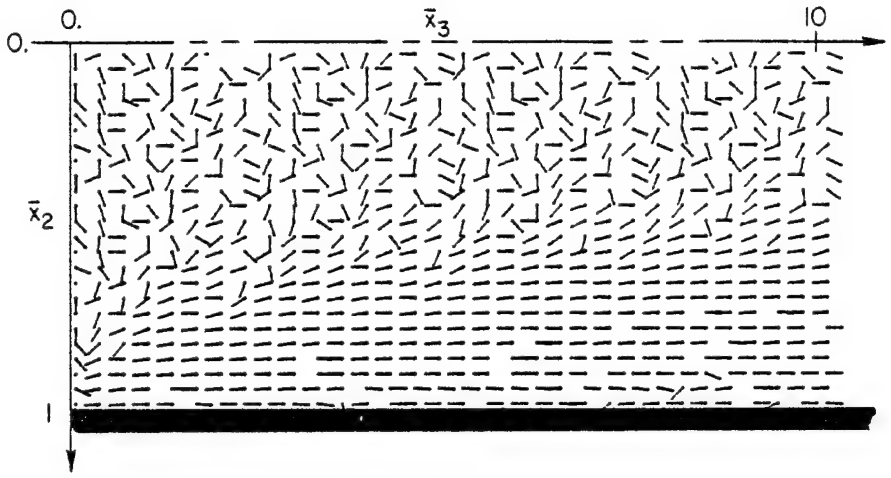

(c)
n=.2

flow direction

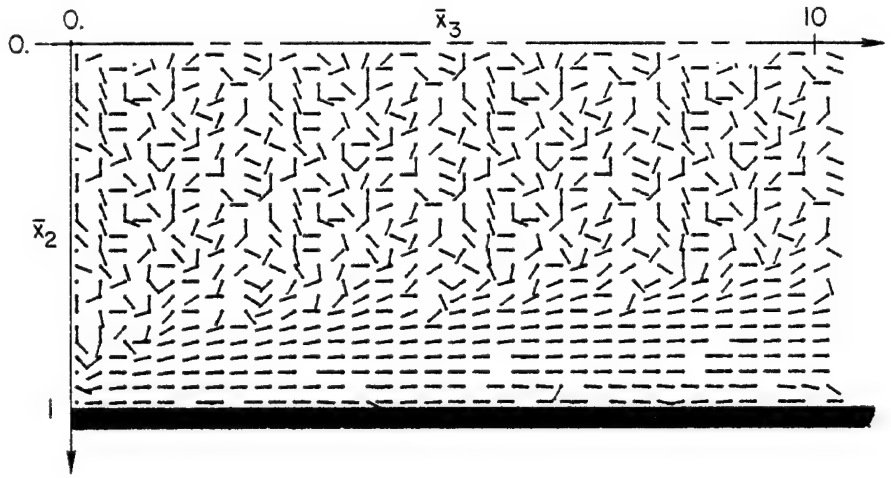

(d)
n=.1

(Figure 4.6 continued)

4.3 Application to the Discretized System

To this point simplified flows have been discussed such that the velocity fields (or derivatives thereof) have been expressed by analytical functions. This was necessary to facilitate the closed-form integration of eq.(4.3). We wish to extend the ideas presented thus far to more complicated domains, where the velocity fields may not be solved exactly. The extension is obvious as one seeks to model the orientation patterns that exist in complex molds.

The flow chart of Figure 4.7 illustrates how the method of solution is altered when the flow becomes complex due to geometry. The initial difference occurs upon implementation of the FEM to solve the fluid mechanics problem. As a result of this approximation to the velocity field, one maintains only a discretized representation of components of velocity. Derived quantities such as stress components, stream function, and vorticity will also be of a discretized nature; thus, all quantities of interest are only known at the nodal points within the domain.

Since the extension of this analysis is to arbitrary flows, one may not assume a priori the components of the

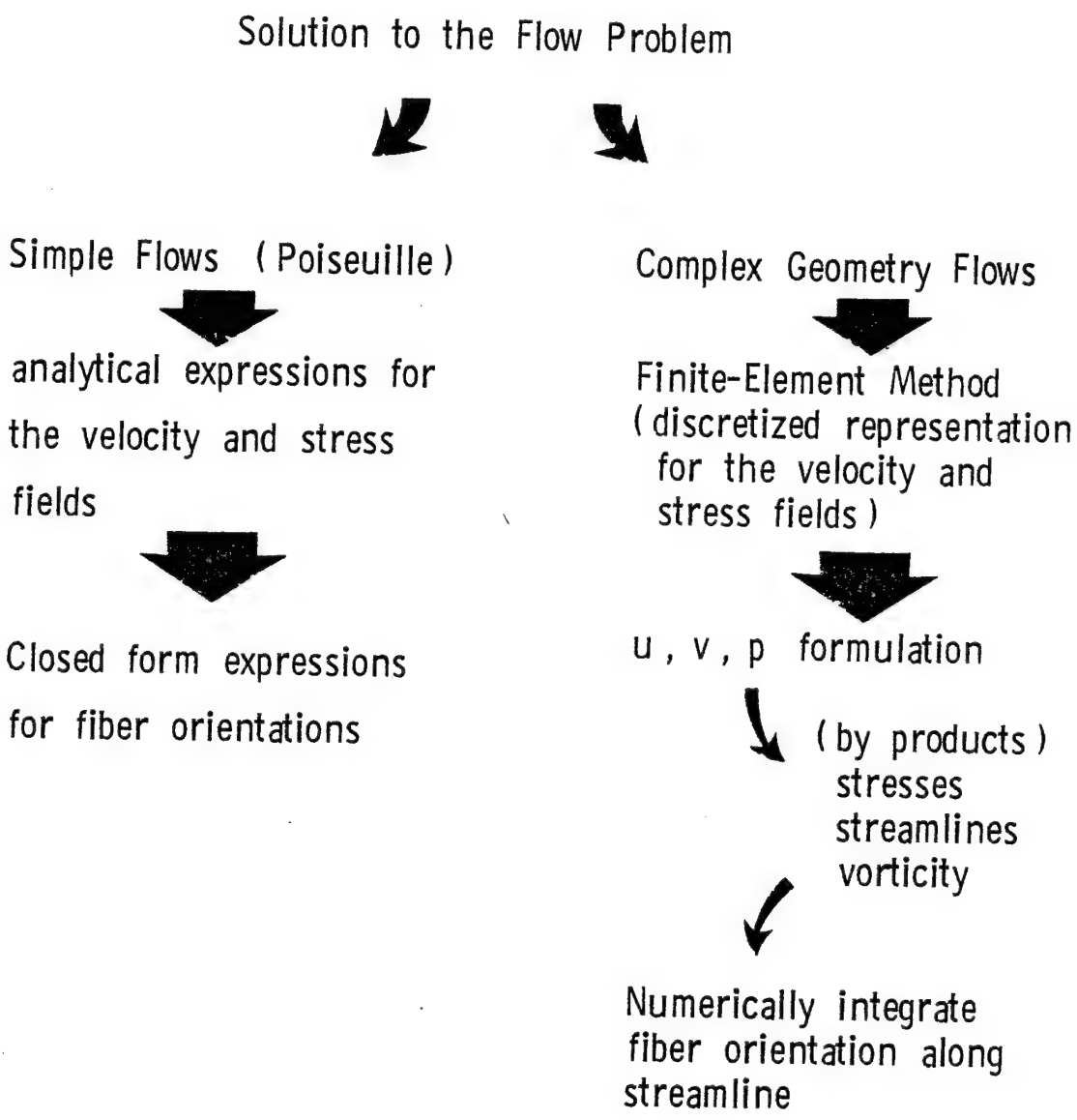

Figure 4.7 Alternative methods of determining fiber orientations in dilute systems

deformation rate tensor to be constant in space on a scale that is large in comparison with the particle. However, by resorting to the discretized domain the original problem of determining fiber orientation has been recast into a series of independent, smaller problems. For each subproblem the components of distortion and rotation are taken to be constant in space and the original assumptions of Jeffery are recovered. The numerical integration of the fiber orientation equation (eq.(4.3)) along a streamline admits a piecewise continuous approximation to the true solution. The components of the deformation rate tensor and vorticity vector are updated at each stage of the integration but remain constant during the integration. The convergence of such a scheme is investigated in section 5.2.

In the following chapter, the methodology of solving for particle orientations when only a discretized velocity field is known is presented in some detail. As in other sections, the subsequent chapter draws on important discussions in the appendices and will culminate with the ability to determine the fiber orientations within molds of complicated designs.

5. THE NUMERICAL ROUTINE "COLINS"

5.1 Methodology

The emphasis in this chapter will be placed upon examining the numerical program COLINS in detail. Incorporated within the program is the methodology allowing one to predict and view fiber orientations within a general flow system. It is assumed that the fluid mechanics problem has been completely solved and a discrete representation of the primitive and derived quantities is in hand. Thus, the input to the program COLINS is a complete knowledge of the flow problem. For the present analysis, it is assumed that the fiber orientations will not alter the velocity field. This criterion may be satisfied if one restricts his considerations to dilute suspensions. Usually the standard for dilute systems is taken to be no greater than 0.05 particulate volume fraction. To correctly model the resulting fiber orientations in a more concentrated material system, an iterative-type solution is required. Here, the effects of fiber orientation on viscosity are predicted and the velocity field is recalculated in light of this updated viscosity function.

Returning to the problem at hand, one seeks to provide a means of solving eq.(4.3) within the discretized domain. The first consideration assumes that the center of gravity of the fiber will translate parallel to fluid streamlines. Streamlines are easily calculated from the discretized representation of the stream function as follows. The entire grid is scanned element by element to identify the nodal points corresponding to a given value of the stream function (ψ). More than likely the desired value of ψ will not intersect an element boundary precisely at a nodal point. Linear interpolation is used to pinpoint the precise location, and hence the coordinate values, for the desired value of ψ. Upon scanning the entire array of elements, a collection of x,y coordinate values is obtained that defines a particular streamline. The next task requires that these points be organized appropriately so as to define a path line of a particle in the direction of the flow.

Scanning element by element will duplicate all of the stream function points excluding the first one and the last. The reason for this can be seen in Figure 5.1, where it is noticed that if a streamline intersects an element, it must intersect an element boundary twice. Given the initial intersecting point of a streamline, P_o,

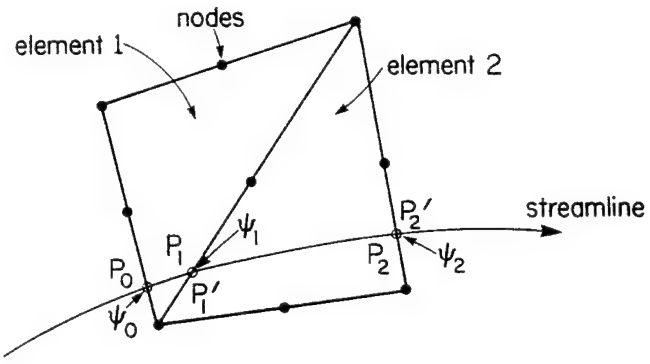

Figure 5.1 Constructing a path line

and its neighboring point, P_1 , the subroutine ARRANG (of the program COLINS) searches until it locates P_1' and hence its neighbor P_2'. The procedure continues until an entire path line is constructed along which a particle will translate.

Now that a typical particle path is known, eq. (4.3) may be numerically integrated along the path line. Since the independent variable is time in eq.(4.3), we need to interpret the distance along the streamline in terms of time steps. Refer to Figure 5.1 and consider the distance between ψ_o and ψ_1 . If one divides the distance by the local fluid velocity at ψ_o , a natural time step is defined. Clearly the accuracy of this procedure is determined by the fineness of the mesh and is investigated in the next section.

The components of the vorticity and distortion tensors have been assumed to vary with position in an arbitrary flow. More particularly, they will vary along the streamline during integration. This situation may be easily handled if the values of Z_i and $\underset{\sim}{d}$ are updated at each time step in the integration. Again, the precise values for Z_i and $\underset{\sim}{d}$ at the points ψ_i (Figure 5.1) are determined via linear interpolation between the nodal values. Hence, the fiber orientation may be numerically integrated via a canned, first-order, nonlinear equation solver. Fiber orientations may be solved for along many streamlines which results in the fiber orientations being known for the entire flow field.

5.2 Convergence of the Numerical Scheme

In this section, the question of convergence of the numerically integrated orientation equation (eq.(4.3)) is investigated. Attention is focused entirely upon the above questions, thus assuming a convergent fluid flow field already exists.[1] Convergence in the context of linear fluid mechanics problems is defined as approaching the exact

[1]This assumption will be satisfied by considering two-dimensional Poiseuille flow, a problem whose finite-element solution yields the exact analytical representation of the velocity and pressure fields.

solution by successive mesh refinements. This idea of convergence will be adopted here, to treat the problem at hand.

Recall that the fiber orientation is solved for by numerically integrating eq.(4.3) along selected path lines. The coefficients of this first-order, nonlinear equation are updated at each point where the path line intersects an element boundary. It stands to reason that the exact solution will be more closely approximated if there is an increased number of such points. Hence, it follows that a continuous refinement of the mesh should lead to convergence of the fiber orientation solution.

Figures 5.2a - c show the three respective grids for 2-D, symmetric Poiseuille flow. The discretized velocity and pressure fields agree exactly with known analytical expressions and the question to be answered concerns the behavior of the fiber orientation response. Figure 5.3 displays the angle of orientation calculated along the same path line per each respective grid. The fibers were initially aligned perpendicularly to the flow direction and the orientations shown in the table were assumed as a function of the axial coordinate.[1]

[1]The process integrates along path lines, but for the case of Poiseuille flow the path lines are parallel to the axial coordinate.

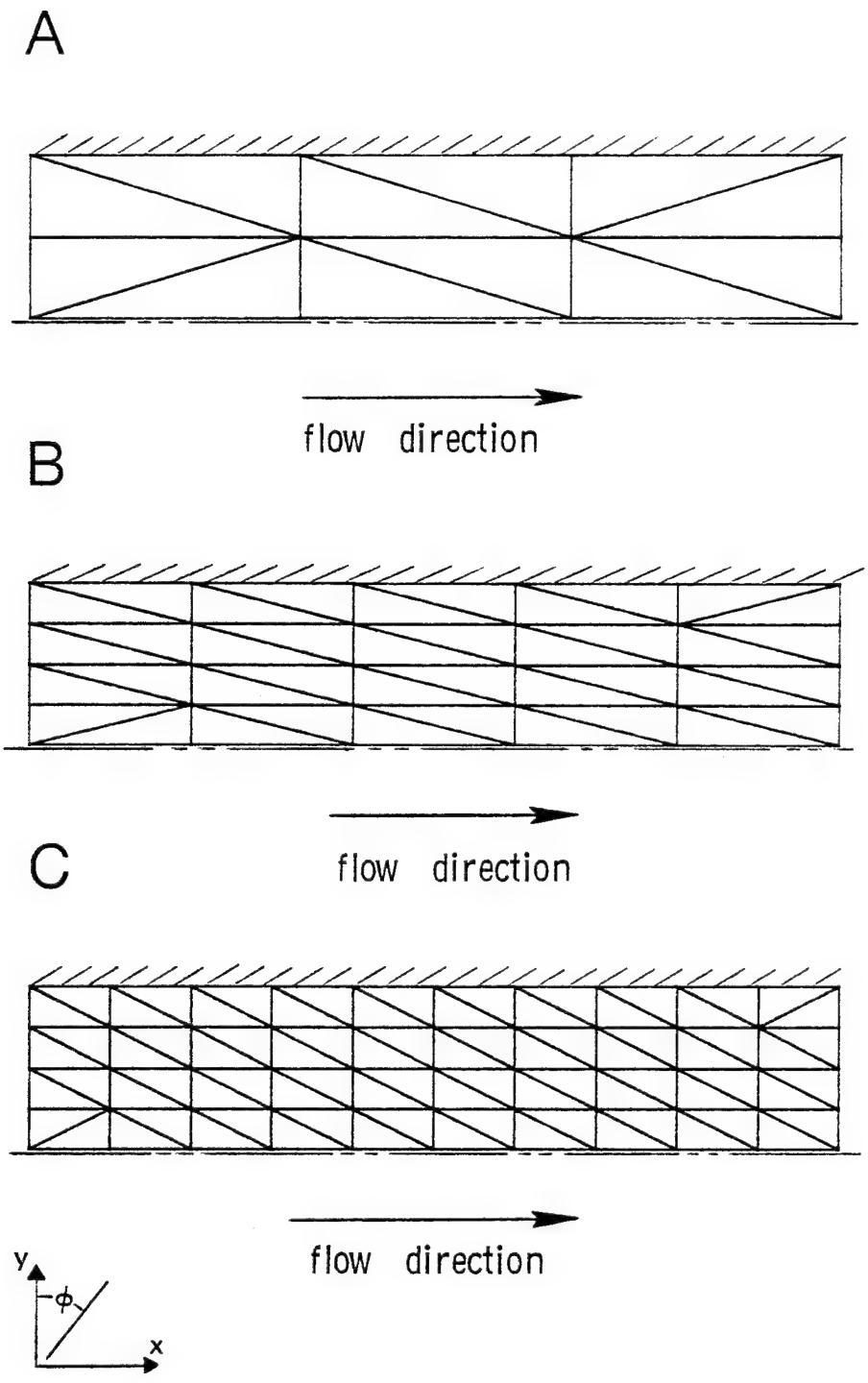

Figure 5.2 Respective grids for conducting a convergence study

Next, it is desirable to approximate the order of convergence from the data of Figure 5.3. Initially, suppose that the truncation error at each step along the streamline can be approximated by the form

$$\phi(x)_{exact} - \phi(x)_{computed} \simeq C(h)^p \qquad (5.1)$$

where C and p are constants and p is the order of the method. Also, h is defined to be the step size (dependent on the mesh refinement), and the left-hand side of eq.(5.1) is the discretized error.

Consider the data labeled "i" in going from the meshes of Figure 5.2a to 5.2b.

$$-0.599884 + 0.616629 \simeq C(\tfrac{1}{3})^p$$
$$-0.599884 + 0.600605 \simeq C(\tfrac{1}{5})^p$$

Dividing these results and solving for p yields

$$23.2 \simeq (\tfrac{5}{3})^p$$

or $p \simeq 6.1$.

For comparison, the data labeled "k" yields

$$-0.939547 + 0.954663 \simeq C(\tfrac{1}{3})^p$$
$$-0.939547 + 0.940057 \simeq C(\tfrac{1}{5})^p$$

Thus,

$$29.6 \simeq (\tfrac{5}{3})^p$$

or $p \simeq 6.6$

and one concludes that the method is of at least sixth order which offers swift convergence. A brief glance

Figure 5.3 Results of the convergence study

A	B	C	Exact
0.0	0.0	0.0	0.0
	-0.136056	-0.136205	-0.135949
	-0.267587	-0.267459	-0.267052
	-0.390068	-0.389928	-0.389422
	-0.501369	-0.501240	-0.500670
-0.616629^{i}	-0.600605^{i}	-0.600491	-0.599884
	-0.687993	-0.687893	-0.687271
	-0.764425	-0.764338	-0.763717
	-0.831099	-0.831024	-0.830415
	-0.889276	-0.889214	-0.888627
-0.954663^{k}	-0.940057^{k}_{m}	-0.940063_{m}	-0.939547

NOTE: All numbers indicate values of orientation along the same streamline, $\psi = -0.8$.

at the data labeled "m" will show that a further mesh refinement from Figures 5.2b to 5.2c is not needed since it appears that we are incurring errors due to the precision of the method. Only six significant digits were carried throughout the calculations and the inaccuracies are most probably due to round-off error. If disturbed by this error, it is encouraging to note the error in the solution of grid B is less than a fraction of a single percent, and for the current work is more than sufficient.

Thus, we have shown the method of calculating fiber orientation to be rapidly convergent in a manner where the discretization error diminishes as $O(h^6)$ as $h \to 0$. It is thus established that the method will converge with increased discretization. Further investigation has clearly dictated the fact that a highly refined mesh is not always the optimum situation. A definite trade-off exists between increased accuracy and additional computation. Reasonable engineering discretion and experience are needed to devise an optimum mesh for computing fiber orientation.

5.3 Defining an Orientation Parameter

In an effort to simulate the actual flow pattern observed in real molding operations, it was necessary to

follow the orientations of many particles. Suppose one designates 10 streamlines of a flow field along which one wishes to monitor fiber orientation. On the average, the orientation shall be recorded approximately 20 times per streamline. Recall that the value for the numerically integrated fiber orientation is found at P_0 , P_1 , ... , P_N , where N equals the number of intersections between streamlines and element boundaries. In addition, if we propose 5 initial orientations, then the total number of discrete fiber orientations is 1,000 . That is to say, there will be 1,000 little fibers plotted at their respective orientation and position within the flow field. While qualitatively appealing, this procedure for representing the fiber orientations becomes cumbersome. Ultimately one seeks a more feasible way of interpreting the fiber orientation data.

It is desired to follow a development that appeals to the experimentalist. Consider a region of the flow field in which the fibers are oriented arbitrarily as shown in Figure 5.4. Initially one defines a set of initial coordinate axes (x,y). With respect to this coordinate system, the arithmetic mean value of the various orientations is calculated and denoted as $\overline{\phi}$. Individual fiber orientations with respect to $\overline{\phi}$ are represented by ϕ_i and

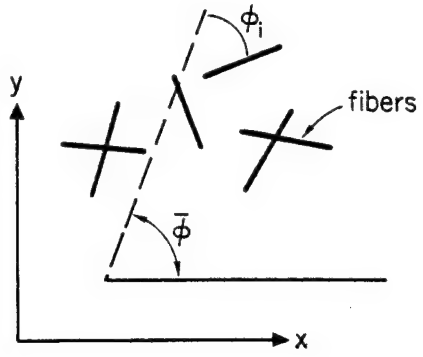

Figure 5.4 Determining the local fiber orientations and their relation with the global coordinate system

are shown in Figure 5.4. From these quantities one may define a root mean square (rms) value of the orientation angle given by eq.(5.2)

$$\Phi_{rms} = \sqrt{\frac{1}{N}\sum_{i=1}^{N}(\phi_i - \bar{\phi})^2} \qquad (5.2)$$

Clearly, due to summetry, the permitted values for Φ_{rms} reside between 0 and $\pi/2$. The symmetry argument stems from the fact that $\phi_i = (\phi + \pi/2)_i$ and $-\phi_i = \phi_i$. To further simplify the orientation idea, one normalizes the value of Φ_{rms} by introducing the orientation parameter f, defined by eq.(5.3)

$$f = 2(\cos^2\phi_{rms}) - 1 \qquad (5.3)$$

The values of f range from -1 to 1 and have the following connotations:

-1 => perfect alignment of fibers transverse to $\overline{\phi}$

0 => random alignment

1 => perfect alignment of fibers parallel to $\overline{\phi}$

Now, having the interpretation of the orientation parameter (f) in hand, one may graphically display the orientation surface, f(x,y), within the domain. Also, quite often contours of f are plotted to describe the relative degree of fiber orientation that exists throughout the region.

6. SELECTED NUMERICAL EXAMPLES

6.1 2-D Poiseuille Flow

In section A2.8, the numerical solution for two-dimensional, pressure driven, shearing flow is presented. Here, the results from the program COLINS are presented to show the close agreement with the analytically predicted orientations. Figure 6.1a shows the resulting fiber orientations for this flow. Four initial fiber orientations at each point at the left-hand side were prescribed to be 0, ±45, 90, in an effort to simulate a random distribution of fibers at the inlet. This is to say that, program COLINS was executed four times with one of the specified initial orientations per each execution. The lucid indication of the orientation mechanisms is borne out in this figure. In regions near the exterior boundary, the fibers are aligned parallel to the streamlines (see Figure A2.20e) regardless of their initial inlet orientations. These were the same findings of the analytic study of section 4.2.1. Contours of the orientation parameter are plotted in Figure 6.1b, which were calculated according to eq.(5.3). The values of this parameter are calculated by COLINS subsequent to

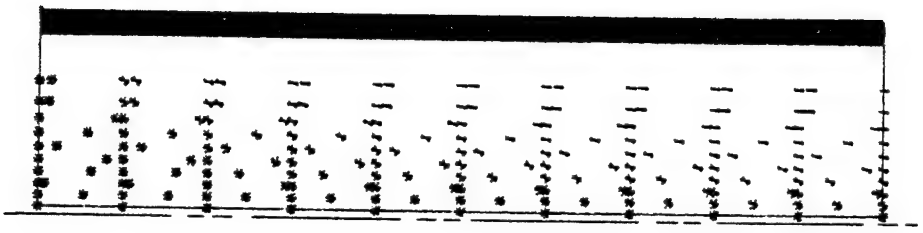

(a) Numerically predicted fiber orientations resulting from wall-bounded shearing flow (Four initial orientations (random distribution) at inlet)

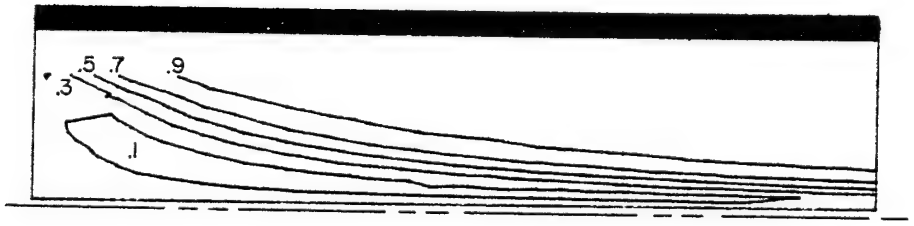

(b) Contours of the orientation parameter

Figure 6.1 Fiber orientation in two-dimensional Poiseuille flow

the solution of the individual fiber distributions. Comparing Figure 6.1b with the previously calculated analytical contours of D (Figure 4.4a), one finds a close agreement in the behavior of the orientation for this wall-bounded shearing flow. Note that equivalence of the parameters D and f is not claimed, but merely the fact that both give rise to the boundary layer concept. In each case, a boundary layer of oriented fibers near the wall is predicted, and the boundary layer thickness is seen to asymptotically approach the channel width at large values of axial coordinate.

The purpose of choosing this example, once again, was to provide consistency among results, as the orientation schemes have been further extended. By maintaining a constant check upon the extensions to the model, a high level confidence is achieved in the model itself. In the next sections, another example to further test the numerical model's ability to accurately predict the resulting fiber orientations in a shear thinning fluid is examined. Finally, an example of expansion flow and the resulting fiber orientations is explored. Here no analytical solution exists for the fiber orientations and the goal of modeling fiber orientations, numerically, is achieved.

6.2 2-D Power Law Flow

6.2.1 Solution of the Problem

The problem of a power law fluid flowing between two parallel walls becomes interesting in itself when a numerical solution is sought. The finite element scheme used previously may be employed again with one major modification. The viscosity of the fluid is a function of the deformation rate tensor, hence its value is not a constant. This suggests an iterative type solution of the problem with one possible approach outlined below.

Initially the Newtonian velocity field is obtained from the finite-element method, assuming μ is constant. Subsequent to the determination of the initial velocity field, the viscosity variation is calculated in terms of the spacial coordinates. This is accomplished by computing the components of the rate of deformation tensor from the calculated Newtonian velocity field. The solution for the velocity field is then repeated using the variable viscosity function, and as before the viscosity function is updated by recomputing the components of the deformation rate tensor in terms of the iterated velocity field. This procedure stops when the numerical values for the components of the velocity field are sufficiently close to the previous

ones. Now assuming that the method of solution is well in hand, one turns to the task of choosing appropriate boundary conditions.

6.2.1.1 Boundary Conditions

Figure 6.2a illustrates the appropriate mesh pattern for the two-dimensional power law flow, taking advantage of the existing symmetry. The boundary conditions along the solid wall and channel centerline are trivially applied in each case. The "no slip" condition at the wall is satisfied by specifying zero velocity there. Since the resulting velocity profile is assumed to be symmetric about the channel centerline, the shear component of the traction vector vanishes on the centerline. In addition, the transverse velocity (v) is prescribed to be zero everywhere on the boundary. There is yet to specify two more boundary conditions to the domain: one each at the upstream and downstream ends of the region. At these boundaries, one may either specify the axial component of the velocity or the normal component of the traction vector. For this example, it has been chosen to prescribe the normal component of the traction vector, F_x. Owing to the fact that the normal deviatoric stresses are zero for this flow, F_x is identical to the pressure. One sets $F_x = 0$ at the downstream boundary and hence only needs to calculate the pressure

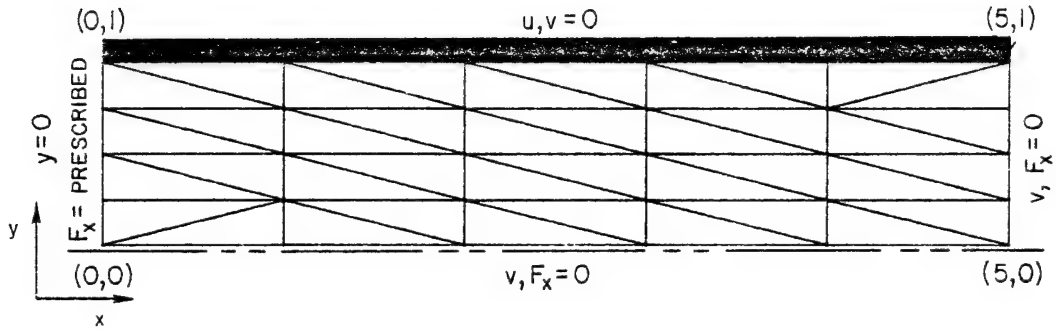

(a) Grid and boundary conditions

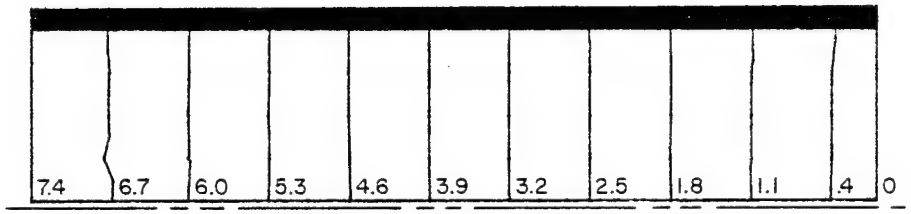

(b) Pressure

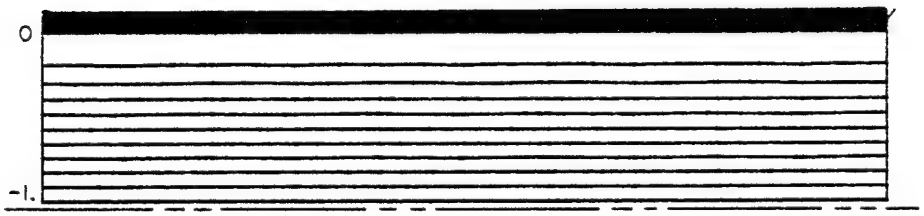

(c) Stream function

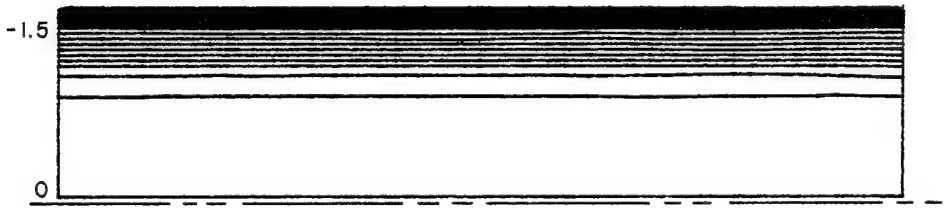

(d) Vorticity

Figure 6.2 Finite element solution to the generalized Newtonian fluid between parallel walls with the power law approximation (n = 0.2)

difference, which shall be applied on the boundary at $x = 0$.

Since F_x being prescribed actually entails a prescribed pressure loading, it is necessary to determine the nodal contributions from the distributed pressure loading. Recall that the nodal forces are given by

$$F_{x_i} = -\int W_i t_x \partial S \qquad (6.1)$$

where F_{x_i} = i-th nodal force,

W_i = i-th shape function,

t_x = surface loading.

This equation may be recast graphically as shown in Figure 6.3. Carrying out the integration of eq.(6.1) and

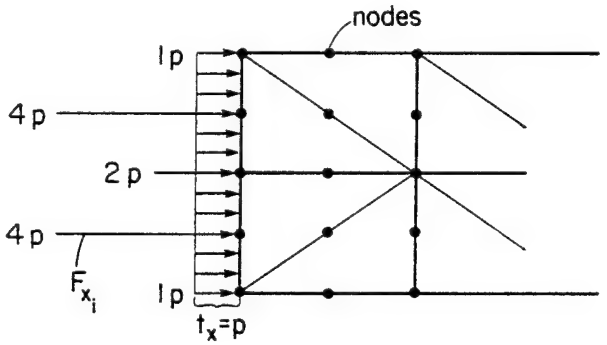

Figure 6.3 Representation of the pressure distribution by concentrated nodal forces for quadratic interpolation

assuming quadratic interpolation functions, the concentrated nodal forces are seen to vary as shown in Figure 6.3. With the calculation of the upstream boundary condition, the boundary value problem becomes completely and uniquely specified. Numerical results from the solution of the problem are given in Figures 6.3b - d and may be contrasted with those of 2-D Poiseuille flow in Figures A2.20b - f. One distinct difference between the flows is seen in the nature of the vorticity function, which is seen to be confined to a narrow region along the wall for the power law fluid. This is characteristic of the shear thinning flows and can be explained by referencing the pseudoplastic velocity profiles of Figure A1.12.

6.2.1.2 Numerically Predicted Fiber Orientations

Here, again one notes the fiber orientations predicted by the model and shown in Figure 6.4a. The power law index was taken to be n = .2 and a random orientation of fibers was prescribed at the left-hand side (inlet). The figure shows the individual fibers plotted within the flow region and it is interesting to note the expanded core region possessing random orientation even at distances away from the inlet. Qualitatively, this behavior could be anticipated from the information describing the flow field.

An equally interesting observation is provided by Figure 6.4b, where the reduction in the boundary layer is associated with increasing shear thinning. The boundary layer for this example has been taken as $f \geq .8$ which corresponds to a highly oriented region of fibers parallel to the wall. As an added note, it can be shown analytically that the boundary layer will approach the channel half-width as $x \to \infty$. The degree of pseudoplasticity will determine the order of the singularity at $y = a$ and hence how fast the boundary layer approaches the channel half-width. This point was also made mention of in section 4.2.2.

6.3 Expansion Flow

Having thus far gained considerable confidence in the numerical scheme for predicting fiber orientations, one arrives at a flow configuration for which nonanalytical solutions exist. It becomes necessary to solve the problem entirely by numerical means. This, of course, has been our ultimate objective all along, but it was important to check the method against known solutions at each stage in the development of the model.

Flow through a 10:1 expansion is investigated in this section to view the fiber orientations in an

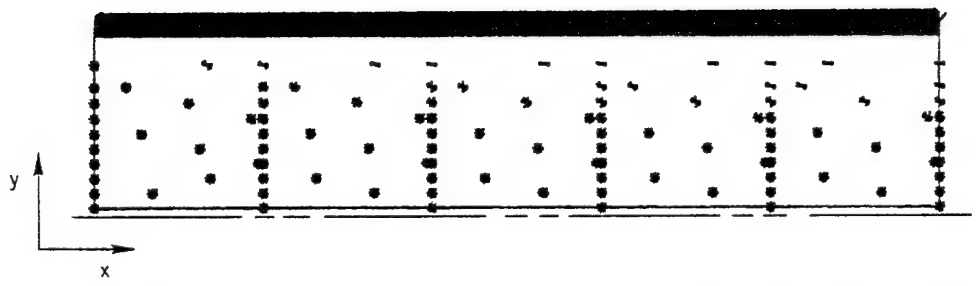

(a) Numerically predicted fiber orientations in a steady power law flow (n=.2) (Four initial orientations (random distribution) at inlet)

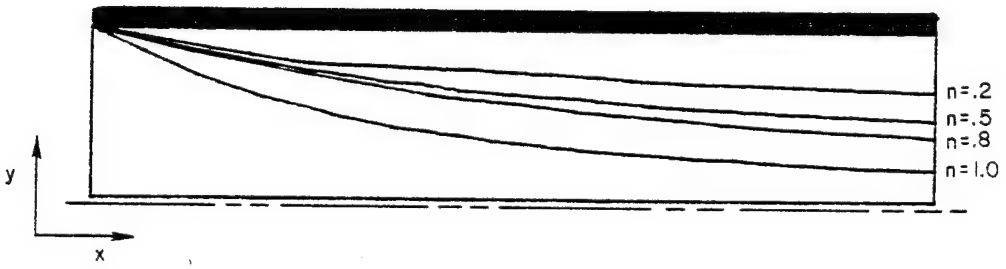

(b) Contours of orientation parameter (f=.8) for varying power law index

Figure 6.4 Fiber orientations in two-dimensional, power law flow

extensional flow situation. While the flow itself is not purely elongational the region removed from the immediate entrance consists mainly of an extensional flow. For this reason the dominant behavior of the normal velocity gradients may not be ignored. The flow configuration under present consideration is encountered in practice at the entrance to a large cavity. As usual we are assuming sufficiently slow motions so that the Stoke's equations of motion are valid. This in essence assumes that all transient and inertia dominated behavior is neglected. The fluid is considered to behave in the Newtonian sense, with the extension to power law fluids following immediately in light of the previous discussion of section 6.2.

6.3.1 Solution of the Problem

6.3.1.1 Boundary Conditions

The appropriate boundary conditions for this problem are labeled in Figure 6.5, which also illustrates the grid design for the problem solution. The boundary conditions by now are rather obvious with the possible exception perhaps of the far field boundary condition applied at $r = 10$. Again, as before, one has the freedom of specifying force components or velocity components on this

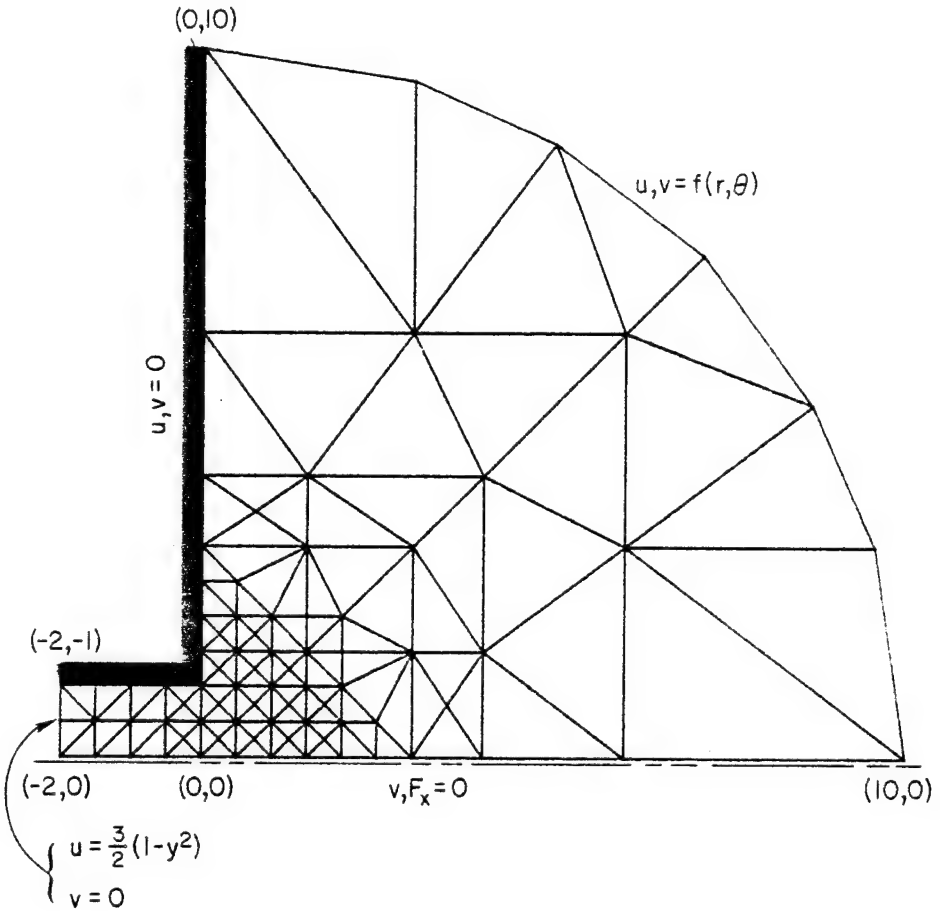

Figure 6.5 Finite element grid for a two-dimensional expansion flow of a Newtonian fluid

portion of the domain. It is desired to prescribe the velocity components at far field since they may be calculated exactly from the solution to the problem of Jeffery-Hamel flow. For source flow in a diverging section at small Reynold's numbers the velocity profile for Jeffery-Hamel flow has been shown to be [35]

$$\frac{u}{u_o} = 1 - \frac{\sin^2\theta}{\sin^2\alpha} \tag{6.2}$$

where $u_o = 4/r\pi$ for unit flow rate and $\alpha = \pi/2$. The u_o is determined from continuity considerations in much the same manner as v_{avg} is determined in eq.(A1.64). Note that this velocity profile is parabolic in the θ-direction and also maintains a radial dependence through the constant

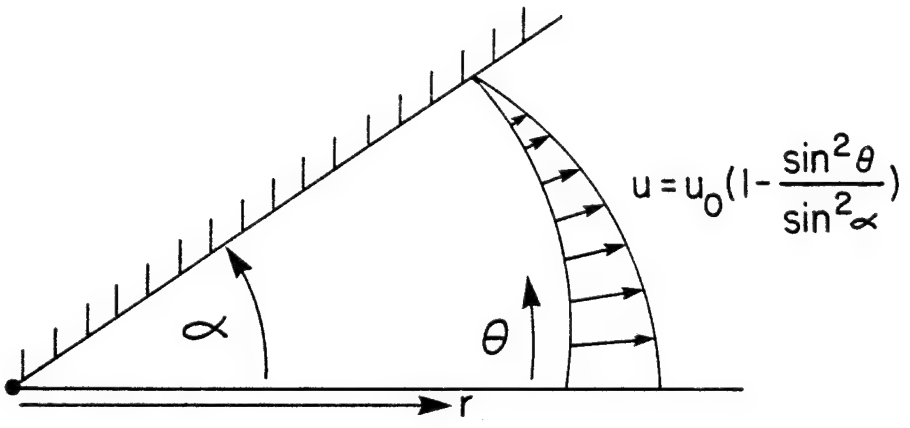

Figure 6.6 Jeffery-Hamel flow in a diverging section

u_o. At large radius values for our expansion flow problem, one may specify the Jeffery-Hamel velocity profile (eq. (6.2)) with good accuracy. It is assumed that when r = 10 the effects of the entrance region are negligible and the flow at this point is as though it emanated from a source. This was the prime consideration for choosing a large value of r at which to apply the final boundary condition.

The solution to the fluid mechanics problem is displayed in Figures 6.7a - d in the usual spirit of contour plots. Unless otherwise noted, ten contours are plotted per each field variable equally spaced between the maximum and minimum values. Contours that are not particularly smooth are a result of plotting a field variable that has a value near zero. Clearly, if the noise level of the solution is even minimal, it will be reflected in such a contour. In any event, perusing Figures 6.7a - d, one may be convinced that the solution to the fluid mechanics problem is a correct one.

6.3.1.2 Numerically Predicted Fiber Orientations

In all the previous examples and discussion, it has been shown how fibers align parallel to streamlines under steady shearing flow. So far, in the present discussion one has dealt with the flow in an expansion and

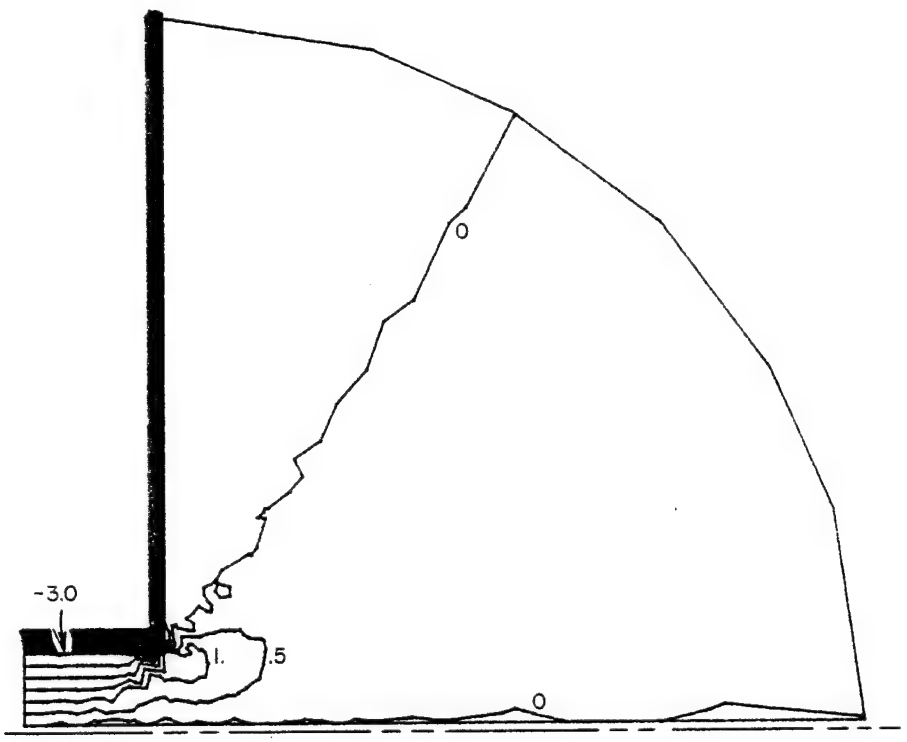

Figure 6.7a Shear stress contours of the expansion flow problem

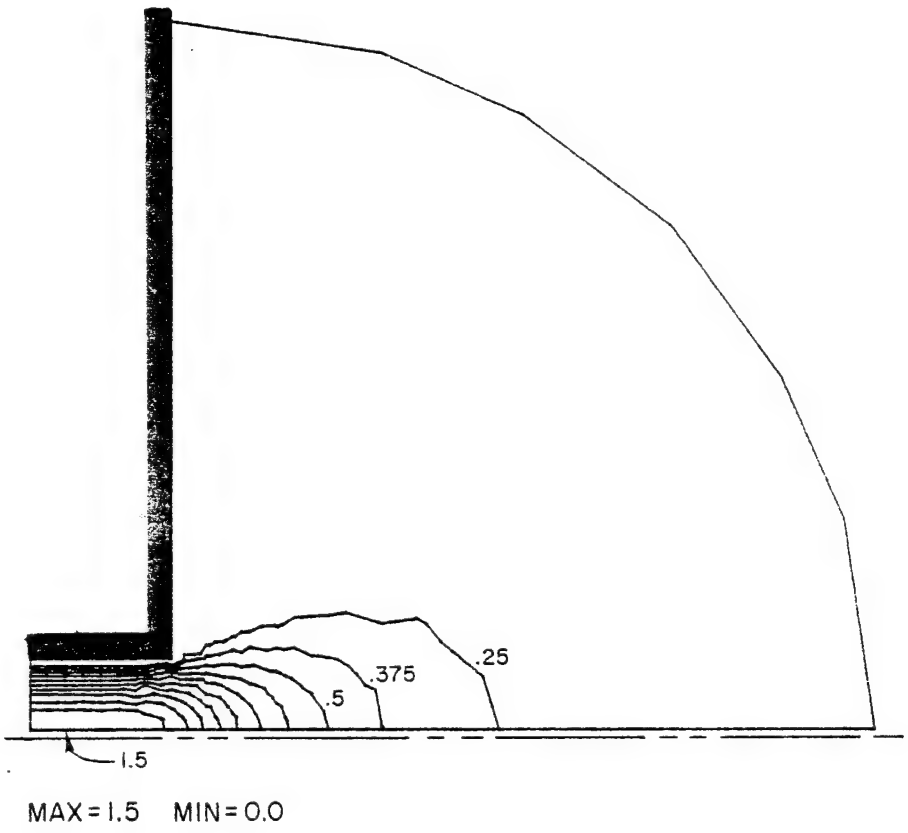

Figure 6.7b Contours of axial veloctiy of the expansion flow problem

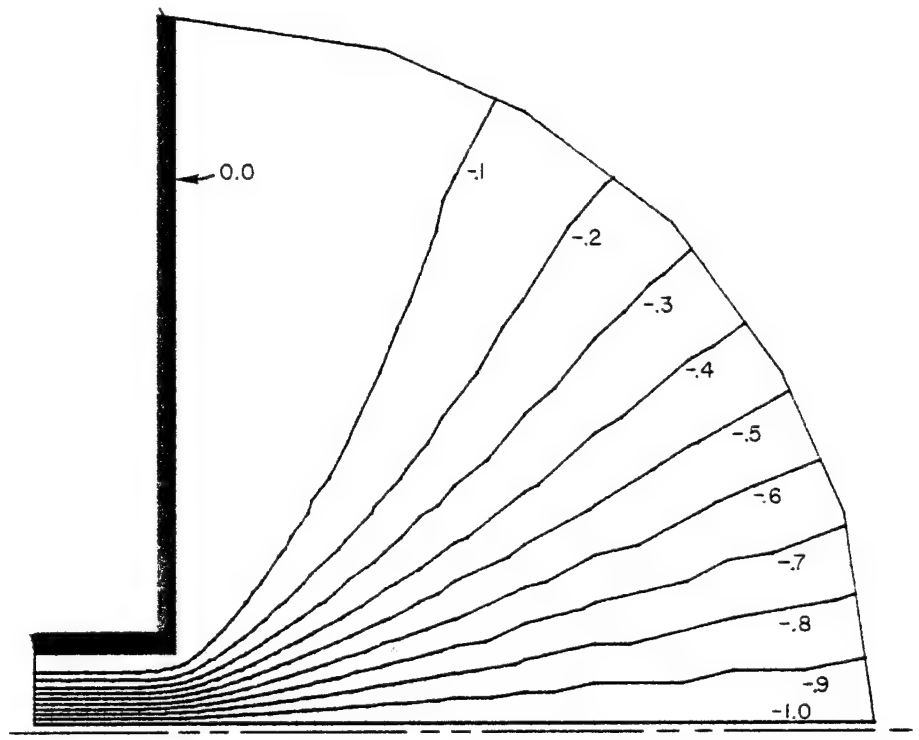

Figure 6.7c Contours of the stream function of the expansion flow problem

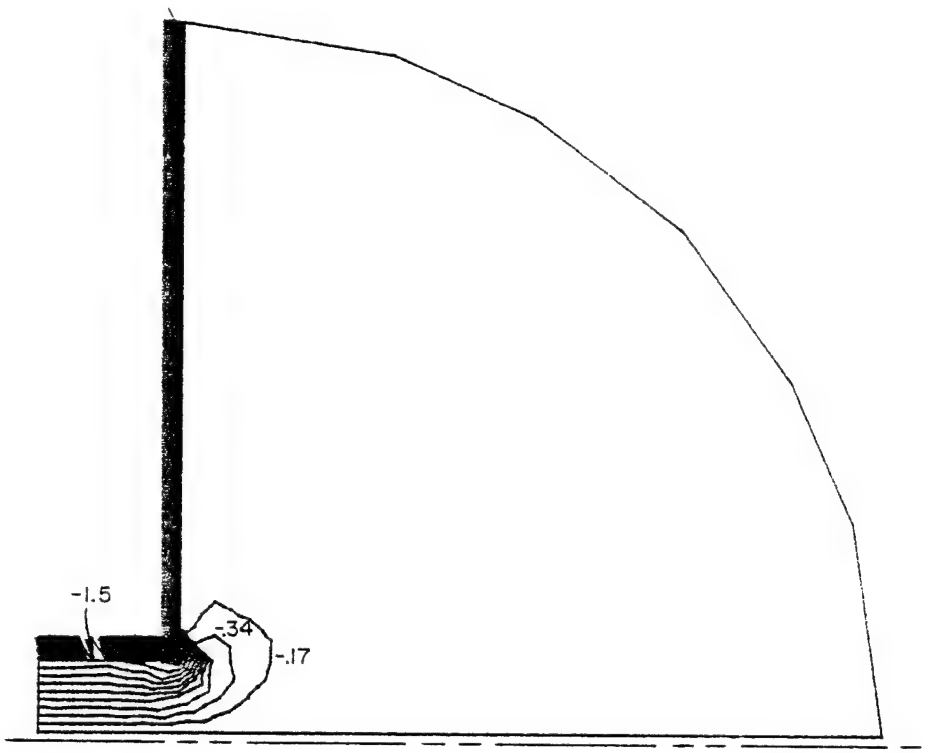

MAX = 0.0 MIN = -1.7

Figure 6.7d Contours of vorticity of the expansion flow problem

now inquires as to the resulting fiber orientations from such a flow. Obviously, from the knowledge of the qualitative orientation mechanisms from section 3.1, one would expect to find transverse orientations of the fibers in the region of the flow where elongational behavior dominates. Figure 6.8 shows exactly this phenomenon. Fibers are completely aligned in the constricted region owing to the high vorticity and shearing components existing there. In practice this region may correspond closely to the behavior experienced in the sprue of the mold. As the fibers enter the mold cavity they are oriented transversely to the streamlines primarily due to the elongational component of the flow. Another interesting point is to note the shearing mechanism for orientation at work all along the wall.

Figure 6.9 displays the orientation parameter for the expansion flow problem. Recall that a contour value of 1.0 corresponds to a completely aligned configuration. The angle of alignment with the global axes may be found in determining the quantity $\bar{\phi}$. (This quantity was defined in section 5.3.) Alternatively, one may deduce the steady state angle of alignment from a knowledge of the local flow kinematics. That is to say, if the local flow characteristics are predominately shearing, then $f = 1.0$

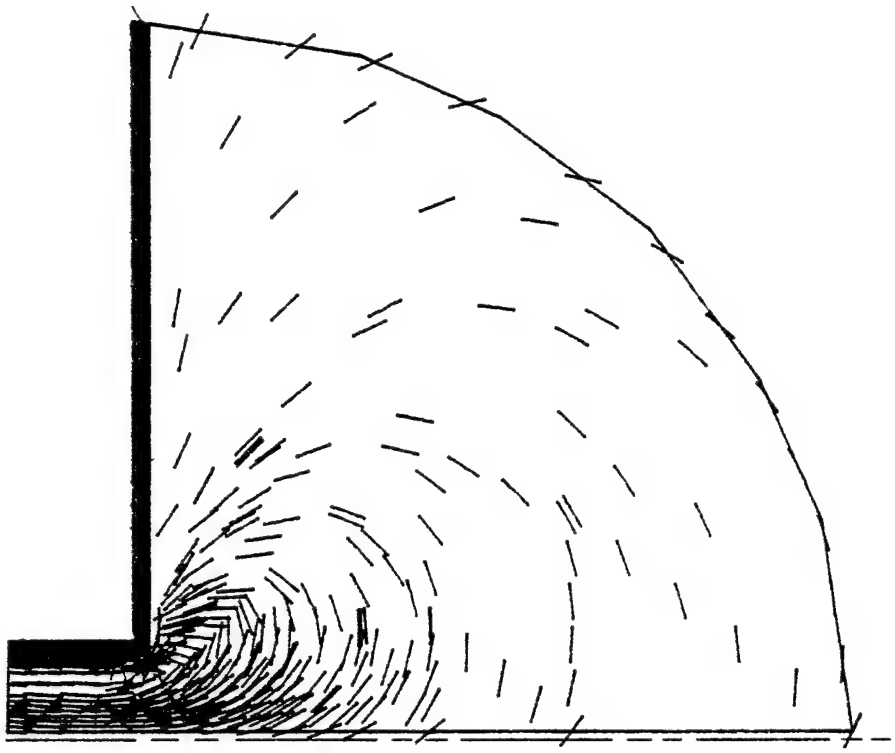

*initial orientation aligned with flow direction

Figure 6.8 Fiber orientation in the expansion flow problem

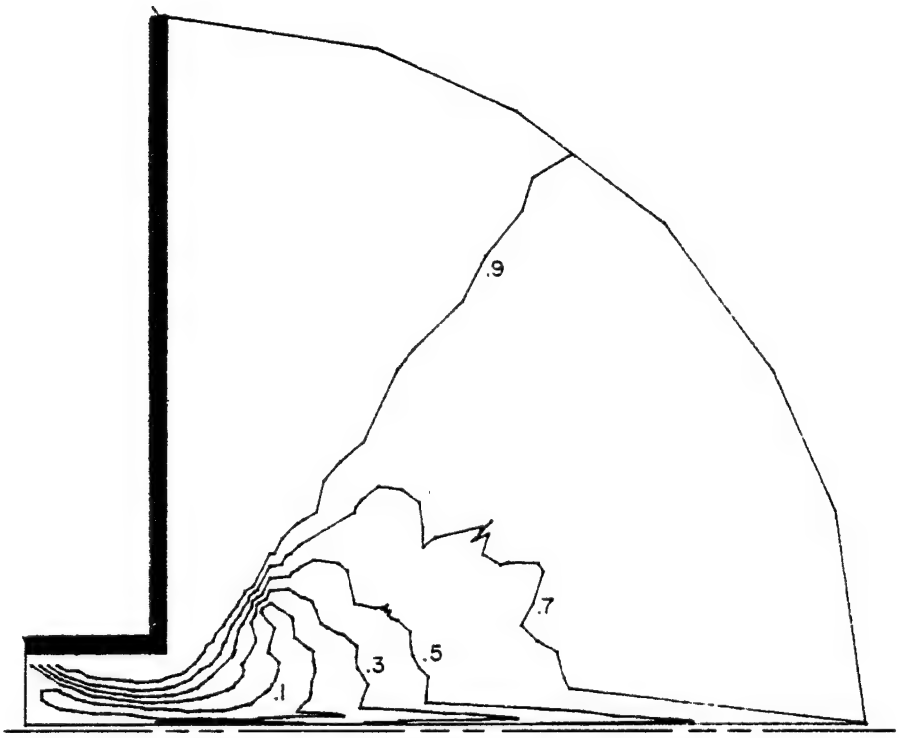

Figure 6.9 Orientation parameter in the expansion flow problem

corresponds to aligned fibers parallel to the streamlines. Transverse orientations to the fluid steamlines at steady state result from regions of the flow dominated by elongational components.

7. EXTENSIONS TO THE THEORY

Throughout this documentation, mention has been made of several shortcomings to the fiber orientation theory as presented herein. While it has been shown to provide excellent results within the assumptions set forth, there are a few extensions to the existing ideas that need to be brought to light.

The extension of the model to include axisymmetric flows is straightforward in theory. It should be realized that both the finite-element method and the orientation equations (eqs.(4.1-2)) need to be generalized to handle axisymmetric flows. Neither is suspected of causing any conceptual difficulties since only a coordinate transformation is encountered. For example, eq.(4.3) may be written in terms of axisymmetric components by the usual rules of tensor transformations. Hence, the present analysis could be extended to include axisymmetric flows directly.

Extending the analysis of the model to a full three dimensions again provides little difficulty conceptually. The limitation of this extension usually becomes apparent

in the solution to the finite element problem. What usually happens, using three-dimensional elements, results in the rapid exhaustion of computer core storage. As a guideline, the consideration of a three-dimensional domain increases the number of unknowns by a factor of

$$2(94/33)\cdot n_3 \simeq O(6n_3)$$

where n_3 is the number of elements through the thickness of the domain. The ratio of (94/33) is the increase in the number of degrees of freedom in going from the 6 node triangular element to the 10 node tetrahedral element. Here, one considers the velocities, stresses and pressure as primitive variables. Indeed, there are methods of solution which reduce the overall core storage requirements (see section A2.6) but considerable effort would be expended to develop the necessary software. In this spirit, the extension to three-dimensional domains seems somewhat less tractable than before.

It has been suggested that many of the practical molding operations poorly approximate steady state flow kinematics, especially in the proximity of the flow front. Tadmor [36] suggests that the flow front actually plays a significant role in the orientation of fibers. For these reasons, it would be beneficial to include the transient

terms of the equations of motion in the solution of the flow problem. This additional modification would be especially helpful if it were developed using a Lagrangian method of solution. Here, the grid is allowed to deform continuously to monitor the actual behavior of the advancing free surface. Thus the mold filling process could be closely modeled by marching out the solution in the time domain with continuous mesh updating and rearrangement. At this point, it is not known how well Jeffery's theory of particle orientations would approximate the true behavior of the solution, since the inclusion of the transient terms has violated Jeffery's assumption of steady flow. This ramification needs to be determined.

The important consideration of including the effect of fiber orientation on the structure of the velocity field has been discussed in section 5.1. This iterative procedure seems highly feasible once the orientation-dependent viscosity is known. Recent work on obtaining such viscosity functions [24] has shown that this effect may be important for certain flow situations. Clearly, this is an avenue for further research.

If the constitutive equation describing the flow includes the possibility for the fluid to possess some elasticity, a viscoelastic model must be employed to

determine behavior of the flow. The numerical solution of the viscoelastic fluids problem can be accommodated by existing computer codes if the elasticity effects within the fluid are not too great. In addition, one other modification needs to be made. The Jeffery equations (eqs.(4.1-2)) that describe particle orientations in viscoelastic fluids must be re-evaluated in light of the non-Newtonian fluid behavior. These modified equations may be referenced in Van Oene [39], for example, and the incorporation of this extension seems straightforward, at least in principle.

Concluding this discussion, then, a final comment is in order. Several possible extensions to the orientation theory have been suggested, whose effects on the fiber orientations are unknown. It is possible that the inclusion of the proposed extensions will not significantly alter the theoretical results in light of the excellent findings predicted by the current theory. The empirical and analytical verification to the present theory yields a high level of confidence in predicting the fiber orientations in real flows, and a more sophisticated model may not deliver additional insight.

8. CONCLUSIONS

A method has been developed to determine the fiber orientations in a dilute suspension undergoing arbitrary, two-dimensional deformations. For flow situations where shearing deformation dominates, the dynamic orientation of the fibers has been predicted. The equilibrium orientation for shearing flows has been shown to be parallel to fluid streamlines. For cases of wall-bounded channel flow, this orientation mechanism is responsible for the occurrence of a boundary layer phenomenon that produces regions of highly aligned fibers along the channel walls. Perturbations from the Newtonian constitutive assumption are possible by considering the analysis to be quasi-Newtonian. Here, the effect of increasing pseudoplasticity reduces the thickness of the boundary layer.

For certain problems where analytical expressions do not exist for the field variables, the finite-element method is employed. Upon solution to the fluid mechanics, the orientation equation may be numerically integrated along a path line to yield the resulting rotations. This

methodology has been incorporated into a computer routine that allows one to calculate the resulting fiber orientations for rather complex geometry flows.

Employing the above methodology to the problems of Newtonian flow in the vicinity of an infinite expansion, the resulting equilibrium orientations have been shown to be transverse to the fluid path lines. These general trends in fiber orientations are also expressed intuitively by considering the stresses acting on a single fiber immersed in a flow of given kinematics.

LITERATURE CITED

1. Batchelor, G. K., "An Introduction to Fluid Dynamics," Cambridge University Press, 1967.

2. Bell, J. P., *J. Composite Materials*, 3, 244, (1969).

3. Bird, R., Armstrong, R., and Hassager, O., "Dynamics of Polymeric Liquids," John Wiley & Sons, 1977.

4. Bird, R., Stewart, W., and Lightfoot, E. N., "Transport Phenomena," John Wiley & Sons, 1960.

5. Brenner, H., *Chem. Eng. Sci.*, 19, 599, (1964).

6. Brenner, H., *Chem. Eng. Sci.*, 19, 631, (1964).

7. Brenner, H., *Chem. Eng. Sci.*, 19, 703, (1964).

8. Bretherton, F. B., *J. Fluid Mech.*, 14, 284, (1962).

9. Broyer, E., et al., *Trans. Soc. Rheol.*, 19, 423, (1975).

10. Chaffey, C. E., et al., *Can. J. Physics*, 43, 1269, (1965).

11. Chan, Y., et al., *Polymer Eng. Sci.*, 18, 268, (1978).

12. Cole, E. A., et al., *Polymer Eng. Sci.*, 19, 12, (1979).

13. Darlington, M. W., et al., *J. Mat. Sci.*, 11, 877, (1976).

14. Finlayson, B. A., "The Method of Weighted Residuals," Academic Press, 1972.

15. Fung, Y. C., "Continuum Mechanics," Prentice-Hall, 1969.

16. Gallagher, R. H., "Finite Elements in Fluids," Volume 1, John Wiley & Sons, 1975.

17. Gandhi, K. D., and Burns, R., *Trans. Soc. Rheol.*, 20, 489, (1976).

18. Goldsmith, H., and Mason, S. G., in "Rheology: Theory and Applications," edited by Erich, Academic Press, 1967.

19. Geottler, L. A., *25th Anniversary Meeting, Reinforced Plastics/Composites Div., SPI*, February 1970.

20. Geottler, L. A., *Modern Plastics*, 144, April 1979.

21. Howard, I. C. and Brierly, P., *Inter. J. Eng. Sci.*, 14, 1151, (1976).

22. Huebner, K. L., "The Finite Element Method for Engineers," John Wiley & Sons, 1975.

23. Irons, B., *Int. J. Num. Meth. Eng.*, 2, 5, (1970).

24. Jarzebski, G., (to be published).

25. Jeffery, G. B., *Proc. Roy. Soc.*, A102, 161, (1922).

26. Kamal, M. R., *Polymer Eng. Sci.*, 17, 96, (1977).

27. Kamal, M. R., *A.I.Ch.E. Journal*, 22, 661, (1976).

28. Kuo, Y., *38th S.P.E. Conference*, April 1978.

29. Marker, L. and Ford, B., *32nd S.P.I. Conference*, (1977).

30. Maschmeyer, R. O., and Hill, C. T., *Montsanto/Wash. Univ. Assoc. Tech. Rep.*, May 1973.

31. Metzner, A. B., "Laminar Flow Theory, with Applications to Non-Linear Fluids," (unpublished).

32. Mill, C. C., "Rheology of Disperse Systems," Pergamon Press, 1959.

33. Owen, M. J., et al., *33rd S.P.I. Conference*, (1978).

34. Owen, M. J. and Whybrew, K., *Plastics and Rubber*, 1, 231, (1976).

35. Schlichting, H., "Boundary Layer Theory," McGraw Hill, 1968.

36. Tadmor, Z., *J. Appl. Pol. Sci.*, 18, 1753, (1974).

37. Takano, M., *Monsanto/Wash. Univ. Assoc. Tech. Rep.*, February 1974.

38. Tong, P. and Fung, Y. C., *J. Appl. Mech.*, 38, 721, (1971).

39. Van Oene, H., *Polymer Blends*, 1, 295, (1978).

40. Wetherhold, R. C., et al., *SAE Technical Paper*, 800813, (1980).

41. Woebcken, W., *Modern Plastics*, 40, 146, (1962).

42. Zienkiewicz, O. C., "The Finite Element Method," (3rd edition), McGraw Hill, 1977.

APPENDIX 1

FLUID MECHANICS

In this chapter the basic conservation concepts that provide a foundation to the fluid mechanics problem are examined. The equations that are discussed are generic in nature, since they apply to all material systems. The question of the behavior of various fluids falls under the category of constitutive relationships to be discussed in section A1.2. It is the coupling of both conservation equations and constitutive approximations that generate the method of solution to practical engineering problems.

A Cartesian reference frame has been adopted to develop the governing equations. For conciseness, indicial or Einsteinian notation will be introduced throughout this discussion, with the usual assumption that repeated indices are summed over the range 1 - 3, unless otherwise noted. A more elegant derivation utilizes general tensorial mathematics to develop a set of governing equations insensitive to any particular coordinate system. The application to a useful reference frame is then only an exercise in manipulation to convert tensorial quantities to physical quantities.

This line of approach tends to be somewhat abstract and physical insight is often overshadowed.

Often, in an effort to grasp new ideas, it is instructive to relate them with a more familiar area. Recall, from linear elasticity, that the general formulation of a problem requires 15 independent equations to completely specify the 15 unknowns. The unknowns are 6 stress components, 6 strain components, and 3 displacement field components; and the equations relating these unknowns are 3 equilibrium equations, 6 constitutive equations, and 6 compatibility conditions. Thus, neglecting the details of the boundary conditions, this set of 15 equations and 15 unknowns forms the basis of a well-posed problem for linear, isothermal elasticity.

Alternatively, one shall see that in the fluid mechanics formulation, that the total number of unknowns is 10: 6 stress components, 3 velocity components, and the density. In order for this problem to be well-posed it is essential that 10 independent equations exist. Conservation of mass provides one equation, while the conservation of linear momentum adds three more independent relations. So, it is apparent that to solve fluid mechanics problems, one must introduce six additional relationships. Some assumptions may result from physical insight into the problem that allows an unknown to be set equal to

zero. Constitutive approximations introducing relationships among stresses and strain rates also allow for additional independent equations. As previously noted, these will be investigated in section A1.2.

A1.1 General Concepts

A1.1.1 Conservation of Mass

As for any continuum, a volume of fluid must satisfy the basic law of conservation of mass, which simply states that all mass within a given control volume must be accounted for at all times. Added to this is the assumption of no atomic disintegration taking place within the specified control volume. Consider the control volume (c.v.) shown below.

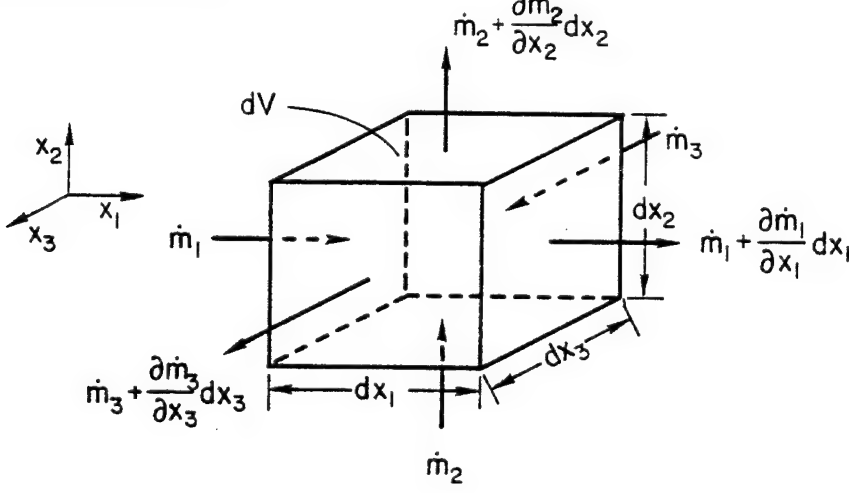

Figure A1.1 Control volume for conservation of mass

Applying the conservation of mass principle, one can write in a statemental form

$$\begin{matrix}\text{rate of mass} \\ \text{into c.v.}\end{matrix} - \begin{matrix}\text{rate of mass} \\ \text{out of c.v.}\end{matrix} = \begin{matrix}\text{rate of mass} \\ \text{accumulation} \\ \text{within c.v.}\end{matrix} \qquad \text{(A1.1)}$$

A suitable expression for the rate of mass ($\dot{m}$) will be given in general by the product of the density and the flow rate, as given by eq.(A1.2),

$$\dot{m} = \rho v \, dA \qquad \text{(A1.2)}$$

where ρ is defined to be the fluid density and (vdA) is the corresponding flow rate through a given face of the control volume. Utilizing the left-hand side of eq.(A1.1) in the x_1 direction yields

$$\dot{m}_1 - (\dot{m}_1 + \frac{\partial \dot{m}_1}{\partial x_1} dx_1) \ , \qquad \text{(A1.3)}$$

and per eq.(A1.2)

$$- \frac{\partial}{\partial x_1} (\rho v_1 dx_2 dx_3) dx_1 = - \frac{\partial}{\partial x_1} (\rho v_1) dV \qquad \text{(A1.4)}$$

If one uses the same procedure for the remaining coordinate directions, it is apparent eq.(A1.1) becomes

$$\left[- \frac{\partial}{\partial x_1} (\rho v_1) - \frac{\partial}{\partial x_2} (\rho v_2) - \frac{\partial}{\partial x_3} (\rho v_3) \right] dV = (\frac{\partial \rho}{\partial t}) dV \qquad \text{(A1.5)}$$

and since the control volume has been chosen arbitrarily

eq.(A1.5) can be simplified to

$$\frac{\partial \rho}{\partial t} + \frac{\partial}{\partial x_i} (\rho v_i) = 0 \qquad \text{(A1.6)}$$

At once, one can see the compactness of eq.(A1.6) in its indicial form. Recall from the previous conventions that the second term of eq.(A1.6) implies three individual terms (the index i is summed from 1 - 3). Eq.(A1.6) is the most general expression for the conservation of mass. Some textbooks also refer to this equation as the continuity equation in that it assures compatibility within the flow domain. Either expression is correct and both shall be utilized throughout this discussion.

Looking at eq.(A1.6), it may be possible to make some simplifying assumptions. If the analysis is one of steady state, this implies that the time dependent term disappears from eq.(A1.6) and one is left with

$$\frac{\partial}{\partial x_i} (\rho v_i) = 0 \quad . \qquad \text{(A1.7)}$$

Next, if it is assumed that the density variation with respect to coordinate positions is negligible, then eq. (A1.7) reduces to

$$\frac{\partial v_i}{\partial x_i} = 0 \quad . \qquad \text{(A1.8)}$$

The last assumption was one of incompressibility, a behavior to which many engineering fluids closely approximate. Again one should be cautioned that eq.(A1.8) applies only to Cartesian coordinate systems, but transformations to other reference frames are found in the literature.

A1.1.2 Conservation of Linear Momentum

If one applies Newton's second law (eq.(A1.9) in inertial coordinates to the same control volume as before, shown for convenience in Figure A1.2, he will arrive at the expression for the conservation of linear momentum.

$$F_i = \frac{\partial}{\partial t}(mv_i) \simeq m\frac{dv_i}{dt} = ma_i = \rho a_i dV \qquad \text{(A1.9)}$$

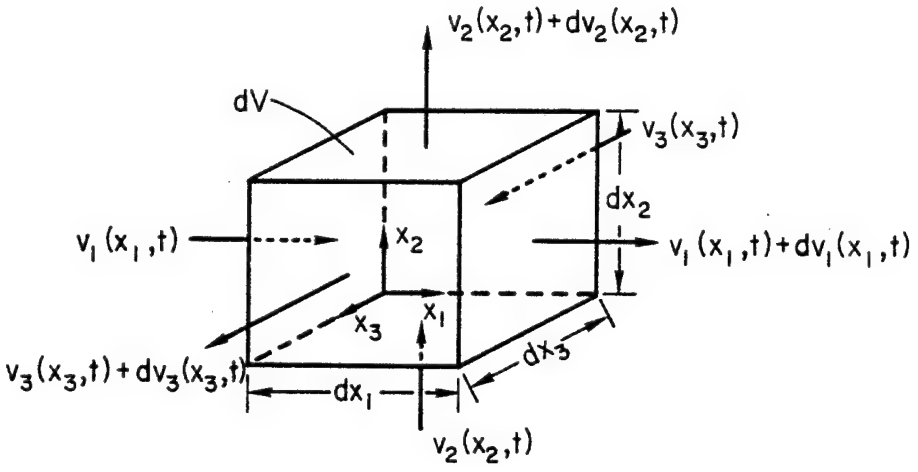

Figure A1.2 Control volume for conservation of linear momentum

The first question to be answered concerns the choice of coordinate systems. It was convenient in section A1.1.1 to choose an inertial frame of reference to discuss the conservation of mass condition. Now it will be necessary to speak of a coordinate system imbedded within the control volume and moving with the local velocity of the fluid. Why does one seek a desired change of reference frame? It is simply for convenience in describing the local accelerations and one shall see that this approach leads to two distinct acceleration terms.

Since one has elected to utilize a material coordinate system, the velocities are functions of both space coordinates and time. Implementing the use of indicial notation, the resultant velocity of the control volume becomes

$$(v_i(x_i,t) + dv_i(x_i,t)) - (v_i(x_i,t)) = dv_i(x_i,t) \tag{A1.10}$$

and per chain rule

$$dv_i(x_i,t) = \frac{\partial v_i}{\partial x_j} dx_j + \frac{\partial v_i}{\partial t} dt \quad . \tag{A1.11}$$

Substituting eq.(A1.11) into eq.(A1.9), which is valid for inertial systems, yields

$$F_i = \rho \left(\frac{\partial v_i}{\partial x_j} \frac{dx_j}{dt} + \frac{\partial v_i}{\partial t} \right) dV = \rho \left(\frac{\partial v_i}{\partial t} + v_j \frac{\partial v_i}{\partial x_j} \right) dV \, . \tag{A1.12}$$

The first term on the right-hand side of eq.(A1.12) is the rate of change in velocity with respect to the material coordinate system, whereas the second term accounts for any accelerations of the material coordinate system with respect to an inertial reference frame. The latter effect is sometimes termed the transport or convective part of the acceleration and together with the local rate of change in velocity represents the total or material derivative of velocity with respect to some inertial reference frame.

To clarify the above discussion, an example is in order. Consider the case of liquid in a long rotating cylinder, where the external wall spins with constant angular velocity. The most natural reference frame to describe the fluid kinematics is one of cylindrical coordinates (r,θ,z), shown in Figure A1.3.

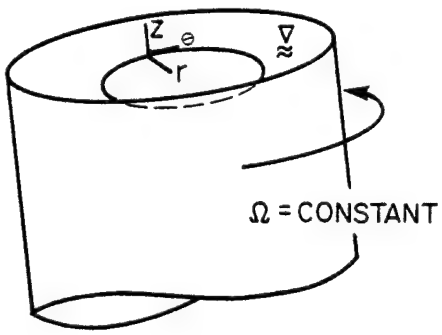

flow kinematics

$v_r = 0$

$v_\theta = f(r)$

$v_z = 0$

Figure A1.3 Fluid in a long, rotating cylinder

Since the flow is steady by assumption, the local acceleration term in eq.(A1.12) is zero. The convective terms, however, are nonzero in that the material coordinate system is rotating with respect to some fixed reference frame.

Next, one may apply a force balance to the control volume of Figure A1.4 in order to compute the forces acting on a fluid element. From the figure it is clear that both body forces and surface tractions act upon the fluid element. The body force may consist of three components, each of which act along the respective coordinate directions. However, the convention pertaining to surface

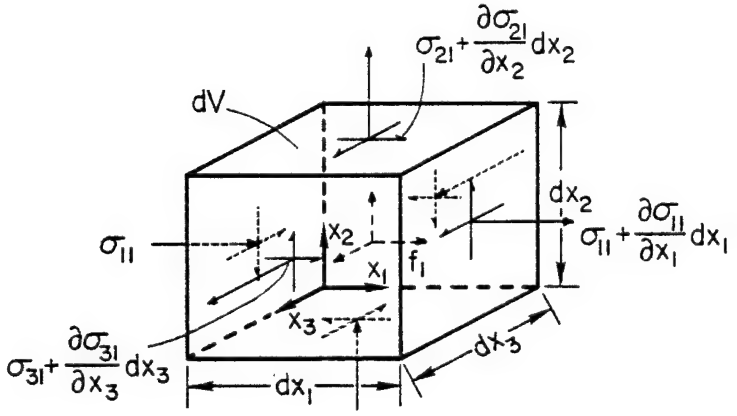

Figure A1.4 Control volume for force balance on a fluid element in the x_1-direction

tractions needs to be elaborated upon. Surface tractions are defined in terms of stresses, whose components transform like those of a second rank tensor. Apparently two subscripts are needed to describe a given component of stress. We adopt the notation such that the first subscript defines the surface upon which the stress acts (the surface is given by the unit outward normal vector) while the second subscript dictates the direction of the stress component. A quick glance at Figure A1.4 will illustrate the use of this convention.

Upon summing the forces in the x_1 direction, one has

$$F_1 = (\sigma_{11} + \frac{\partial \sigma_{11}}{\partial x_1} dx_1) dx_2 dx_3 - \sigma_{11} dx_2 dx_3$$

$$+ (\sigma_{21} + \frac{\partial \sigma_{21}}{\partial x_2} dx_2) dx_1 dx_3 - \sigma_{21} dx_1 dx_3$$

$$+ (\sigma_{31} + \frac{\partial \sigma_{31}}{\partial x_3} dx_3) dx_1 dx_2 - \sigma_{31} dx_1 dx_2$$

$$+ \rho f_1 dV$$

$$F_1 = \left(\frac{\partial \sigma_{11}}{\partial x_1} + \frac{\partial \sigma_{21}}{\partial x_2} + \frac{\partial \sigma_{31}}{\partial x_3} + \rho f_1 \right) dV \qquad \text{(A1.13)}$$

Force balances in the x_2 and x_3 coordinate directions yield similar expressions and using indicial notation

may be combined to read

$$\left(\frac{\partial \sigma_{ji}}{\partial x_j} + \rho f_i\right) dV = F_i \quad . \tag{A1.14}$$

Substituting eq.(A1.14) into eq.(A1.12)

$$\rho\left(\frac{\partial v_i}{\partial t} + v_j \frac{\partial v_i}{\partial x_j}\right) = \frac{\partial \sigma_{ji}}{\partial x_j} + \rho f_i \tag{A1.15}$$

one arrives at the final expression for the principle of conservation of linear momentum.

A1.1.3 The Stress Tensor

One of the most difficult points to understand when first learning fluid mechanics is the relation between normal stresses and pressure. The ideas to be introduced here are compatible with those learned from an undergraduate fluid mechanics course, say, and some comparison may be helpful.

Thus far, the stresses that have been referred to were total stresses (σ_{ij}). The components of the total stress tensor represent a fully populated second rank tensor, shown below. Diagonal components represent

$$\sigma_{ij} = \begin{Bmatrix} \sigma_{11} & \sigma_{12} & \sigma_{13} \\ \sigma_{21} & \sigma_{22} & \sigma_{23} \\ \sigma_{31} & \sigma_{32} & \sigma_{33} \end{Bmatrix} \qquad i,j=1-3$$

stresses which tend to dilate the fluid, while off-diagonal stresses correspond to shearing stresses. Recall now that the term "pressure" refers to only dilatational behavior and must therefore be related uniquely to the normal stresses (σ_{11} , σ_{22} , σ_{33}). Hence, it seems reasonable to define the pressure as the average value of the normal stresses given by eq.(A1.16)

$$p = - \tfrac{1}{3}(\sigma_{11} + \sigma_{22} + \sigma_{33}) \qquad \text{(A1.16a)}$$

$$= - \tfrac{1}{3}\sigma_{ii} \ . \qquad \text{(A1.16b)}$$

The negative sign indicates that pressure is inherently compressive in nature. Note that this definition is compatible with the notion of hydrostatic pressure if the fluid is at rest. In this case, all three normal stresses are identical and their average defines the hydrostatic pressure.

Next, one may introduce the important concept of deviatoric stress. As a consequence of eq.(A1.16), the total stress tensor may be represented by two terms:

$$\sigma_{ij} = -p\delta_{ij} + P_{ij} \qquad \text{(A1.17)}$$

$$\sigma_{ij} = \begin{bmatrix} -p+P_{11} & P_{12} & P_{13} \\ P_{21} & -p+P_{22} & P_{23} \\ P_{31} & P_{32} & -p+P_{33} \end{bmatrix} \qquad \text{(A1.18)}$$

in which the δ_{ij} is defined to be the Kronecker delta. It takes on the value of unity for i=j and is zero otherwise. The P_{ij} tensor represents that part of the stress tensor as a result of fluid motion or deformation. It is commonly called the deviatoric stress tensor. An alert reader usually inquires as to the nature of the diagonal terms of the P_{ij} tensor. Quite simply they are the normal stresses that arise from deforming the fluid. They are not related to the pressure, since the pressure has been extracted as a consequence of eq.(A1.17). The confusion usually stems from the fact that a first course on the subject only emphasizes the shearing behavior of fluids, say for instance, water flowing in a tube. Little reference was made of the fact that some fluid systems exhibit anomalous normal stresses. As an example, egg whites hanging from their shell (Figure A1.5) produce substantial normal stresses (P_{33}) within the bulk of the fluid. These normal stresses are seen to be at least large enough to support the weight of the fluid in tension. Other such fluids exhibiting this exotic behavior include body mucuses and a slew of industrial polymers. Even the familiar concept of surface tension is really another illustration of normal stresses, that can develop under many circumstances.

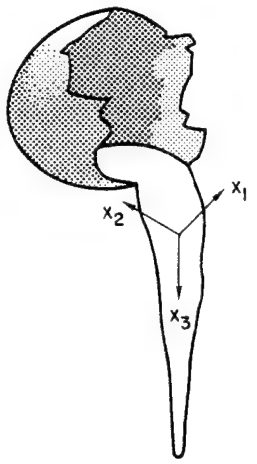

Figure A1.5 An illustration of the normal stresses found in egg whites

Before leaving this discussion of normal stresses, one last comment is in order. When one experimentally measures "pressure" in the laboratory, he is actually measuring a total stress component (for definiteness σ_{11}). From eq.(A1.18) it is apparent that the total stress is really the sum of the isotropic pressure and the deviatoric stress component. It is only through an appropriate rheological constitutive equation that one usually claims P_{11} to be zero. Hence, inadvertantly one is measuring the quantity known as pressure, but the reader is cautioned that occasionally normal deviatoric stresses result from the fluid motion and one no longer measures just the "pressure".

A1.1.4 Conservation of Angular Momentum

Consider, again, the control volume of Figure A1.4. In addition to the linear motion that these stresses produce, there also exists angular motion (rotation) that must be conserved. The conservation of angular momentum is the analogue of eq.(A1.9), with forces being replaced by torques and angular velocities substituted for linear ones. So,

$$T_i = \frac{\partial}{\partial t} (I_{ij}\Omega_j) \qquad \text{(A1.19)}$$

where T_i = torque vector

I_{ij} = moment of inertia tensor

Ω_j = angular velocity vector.

Figure A1.6 shows the same control volume as Figure A1.4 with some of the stresses deleted for clarity. Also

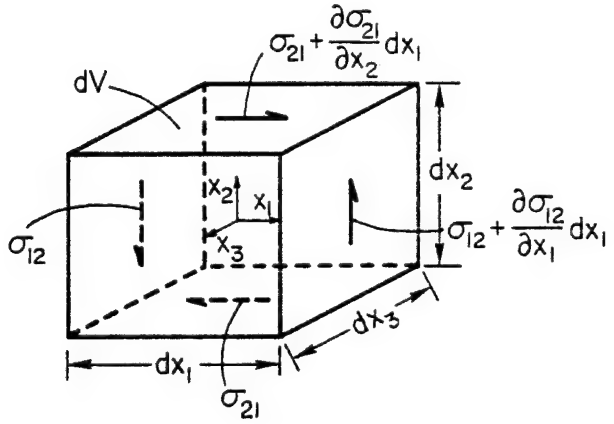

Figure A1.6 Control volume for moment balance about the x_3 axis

note that the coordinate system has been placed at the center of the control volume and will be considered as inertial. In terms of inertial coordinates, then, consider a rotation about the x_3 axis for definiteness. Eq.(A1.19) becomes specifically

$$T_3 = \frac{\partial}{\partial t} (I_{33}\Omega_3) \quad .$$

Substitution for the moment of inertia and noting that it is independent of time yields

$$T_3 = \frac{\partial}{\partial t} (mr_{g_3}^2\Omega_3) = \rho dV r_{g_3}^2 \frac{\partial \Omega_3}{\partial t} \tag{A1.20}$$

where r_{g_3} is the radius of gyration about the x_3 axis. The torque that the stresses produce may be summed as

$$T_3 = \sigma_{12}dx_2dx_3\frac{dx_1}{2} + (\sigma_{12} + \frac{\partial \sigma_{12}}{\partial x_1} dx_1)dx_2dx_3\frac{dx_1}{2}$$
$$- \sigma_{21}dx_1dx_3\frac{dx_2}{2} - (\sigma_{21} + \frac{\partial \sigma_{21}}{\partial x_2} dx_2)dx_1dx_3\frac{dx_2}{2} \quad . \tag{A1.21}$$

Note that the normal stresses do not contribute to the moment as a result of a convenient placing of the coordinate system at the centroid of the control volume. If one retains only the first-order terms of eq.(A1.21) and substitutes into eq.(A1.20), the resulting expression for conservation of angular momentum in the x_3 direction is

$$(\sigma_{12} - \sigma_{21}) = \rho r_{g_3}^2 \frac{\partial \Omega_3}{\partial t} \quad . \tag{A1.22}$$

Since eq.(A1.22) must hold in the limit of the continuum, the size of the control volume of Figure A1.6 is allowed to approach zero. Note that the right-hand side of eq. (A1.22) tends to zero since $r_{g_3} \to 0$ as c.v. $\to 0$. Thus, it must be that $\sigma_{12} = \sigma_{21}$ for the equality to hold.

The conclusion to be drawn from this exercise is that the order of subscripts pertaining to the stresses does not matter (i.e. $\sigma_{ij} = \sigma_{ji}$). Therefore, the stress tensor is seen to be symmetric in nature and the total number of unknown independent stress components reduces from nine to six. This point was mentioned previously; now the justification is established for such a claim.

A1.1.5 Material Motion

It is natural when referring to fluid flow to express the motion of the continuum in terms of the velocity field. Consider a fluid continuum undergoing an arbitrary motion, shown in Figure A1.7.

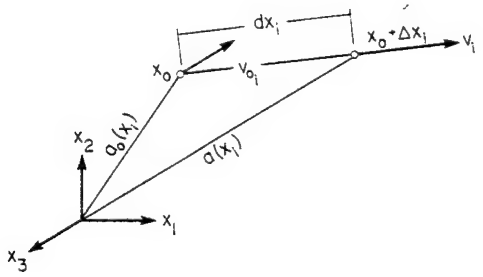

Figure A1.7 Material motion for a fluid continuum

An inertial Cartesian reference frame is established to assist in describing the particle motions. Unlike the methodology in linear elasticity, it is undesirable to use displacement gradients in order to describe material motion. The primary reason is that the displacements are usually far greater than those encountered in solid mechanics.

The difference in local velocity vectors for two neighboring points x_{o_i} and $x_{o_i}+\Delta x_i$ is given by eq.(A1.23)

$$v_i - v_{o_i} = dv_i = \frac{\partial v_i}{\partial x_j} dx_j \quad . \tag{A1.23}$$

Again, since the coordinate system is fixed, the velocities are function only of position. Clearly, differences in velocities between points x_{o_i} and $x_{o_i}+\Delta x_i$ must introduce a deformation to the fluid continuum. Thus, one arrives at the conclusion that fluid deformation is related to the velocity gradients. As is customary, the velocity gradient tensor may be written as two distinct parts with individual characteristics.

$$\frac{\partial v_i}{\partial x_j} = \tfrac{1}{2}\left(\frac{\partial v_i}{\partial x_j} + \frac{\partial v_j}{\partial x_i}\right) + \tfrac{1}{2}\left(\frac{\partial v_i}{\partial x_j} - \frac{\partial v_j}{\partial x_i}\right) \tag{A1.24}$$

The first term on the right-hand side of eq.(A1.24) is responsible for actual deformation of a fluid element.

Hence, it will be referred to as the deformation rate tensor d_{ij}. Upon interchanging i and j, it is obvious that this "strain rate" tensor is symmetric.

$$d_{ij} = \tfrac{1}{2}\left(\frac{\partial v_i}{\partial x_j} + \frac{\partial v_j}{\partial x_i}\right) \tag{A1.25a}$$

$$= \begin{pmatrix} d_{11} & d_{12} & d_{13} \\ d_{12} & d_{22} & d_{23} \\ d_{13} & d_{23} & d_{33} \end{pmatrix} \tag{A1.25b}$$

The second term of eq.(A1.24) does not participate in fluid deformation and acts only to rigidly rotate a fluid element. The effect of this term defines the fluid vorticity and can be shown to be antisymmetric.

$$\omega_{ij} = \tfrac{1}{2}\left(\frac{\partial v_i}{\partial x_j} - \frac{\partial v_j}{\partial x_i}\right) \tag{A1.26a}$$

$$= \begin{pmatrix} 0 & \omega_{12} & -\omega_{13} \\ -\omega_{12} & 0 & \omega_{23} \\ \omega_{13} & -\omega_{23} & 0 \end{pmatrix} \tag{A1.26b}$$

The antisymmetry of the vorticity tensor insures that only three independent components exist. It is sometimes helpful to define a vorticity vector such that:

$$Z_k = e_{ijk}\omega_{ij}$$

$$e_{ijk} = \begin{cases} 1 & i \neq j \neq k \text{ ; } i,j,k \text{ form a right-handed system. . . . . .cyclic sequence} \\ -1 & i \neq j \neq k \text{ ; } i,j,k \text{ form a left-handed system. . . .anticyclic sequence} \\ 0 & \text{everywhere else. acyclic sequence} \end{cases}$$

A1.1.6 The Stream Function

Consider the two-dimensional flow field defined by Figure A1.8. The region of interest for this discussion lies between two streamlines. Since by definition, the local velocity vectors are tangential to a streamline, no fluid particles may cross that imaginary boundary.

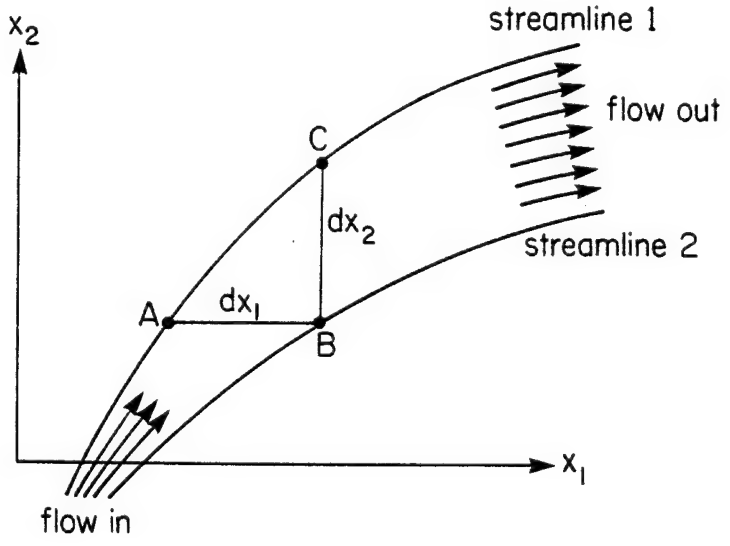

Figure A1.8 Flow between two streamlines

Concentrating on the control volume ABC, one may apply the conservation of mass principle for an incompressible fluid.

$$\begin{matrix}\text{mass efflux} \\ \text{across AB}\end{matrix} + \begin{matrix}\text{mass efflux} \\ \text{across BC}\end{matrix} = 0$$

$$(\rho v_2 dx_1) + (\rho v_1 dx_2) = 0 \qquad \text{(A1.27)}$$

The stream function is defined according to eq.(A1.28).

$$d\psi \equiv -v_2 dx_1 = v_1 dx_2 \qquad \text{(A1.28)}$$

Qualitatively then, the stream function can be viewed as a measure of the flow between two given streamlines in the velocity field.

Often it is advantageous to define the velocities in terms of a stream function. It may be possible in certain problems to substitute the equivalent of the velocity components in terms of the stream function.

$$v_1 = \frac{\partial \psi}{\partial x_2} \quad , \quad v_2 = \frac{-\partial \psi}{\partial x_1} \qquad \text{(A1.29)}$$

This maneuver reduces the number of dependent variables to be solved for at the expense of raising the order of the differential equation. Despite the drawbacks, many problems have been solved using this technique.

A1.2 Constitutive Relationships

The general conservation laws that were developed in the previous section made no mention of any particular material system. Clearly, when one attempts to solve real engineering problems in fluid mechanics, the behavior of the fluid is an important consideration. One usually wishes to relate the response of the fluid to the applied stresses. The expressions that link the stresses and the fluid motion are called constitutive relationships. It should be pointed out that these relationships are not derivable from basic conservation principles, but are merely approximations at best. Many times the expressions are such that they seem to fit the data over a wide range of deformation rates. Other approximations result from experience or intuition that have worked well over the years.

A1.2.1 The Inviscid Fluid

The simplest constitutive relationship that could be proposed is one in which the stress tensor is isotropic, namely

$$\sigma_{ij} = -p\delta_{ij} \tag{A1.30a}$$

$$= \begin{bmatrix} -p & 0 & 0 \\ 0 & -p & 0 \\ 0 & 0 & -p \end{bmatrix} \tag{A1.30b}$$

From eq.(A1.30) it is apparent that the stress tensor is independent of the deformation rate of the fluid. Also, notice that the viscous effects do not enter into the rheological characterization of the fluid, as implied in the definition of inviscid.

If the fluid is gaseous and compressible then the pressure may be related to the temperature and the density via the ideal gas law

$$p/\rho = RT \tag{A1.31}$$

where R is the gas constant.

A much broader class of fluids may be investigated if one assumes that the fluid approximates the incompressibility criterion. As usual, one begins with the basic conservation of mass principle. In general vector notation, recall eq.(A1.7) given by

$$\nabla\cdot(\rho q) = 0 \tag{A1.32}$$

where ∇ is defined to be the del operator and q is the velocity vector. Incompressibility states that

$$\rho \equiv \text{constant}$$

and so eq.(A1.32) becomes

$$\nabla\cdot q = 0 \tag{A1.33}$$

This last equation states that the flow field is solenoidal and it is seen that the divergence of the velocity vector is zero everywhere.

Now if the vorticity (defined by eq.(A1.26)) vanishes identically throughout the flow, it will be said that the flow field is irrotational. In fact, if the vorticity is initially zero for our inviscid fluid, even then the velocity field is irrotational. To see this, suppose that initially (either in time or space) the flow possesses no rigid body rotation. The only way that a fluid element could assume angular motion is through the action of surface tractions in the form of shear stresses along its edges. Clearly the assumption of inviscid flow prohibits the development of any such shear stresses. This fact was borne out by the constitutive relationship of eq.(A1.30). Mathematically, for a flow field to be irrotational, the curl of the velocity field must vanish.

$$\nabla \times q = 0 \quad . \tag{A1.34}$$

In addition, eq.(A1.34) assures us that a velocity potential exists such that

$$q = \nabla \Phi \quad . \tag{A1.35}$$

Inserting eq.(A1.35) into eq.(A1.33) yields the well-known Laplace equation which governs potential flow theory.

Notice the simplifications that result from the above substitution. The governing differential equation contains only the unknown scalar function Φ instead of three unknown velocity components,

$$\nabla^2\Phi = 0 \quad . \tag{A1.36}$$

Comparing with eq.(A1.32), one sees that a trade-off exists in that the order of the differential equation has been increased. Fortunately, many solution techniques are available for solving the Laplace equation.

The addition of appropriate boundary conditions establishes the well-posed nature of such problems solved under these assumptions. Potential theory is applicable to flows in which the fluid viscosity is negligible. A convenient non-dimensional parameter defined to be the Reynold's number

$$\text{Re} = \frac{\text{inertial forces}}{\text{viscous forces}} \tag{A1.37}$$

determines the range of applicability of potential theory. Large values of the Reynold's number are indicative of flow conditions dominated by inertial effects and thus the approximation of an inviscid fluid is quite good.

A1.2.2 The Newtonian Fluid

Unlike the inviscid fluid of section A1.2.1, the Newtonian fluid behaves as a viscous fluid. The stress tensor is linearly related to the rate of deformation by a single constant known as the viscosity of the fluid.

$$\sigma_{ij} = -p\delta_{ij} + 2\mu d_{ij} \qquad \text{(A1.38)}$$

When one limits the response of the stress tensor to a linear dependence on the rate of deformation tensor, the claim is made that the parameter μ is not a function of d_{ij}. The viscosity may still depend upon the temperature, however. Quite often the temperature effect upon the viscosity may be an important consideration and not at all negligible.

Returning to eq.(A1.38), one may note that a scale factor of 2 is placed in front of the second term. This is purely for convenience in that it exactly cancels the $\frac{1}{2}$ which is found in the definition of d_{ij} (eq.(A1.26)). When the Newtonian constitutive relationship is substituted into the equations of motion the resulting expressions are known as the Navier-Stokes equations. They are quite important and have received widespread attention over the years. Often they are used as a first approximation to difficult flow problems as a means of obtaining useful insight.

A1.2.3 The Generalized Newtonian Fluid

Here, the viscosity is seen to depend upon the deformation rate tensor as indicated by eq.(A1.39),

$$\sigma_{ij} = -p\delta_{ij} + \eta d_{ij} \tag{A1.39}$$

where η = variable viscosity function.

We anticipate expressing the viscosity function η in terms of the invariants of the deformation rate tensor. It is a logical choice since one expects the constitutive relation of eq.(A1.39) to be unchanged by a coordinate transformation. The three invariants of the tensor $\underset{\sim}{d}$ are shown below.

$$I_{\underset{\sim}{d}} = d_{ii} \tag{A1.40}$$

$$II_{\underset{\sim}{d}} = \tfrac{1}{2}((\mathrm{tr}\,\underset{\sim}{d})^2 - \mathrm{tr}(\underset{\sim}{d})^2) \tag{A1.41}$$

$$III_{\underset{\sim}{d}} = \det(\underset{\sim}{d}) \tag{A1.42}$$

where "tr" is the abbreviation for the trace of a matrix. Simply, it is seen to be the sum of the components along the main diagonal. Since it has been decided that the viscosity should be some function of the above invariants, one proceeds to determine this dependence.

Looking at the first invariant, one easily recognizes this to be the conservation of mass condition. For

Cartesian coordinates and assuming the fluid to be incompressible, this was shown to be identically zero in eq.(A1.8). As a result, it is permissible to ignore any dependence from $I_{\underset{\sim}{d}}$ on the viscosity. It is also customary to ignore the $III_{\underset{\sim}{d}}$ dependence upon the viscosity. In doing so one is neglecting the extensional flow effects upon the rheological approximation. Essentially then, the model will be limited to shearing type flows. This is an acceptable simplification in lieu of the fact that many important problems may still be solved if extensional effects are ignored.

Thus far, it has been shown that the viscosity function for the generalized Newtonian fluid depends on the second invariant of the deformation rate tensor $II_{\underset{\sim}{d}}$.

$$\eta = f(II_{\underset{\sim}{d}}) \tag{A1.43}$$

There have been many models which have specified the exact nature of eq.(A1.43) in terms of the flow conditions. Most of the models are empirical in nature and have been derived as a result of curve fitting schemes with adjustable parameters. The best expressions have a minimum of parameters that must be determined experimentally and also exhibit a wide range of applicability. Perhaps the best known two-parameter model is that of the power law fluid.

The viscosity function for the power law model is given below for laminar shearing flow.

$$\eta = M|\Gamma|^{n-1} \tag{A1.44}$$

The constant M corresponds most naturally to the viscosity for the Newtonian fluid, while Γ represents the shear rate of the fluid. The shear stress is related to an arbitrary power of the deformation rate, hence the nomenclature: power law model. Comparing this expression to eq.(A1.38) it is evident that for n = 1 the equations are identical and the Newtonian constitutive relation is recovered. Figure A1.9 shows the variation of shear stress with deformation rate for both Newtonian and power law fluids.

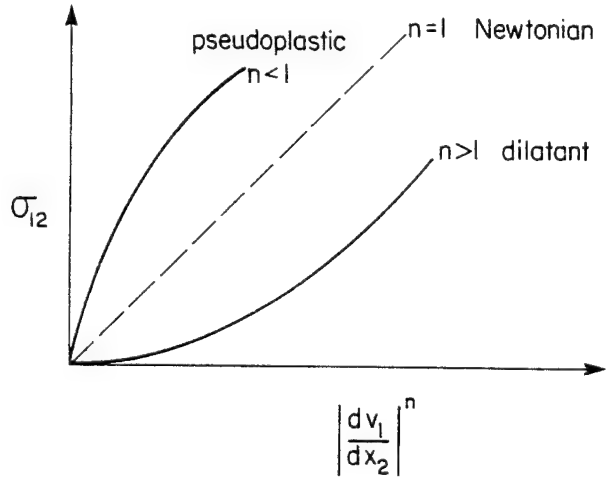

Figure A1.9 Variation of shear stress with deformation rate for a power law fluid

Values of the power law index (n) less than unity correspond to pseudoplastic or shear thinning behavior. Index values greater than one represent dilitant or shear thickening fluids.

An example is given below which illustrates the derivation of the power law model for steady-shearing flow. Consider the two-dimensional Couette type flow shown in Figure A1.10. The kinematics of the flow are quite straightforward and are listed here for convenience.

$$v_1 = f(x_2) \qquad \text{(A1.45a)}$$

$$v_2 = 0 \quad . \qquad \text{(A1.45b)}$$

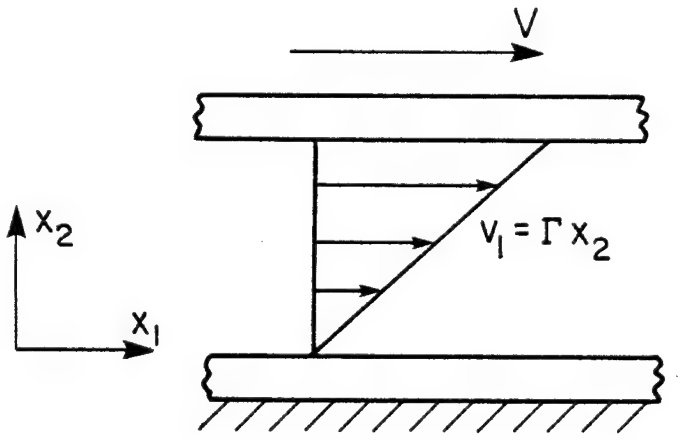

Figure A1.10 Two-dimensional Couette flow

The only deviatoric stress resulting from this type of flow happens to be P_{12}. To justify this claim, recall that from eq.(A1.39)

$$P_{ij} = \eta d_{ij}$$

and that the only nonzero component of the deformation rate tensor for the above kinematics was d_{12}.

$$d_{ij} = \begin{pmatrix} 0 & \frac{1}{2}\Gamma & 0 \\ \frac{1}{2}\Gamma & 0 & 0 \\ 0 & 0 & 0 \end{pmatrix} \tag{A1.46}$$

From eq.(A1.41), it is easy to calculate the second invariant of the deformation rate tensor

$$\begin{aligned} II_{\underset{\sim}{d}} &= d_{11}d_{22} - d_{12}^2 \\ &= -d_{12}^2 = -\tfrac{1}{4}\Gamma^2 \end{aligned}$$

and by solving for the shear rate (Γ), one finds

$$\Gamma = 2\sqrt{-II_{\underset{\sim}{d}}} \tag{A1.47}$$

Substituting eq.(A1.47) into eq.(A1.44), the viscosity function is now found in terms of the second scalar invariant.

$$\eta = M2^{n-1}(-II_{\underset{\sim}{d}})^{\frac{n-1}{2}} \tag{A1.48}$$

Again note that if $n = 1$, $\eta = M =$ constant then the viscosity function reduces to the value of the Newtonian viscosity.

Thus, one may summarize the findings of the above discussion. As written, the power law model is generally applicable to the shearing-type flows, hence stress terms such as P_{11} , P_{22} , etc. do not arise. Secondly, for viscous flows that satisfy the kinematics of eq.(A1.45) the rheological constitutive relationship becomes

$$P_{ij} = M|\Gamma|^{n}$$

A1.2.4 The Oldroyd-Maxwell Fluid

So far the constitutive equations that have been discussed have been independent of time. The stress tensor has been shown to depend upon the deformation rate tensor for both Newtonian and power law fluids. Now, the stresses are allowed to depend upon the time domain. Physically, the stresses will be time-dependent if the fluid possesses some elasticity. In this case one would expect normal deviatoric stresses to be present and thus give rise to anomalous effects.

In essence, a relationship is proposed to describe time-dependent rheological behavior which suggests the idea

of viscoelasticity. In fact, the Maxwell model is probably the best known viscoelastic model and also the easiest to understand. The constitutive relationship for the Oldroyd-Maxwell fluid is given by eq.(A1.49).

$$P_{ij} + \theta \frac{\delta P_{ij}}{\delta t} = 2\mu d_{ij} \qquad \text{(A1.49)}$$

With the exception of the second term, eq.(A1.49) is identical to that of the Newtonian fluid. In eq.(A1.49) θ is defined to be a relaxation time constant. It may be further defined as the viscosity divided by the shear modulus (μ/G) which has the units of time. The derivative $\delta/\delta t$ is defined as the Oldroyd convective derivative (OCD). Assuming Cartesian coordinates, the OCD may be expanded to

$$\frac{\delta P_{ij}}{\delta t} = \frac{\partial P_{ij}}{\partial t} + v_m \frac{\partial P_{ij}}{\partial x_m} - P_{im} \frac{\partial v_j}{\partial x_m} - P_{mj} \frac{\partial v_i}{\partial x_m} \quad . \qquad \text{(A1.50)}$$

As before, it is convenient to describe the stresses in a moving coordinate system. The variations in the stress tensor with respect to time are then given by the OCD. The first term of the OCD (eq.(A1.50)) records the variation in stress with respect to the local coordinate system. The remaining terms take into account the time variations as a result of the fluid velocity and nonlinearities, respectively. Together, they model the total derivative of stress with respect to time.

To best illustrate the implications of the Maxwell model (eq.(A1.49)), an example is worked out below. Consider the same two-dimensional steady, shearing, flow of Figure A1.10. Recall that the kinematics were

$$v_1 = \Gamma x_2$$
$$v_2 = 0$$

and the deformation rate tensor was shown to be

$$d_{ij} = \begin{pmatrix} 0 & \frac{1}{2}\Gamma & 0 \\ \frac{1}{2}\Gamma & 0 & 0 \\ 0 & 0 & 0 \end{pmatrix}$$

Both the kinematics and the strain rate tensor are identical for this problem. The difference arises when one applies a constitutive relationship. Applying eq.(A1.49) with the known components of $\underset{\sim}{d}$, it is not hard to show that the only nonzero stress terms are contained in the equations

$$P_{11} + \theta \frac{\overset{\nabla}{P}_{11}}{\nabla t} = 0 \qquad \text{(A1.51a)}$$

$$P_{12} + \theta \frac{\overset{\nabla}{P}_{12}}{\nabla t} = \mu\Gamma \qquad \text{(A1.51b)}$$

Working out the Oldroyd derivatives, one sees that

$$\frac{\overset{\nabla}{P}_{11}}{\nabla t} = -2P_{m1}\frac{\partial v_1}{\partial x_m} = -2\mu\Gamma^2 \qquad \text{(A1.52a)}$$

$$\frac{\partial P_{12}}{\partial t} = 0 \qquad \text{(A1.52b)}$$

Substituting eqs.(A1.52) into eqs.(A1.51) and solving for the deviatoric stresses, it may be shown

$$P_{11} = 2\theta\mu\Gamma^2$$

$$P_{12} = \mu\Gamma$$

In matrix form the deviatoric stress tensor is given by eq.(A1.53)

$$P_{ij} = \begin{pmatrix} 2\theta\mu\Gamma^2 & \mu\Gamma & 0 \\ \mu\Gamma & 0 & 0 \\ 0 & 0 & 0 \end{pmatrix} \qquad \text{(A1.53)}$$

If one compares the structure of the stress tensor (P_{ij}) with that of the deformation rate tensor, an interesting observation can be made. The normal stress P_{11} is nonzero even though the d_{11} component of the $\underset{\sim}{d}$ tensor is zero. What is happening is that the Maxwell fluid develops inherent normal stresses when subjected to pure shearing flow. This anomalous effect is common among many polymeric solutions. In many instances, these normal stresses may be far greater than the shearing stresses needed to deform the material; hence, they may not be neglected.

A1.3 Selected Analytical Examples

In an effort to reinforce some of the concepts presented in this discourse and also illustrate the method of problem solving, two examples are presented in this section. These problems serve to introduce the reader to the basic idea of simple shearing flow in a channel. Contrasting behavior in the fluid velocity fields result from employing two different constitutive equations.

As one shall see, solving problems in fluid mechanics is basically intuitive. However, there is a logical sequence of events that should be discussed briefly. First, one must make an educated guess as to the flow kinematics. This initial guess can be only as good as one's insight or experience may dictate. Clearly, the kinematics that are chosen must satisfy the boundary conditions of the physical problem. The next step usually involves choosing a suitable constitutive equation. If this is not explicitly given in the problem definition, one must rely on past experience. With the assumed fluid behavior in hand, the above information is substituted into the equations of motion. This step acts to solve for the missing information in terms of unknown stresses

and/or the exact expressions for the velocity components. If the initial guess as to the kinematics was incorrect, that fact will frequently be borne out during the solution to the equations of motion. Since the details of the flow problem are a direct consequence of the assumed kinematics, incorrect guesses as to the kinematics result in invalid and often contradictory details. If need be, added information from the continuity equation can be used as a check to verify the final solution. One shall see how to apply this methodology in the problems that follow.

A1.3.1 Planar Poiseuille Flow

Consider the flow of a very viscous fluid between two stationary walls as shown in Figure A1.11.

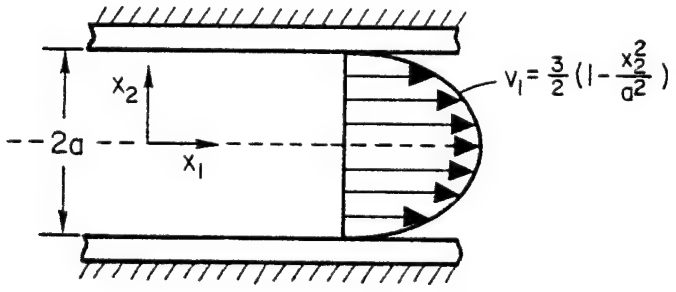

Figure A1.11 Normalized velocity profile for two-dimensional Poiseuille flow

As instructed, a set of reasonable kinematics is proposed.

$$v_1 = f(x_2) \tag{A1.54a}$$

$$v_2 = 0 \tag{A1.54b}$$

$$v_3 = 0 \tag{A1.54c}$$

In the problem formulation it is assumed that the dimension of x_3 is sufficiently large so that no variation in the flow takes place in that direction. In fact, one further specifies that in addition to being a constant, v_3 *is* zero. For clarity, one many draw on the analogy from the plane strain approximation in linear two-dimensional elasticity. The velocity component in the x_2 direction is also seen to be zero since one expects no velocity fluctuations transverse to the flow direction. Finally, v_1 is considered to be a function of x_2 since it is known from the "no slip" boundary condition at the solid wall that $v_1 = 0$ at this interface and yet v_1 must be finite within the channel for flow to take place. The velocity component v_1 is not a function of x_1 since one is assuming shearing flow. Hence, it may be justified that the kinematics of eqs.(A1.54) are reasonable.

The equations of motion for steady inertialess flow in Cartesian coordinates are written below.

$$0 = \frac{\partial \sigma_{ij}}{\partial x_j} = \begin{cases} \dfrac{\partial \sigma_{11}}{\partial x_1} + \dfrac{\partial \sigma_{12}}{\partial x_2} + \dfrac{\partial \sigma_{13}}{\partial x_3} & \text{(A1.55a)} \\ \dfrac{\partial \sigma_{12}}{\partial x_1} + \dfrac{\partial \sigma_{22}}{\partial x_2} + \dfrac{\partial \sigma_{23}}{\partial x_3} & \text{(A1.55b)} \\ \dfrac{\partial \sigma_{13}}{\partial x_1} + \dfrac{\partial \sigma_{23}}{\partial x_2} + \dfrac{\partial \sigma_{33}}{\partial x_3} & \text{(A1.55c)} \end{cases}$$

Usually, when the transient and inertial terms (the left-hand side of the equations of motion) are ignored, the flow is such that viscous effects dominate the inertial effects. Recall from section A1.2.1 the definition of the Reynold's number. For slow, viscous flows the Re number approaches zero and the equations of motion reduce to those of eqs.(A1.55).

From the kinematics, eqs.(A1.54), one may at once write down the deformation rate tensor.

$$d_{ij} = \tfrac{1}{2}\left(\frac{\partial v_i}{\partial x_j} + \frac{\partial v_j}{\partial x_i}\right)$$

$$= \tfrac{1}{2}\begin{pmatrix} 0 & \dfrac{\partial v_1}{\partial x_2} & 0 \\ \dfrac{\partial v_1}{\partial x_2} & 0 & 0 \\ 0 & 0 & 0 \end{pmatrix} \qquad \text{(A1.56)}$$

Upon employing the Newtonian constitutive relationship

$$\sigma_{ij} = -p\delta_{ij} + 2\mu d_{ij} \qquad \text{(A1.57)}$$

it may be concluded that the only nonzero deviatoric stress component is P_{12}. This is due to the linear relationship between the $\underset{\sim}{P}$ and $\underset{\sim}{d}$ tensors. Hence, eqs. (A1.55) become

$$0 = \frac{-dp}{dx_1} + \frac{\partial}{\partial x_2}\left(2\mu \tfrac{1}{2}\frac{\partial v_1}{\partial x_2}\right) \qquad \text{(A1.58a)}$$

$$0 = \frac{\partial}{\partial x_1}\left(2\mu \tfrac{1}{2}\frac{\partial v_1}{\partial x_2}\right) - \frac{dp}{dx_2} \qquad \text{(A1.58b)}$$

respectively. Eq.(A1.55c) provides no information in that it is identically zero; thus it will be ignored in the remaining discussion.

From eq.(A1.58b) it is apparent that

$$\frac{dv_1}{dx_2} = f(x_2) \qquad \text{(A1.59)}$$

which reinforces the original choice of kinematics. To solve for v_1 eq.(A1.58a) is integrated twice with respect to x_2

$$v_1 = \frac{1}{\mu}\frac{dp}{dx_1}\frac{x_2^2}{2} + \frac{C_1}{\mu}x_2 + \frac{C_2}{\mu} \quad . \qquad \text{(A1.60)}$$

Upon the application of the two boundary conditions

$$v_1 = 0 \qquad x_2 = \pm a \qquad \text{(A1.61a)}$$

$$\frac{dv_1}{dx_2} = 0 \qquad x_2 = 0 \qquad \text{(A1.61b)}$$

it turns out that $c_1 = 0$ and $c_2 = (-a^2/_2)\,dp/dx_1$ where "a" is defined as half of the channel width. Therefore, eq.(A1.60) becomes

$$v_1 = \frac{1}{2\mu}\frac{dp}{dx_1}(x_2^2 - a^2) \quad . \tag{A1.62}$$

Since (dp/dx_1) is negative (a pressure drop is experienced for viscous flow), one may multiply eq.(A1.62) by (-1) and deal with $|dp/dx_1|$ which may be written simply as dp/dx_1 with no confusion intended. Upon rearranging eq.(A1.62)

$$v_1 = \frac{a^2}{2\mu}\frac{dp}{dx_1}\left(1 - \frac{x_2^2}{a^2}\right) \quad . \tag{A1.63}$$

If one considers a flow with a centerline velocity of unity, then setting $x_2 = 0$ in eq.(A1.63) it is evident that the collection of constants

$$\frac{a^2}{2\mu}\frac{dp}{dx_1}$$

must equal 1. Now one may use the remaining continuity equation to determine the average value of the velocity.

$$\int_{-a}^{+a} v_1 dx_2 = v_{avg}\int_{-a}^{+a} dx_2 \tag{A1.64}$$

so that upon carrying out the integration one finds $v_{avg} = {}^2/_3\, v_{max}$. At last, the desired expression for

the normalized velocity profile is obtained for Newtonian channel flow.

$$v_1 = \tfrac{3}{2}\left(1 - \frac{x_2^2}{a^2}\right) \qquad \text{(A1.65)}$$

This result illustrates the well-known parabolic velocity profile characterisitc of planar Poiseuille flow. This relationship is referenced several times throughout the preceding chapters.

A1.3.2 Planar Power-Law Fluid

Consider again the flow conditions of Figure A1.11. In this example, one endeavors to solve the same problem as in section A1.3.1, with the exception of the constitutive equation. The kinematics remain precisely the same as do the equations of motion. From eq.(A1.58a) the governing equation in the x_1 direction was found to be

$$0 = -\frac{dp}{dx_1} + \frac{\partial P_{12}}{\partial x_2} \qquad \text{(A1.66)}$$

For the power law fluid, undergoing simple shearing flow, recall that the desired relationship between the stress and strain rate was shown to be

$$P_{12} = \eta d_{12} \qquad \text{(A1.67)}$$

where from eq.(A1.43) for simple shearing flow

$$\eta = M\left|\frac{\partial v_1}{\partial x_2}\right|^{n-1}$$

Recall that M is interpreted to be the consistency of the fluid and n is defined to be the power law index. Substituting for P_{12} in eq.(A1.66) yields a second order ordinary differential equation in terms of v_1

$$\frac{dp}{dx_1} = \frac{d}{dx_2}\left[M\left(\frac{dv_1}{dx_2}\right)^n\right] \quad . \tag{A1.68}$$

Integrating eq.(A1.68) twice and making use of the boundary conditions of eqs.(A1.61) the resulting velocity field is shown to be

$$v_1 = \frac{n}{n+1}\,\frac{1}{M^{1/n}}\left(\frac{dp}{dx_1}\right)^{1/n}\left(x_2^{\frac{n+1}{n}} - a^{\frac{n+1}{n}}\right) \quad . \tag{A1.69}$$

Resorting to similar arguments as in the previous section, let it be assumed that the maximum centerline velocity is equal to unity. The average velocity may be calculated from the continuity equation to be

$$v_{avg} = \left(1 - \frac{n}{2n+1}\right) v_{max} \quad . \tag{A1.70}$$

As before, one may normalize eq.(A1.69) with respect to the average velocity to obtain the general velocity profile for a power law fluid.

$$v_1 = \frac{1+2n}{1+n}\left[1 - \left(\frac{x_2}{a}\right)^{\frac{n+1}{n}}\right] \tag{A1.71}$$

In general, these velocity profiles will not be parabolic except in the special case where n = 1 and eq.(A1.71) collapses to that derived for the Newtonian fluid (eq.(A1.65)). Figure A1.12 shows the variation of the velocity profile with power law index. These are the characteristic profiles for pseudoplastic or shear thinning fluids. We will be concerned primarily with the response of such fluids undergoing shearing deformation.

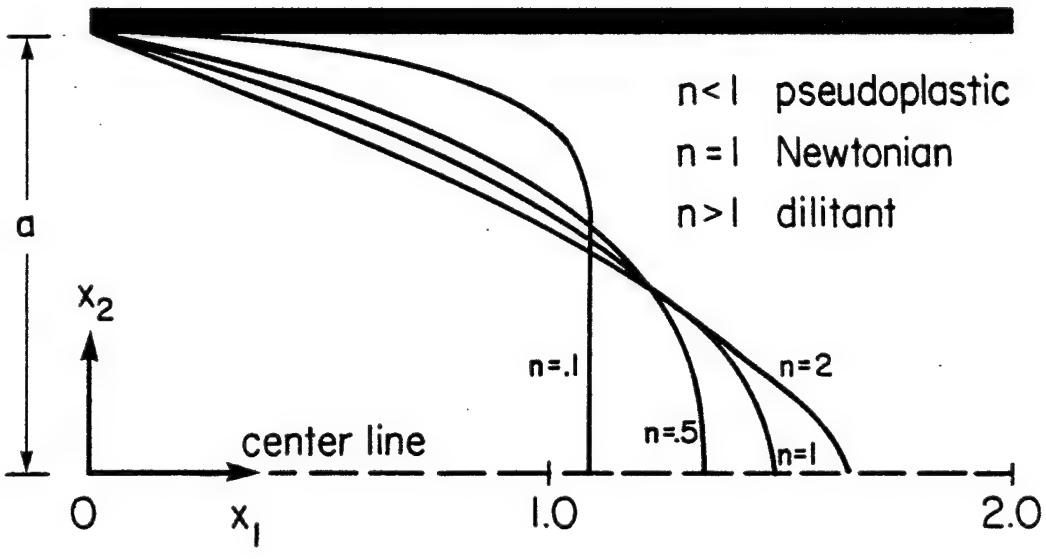

Figure A1.12 Velocity profile for the power law fluid

APPENDIX 2

FINITE ELEMENTS IN FLUID MECHANICS

A2.1 Introduction

One important aspect of the determination of fiber orientation within a flow field relies on the ability to completely solve the fluid mechanics problem. By completely, it is meant that all the components of the velocity field (v_i) and the independent components of stress (σ_{ij}) are known, as well as approximations to the stream function and vorticity. In Appendix A1, it was apparent that only a limited number of problems could be solved by obtaining analytical solutions for the velocity field. For a simple two-dimensional flow field the equations of motion were integrated directly. As the kinematic expressions increase in complexity, such a simplified approach fails. Even for Stoke's flow, where the equations of motion are relatively simple, it becomes formidable to obtain a closed form solution if the domain geometry becomes too complex. As one anticipates the nonuniform mold shapes that may arise, it becomes

necessary to seek an approximation to the actual solution. The finite element method shall be employed for this purpose. Irregular boundaries will be shown to present no difficulty with this type of formulation. In fact, through proper discretization some rather exotic boundary shapes may be modeled quite closely, thus insuring a good representation of the solution domain.

In discussing the application of the FEM to specific problems, one shall assume that the reader has a limited but working knowledge of the subject. Many excellent texts are listed in the references for introductory or additional reading. What is intended here is to present a logical sequence of steps that will provide a basis toward understanding the FEM as applied to fluid mechanics for this work. Many techniques such as domain discretization, the assembly of elements, etc., are direct carry-overs from the solid mechanics area. Other similarities will be mentioned as they arise to assist the reader in his understanding. The main difference between solid and fluid mechanics formulations lies in the derivation of the element equations. Again, the material contained in Appendix A1 will be of paramount importance in the development of such equations.

In section A2.2, a quick glance at the variational methods is presented in relation to the finite element method. It is useful to introduce variational methods to present an alternate approach to the general formulation via the direct stiffness approach. Most treatises introduce the FEM by the direct stiffness approach because of its simplicity. Our goal is to compare the formulations due to the direct stiffness approach and variational methods. Also an illuminating example is included to illustrate the link between the governing differential equation and the discretized matrix representation of a problem.

The six node triangular element is developed in section A2.3. Included within this scope are references to the standard element and the interpolation functions. Having chosen a suitable element with prescribed shape functions, the actual solving of the differential equation is anticipated. The method of weighted residuals (MWR) allows one to approximate the solution within the domain to an artibrary degree of accuracy. In section A2.4, a particular form of the MWR, the Galerkin method, is introduced for this purpose.

The element equations governing Stoke's flow are derived in section A2.5. Ideas from sections A2.3 and A2.4 are utilized to arrive at the final set of discretized equations. The solution of the linear system of equations is enhanced with a frontal elimination method, and the procedure is outlined in section A2.6. A procedure that utilizes the Galerkin method and determines the behavior of the derived quantities of stream function and vorticity is outlined in section A2.7. These two functions are needed in the development of the fiber orientation model. Lastly, an example is solved via the FEM that draws on many of the ideas presented in Appendix A1. A simple, two-dimensional, shearing flow problem is solved numerically to show the validity in the FEM.

A2.2 The Finite Element Approach

A2.2.1 Direct Stiffness Approach

There are two possible avenues to traverse when introducing the finite element method. The first, and perhaps the most widely adopted, is called the direct stiffness approach. Its derivation originated in the area of solid mechanics primarily because initial

investigations into the finite element approach were made in this area. However, direct analogies exist in other disciplines as well, which should emphasize that it is a rather general methodology. This procedure shall be briefly outlined below, for the purpose of comparing this method with that of the variational approach to be discussed subsequently. As one will appreciate, each approach has its advantages, but both paths of pursuit yield identical results.

Consider the one-dimensional domain D shown in Figure A2.1. For definiteness it may be considered to be a uniform rod subject to compressive forces. The independent variable is defined as x while the dependent

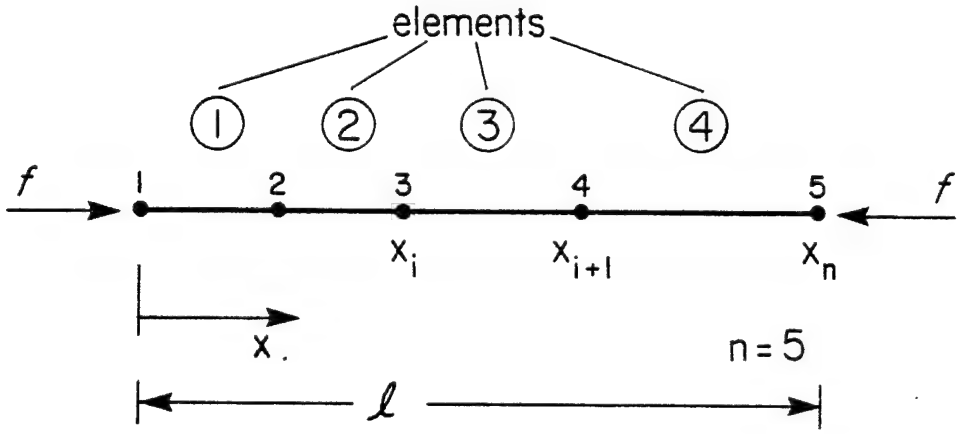

Figure A2.1 One-dimensional domain, D, for the FEM

or solution variable shall be denoted as y. Since it was chosen to consider a rod in compression, the variable y many be viewed as in-plane displacements. To illustrate the discretization procedure one may divide the original domain D into four elements that connect a total of five nodes. Each node in this simple example is to possess one degree of freedom (i.e. a single displacement). A typical element is shown in Figure A2.2. Note that each element possesses two degrees of freedom y_i and y_{i+1} and that the variation of the dependent variable is assumed to be linear within the individual element. We shall expand upon the ideas presented here later when discussing the representation of the unknown field variable in terms of shape functions.

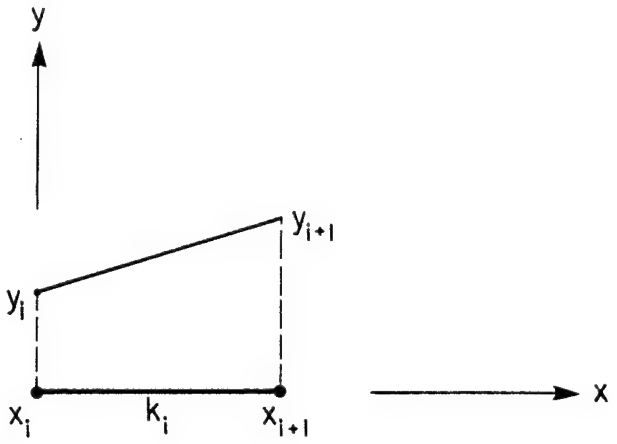

Figure A2.2 A one-dimensional element with two degrees of freedom

If one turns to solid mechanics to borrow a constitutive relation in which to relate these dependent variables, one finds from Hooke's law that

$$ky = f \tag{A2.1}$$

where k = stiffness coefficient

y = displacement

f = force

The analogy with forces and displacements is one that usually allows the reader to think in terms of familiar quantities. Now, typical with the finite element process one asks that eq.(A2.1) be satisfied within each subdivision or element. Thus, writing eq.(A2.1) for each element, one arrives at a system of simultaneous equations to be solved. In matrix or operator notation these equations are seen to be

$$\underset{n\times n}{[k]}\ \underset{n\times 1}{\{y\}} = \underset{n\times 1}{\{f\}} \tag{A2.2}$$

The labor involved in this procedure results from the computation of the individual "stiffness coefficients". It is not hard to show that this approach will always render the stiffness matrix symmetric. An additional important point to realize from eq.(A2.2) is that the maximum size of the matrices depends upon the number

of variables contained in the overall system. In this example, the number of variables equals the number of nodes.

A2.2.2 Variational Methods

One begins this section by considering a family of functions on the interval between two given points, say x_o and x_i as shown in Figure A2.3. Clearly there are a vast number of possible relationships that satisfy the above criterion. The number of admissible functions may be restricted by requiring that they all contain continuous derivatives of at least second order. In addition, it may be assumed that they all satisfy the essential boundary conditions at the two endpoints.

$$y(x_o) = y_o \tag{A2.3a}$$

$$y(x_i) = y_i \tag{A2.3b}$$

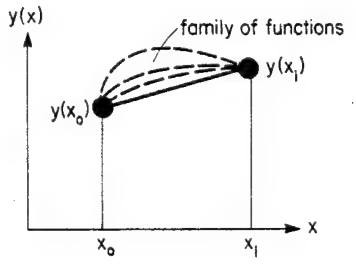

Figure A2.3 The variation of y(x) on the interval $(x_i - x_o)$

Assume that the family of curves may be represented by the integral

$$I(y(x)) = \int_{x_o}^{x_i} F(x,y,y')dx \qquad (A2.4)$$

where the prime denotes differentiation with respect to x. The value of the integral inherently depends upon the particular choice of the function F. The function F is seen to depend only on x, y and y'. More general derivations include dependence upon higher order derivatives, but for current purposes the noted dependence will suffice. Also, the integral I contains only one independent variable whereas more general procedures might include more. Ultimately, I(y(x)) is seen to be a function of a function and one many define this type of relationship by the term functional.

It will be of concern to determine the stationary value of the functional I. It will be apparent that this extremal condition will lead to a differential equation that must be satisfied if the functional is to be an extremum. This differential equation, often called the Euler equation, will often be identical to the equations that govern various physical phenomena. Thus, one shall see that for certain problems, it will be possible to

work with the minimizing of a functional instead of dealing directly with the differential equation. This is not always possible since differential equations that govern some physical circumstances possess no variational counterpart. With the motivation now in place, one may therefore proceed to minimize the function of eq.(A2.4).

Assume that $y(x)$ is the true solution in that it extremizes I. Next, one allows for the following perturbation on the function $y(x)$ of the form

$$\bar{y}(x) = y(x) + \varepsilon\eta(x) \tag{A2.5}$$

where ε is a small number. The new function $\eta(x)$, which may be chosen arbitrarily, satisfies the boundary conditions $\eta(x_0) = 0$ and $\eta(x_1) = 0$. Schematically, the functions of eq.(A2.5) are shown in Figure A2.4. We shall

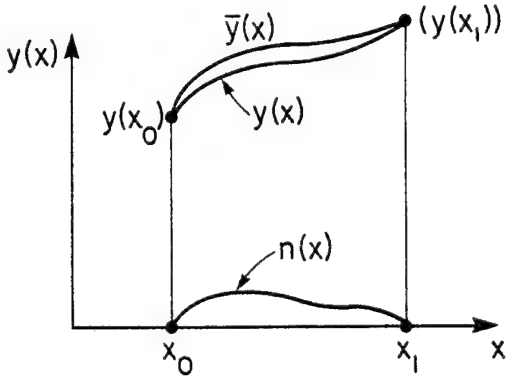

Figure A2.4 The function $\eta(x)$

consider these functions as fixed and the only variable is the scalar parameter ε. Substitute eq.(A2.5) into eq.(A2.4) and arrive at the following function.

$$I(\bar{y}(x)) = \int_{x_o}^{x_1} F(x,y+\varepsilon\eta(x),y'+\varepsilon\eta'(x))dx \qquad (A2.6)$$

Since eq.(A2.6) is a function only of the parameter ε, one may find the extremum by ordinary means. The derivative of the function with respect to the parameter ε will provide the necessary condition for an extremum to occur.

$$\left.\frac{dI(\bar{y}(x))}{d\varepsilon}\right|_{\varepsilon=0} = 0 \qquad (A2.7)$$

If one applies eq.(A2.7) to eq.(A2.6),

$$\left.\frac{dI(\bar{y}(x))}{d\varepsilon}\right|_{\varepsilon=0} = \int_{x_o}^{x_1}\left(\left(\left.\frac{\partial F}{\partial y}\right|_{\varepsilon=0}\right)\eta + \left(\left.\frac{\partial F}{\partial y'}\right|_{\varepsilon=0}\right)\eta'\right)dx \qquad (A2.8)$$

and integrating the second term of eq.(A2.8) by parts

$$\left.\frac{dI(\bar{y}(x))}{d\varepsilon}\right|_{\varepsilon=0} = \frac{\partial F}{\partial y'}\eta(x)\Big|_{x_o}^{x_1} + \int_{x_o}^{x_1}((\partial F/\partial y) - \frac{d}{dx}(\partial F/\partial y'))\eta\,dx$$

$$= 0 \qquad (A2.9)$$

The first term of eq.(A2.9) vanishes because of the

essential boundary conditions placed upon the function $\eta(x)$. The remaining terms must then equal zero per eq.(A2.7).

$$\int_{x_o}^{x_1} \left(\frac{\partial F}{\partial y} - \frac{d}{dx}\left(\frac{\partial F}{\partial y'} \right) \right) \eta(x)\, dx = 0 \qquad \text{(A2.10)}$$

The function $\eta(x)$ is not necessarily zero everywhere; thus in order to satisfy the equality, the bracketed portion of eq.(A2.10) must be identically zero.

$$\frac{\partial F}{\partial y} - \frac{d}{dx}\left(\frac{\partial F}{\partial y'} \right) = 0 \qquad \text{(A2.11)}$$

Eq.(A2.11) is the Euler equation and is a necessary condition for extremizing the functional of eq.(A2.6). The question of a sufficient condition for minimum extrema may be investigated by computing the second variation of the functional with respect to ε, namely $\frac{d^2 I}{d\varepsilon^2}$.

How can the above mathematics be applied to the finite element method as introduced in the previous section? The so-called variational approach will be illustrated through the following example. Suppose one knows that the governing differential equation to a particular problem admits the functional

$$I(y(x)) = \int_{x_0}^{x_1} (\tfrac{1}{2}(dy/dx)^2 - f(x)y)\,dx \quad . \qquad \text{(A2.12)}$$

As shown above, it is desired to minimize this functional subject to the appropriate boundary conditions. In doing so, one will satisfy the necessary condition of eq.(A2.11) and thus satisfy the differential equation. Consider, for definiteness, the same domain as outlined in Figure A2.1. Since one is about to apply the FEM, the initial consideration is concerned with representing the solution in a discretized manner. The unknown variable, y, may be represented by the series expansion

$$y = \sum_{i=1}^{2} W_i y_i \qquad \text{(A2.13)}$$

within each element, where y_i denotes nodal values of the unknown field variable and W_i corresponds to the interpolation functions. The interpolation functions dictate the variation of the field variable within any element. Assuming a one-dimensional, linear element as described by Figure A2.2, the shape functions become

$$W_1 = \frac{x_i - x}{x_i - x_o} = 1 - \xi \qquad \text{(A2.14a)}$$

$$W_2 = \frac{x - x_o}{x_i - x_o} = \xi \qquad \text{(A2.14b)}$$

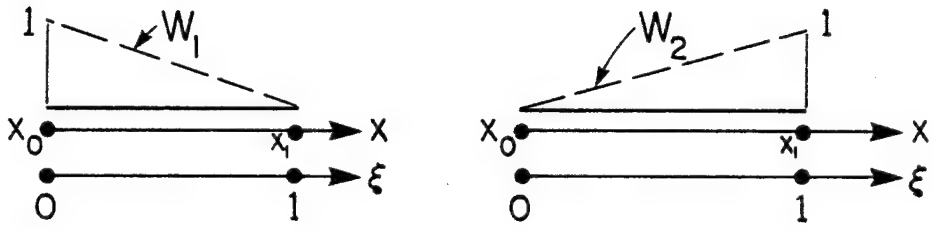

Figure A2.5 Linear shape functions

Characteristic of all shape functions, the i-th shape function takes on the value of unity at the i-th local node and equals zero at all other element nodes. In this fashion one is able to approximate the solution in terms of the nodal values of the unknown function.

Also, the standard element is introduced as a means of calculating derivatives with repect to space coordinates. On a given element the normalized coordinate ξ ranges from 0 to 1 and is related to the global coordinate x by the transformation shown in Figure A2.6. The advantage of working on a standard element will be shown as opposed to working with global coordinate values.

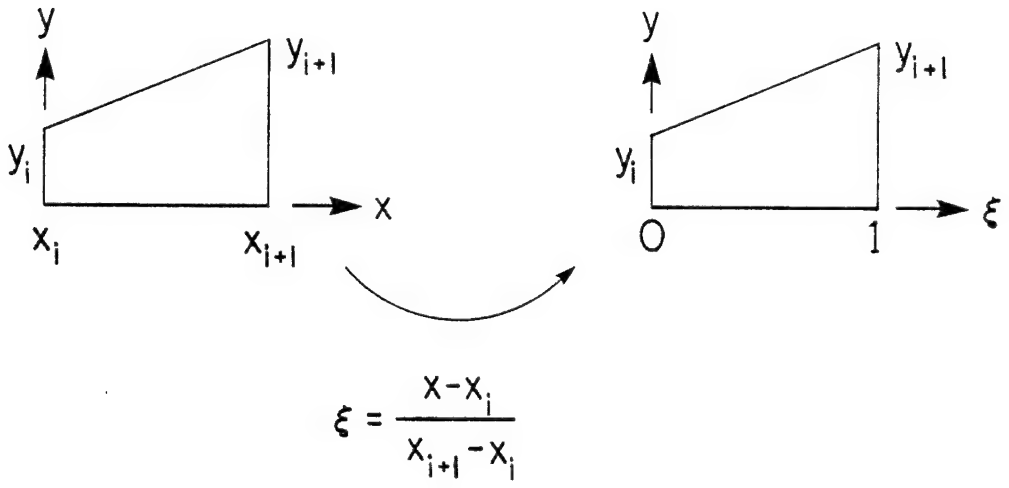

Figure A2.6 Transformation to local coordinates

Integrations which need to be performed will be over a unit interval and this idea is useful when implementing numerical integration schemes.

Thus, returning to the functional to be minimized, eq.(A2.12) becomes

$$I = \int_0^L (\tfrac{1}{2}(dy/dx)^2 - f(x)y)dx \ , \ y(0)=y(L)=0 \qquad (A2.15)$$

where L ranges over the full domain. Next, it is natural to discretize the domain and sum up the contributions from all the elements.

$$I = \sum_{i=1}^{N} \int_{x_i}^{x_{i+1}} (\tfrac{1}{2}(dy/dx)^2 - f(x)y)\,dx \qquad \text{(A2.16)}$$

By chain differentiation, one may write the contribution from the j-th element in terms of the standard element.

$$I_j = \int_0^1 \tfrac{1}{2}(dy/d\xi)^2 (d\xi/dx)^2 (dx/d\xi)\,d\xi - \int_0^1 f(x(\xi))y\ (dx/d\xi)\,d\xi \qquad \text{(A2.17)}$$

Following immediately, one may rewrite the approximation for the field variable (eq.(A2.13)) in terms of the shape functions and unknown nodal values as

$$y(\xi) = y_i(1 - \xi) + y_{i+1}\xi \qquad \text{(A2.18)}$$

The needed derivatives in eq.(A2.17) are calculated directly from either eq.(A2.18) or eq.(A2.14), namely

$$\frac{dy}{d\xi} = -y_i + y_{i+1} \qquad \text{(A2.19a)}$$

$$\frac{dx}{d\xi} = x_{i+1} - x_i \qquad \text{(A2.19b)}$$

Substituting eqs.(A2.19) and eq.(A2.18) into the functional expression of eq.(A2.17) yields

$$I_j = \frac{(y_{i+1}-y_i)^2}{2(x_{i+1}-x_i)} - \int_0^1 f(x(\xi))\,[y_i(1-\xi)+y_{i+1}\xi]\,(x_{i+1}-x_i)\,d\xi \qquad \text{(A2.20)}$$

or equivalently

$$I_j = \frac{1}{2(x_{i+1}-x_i)}\,(y_i^2 - 2y_iy_{i+1} + y_{i+1}^2) - y_i(x_{i+1}-x_i)\int_0^1 (1-\xi)\,f(x(\xi))\,d\xi - y_{i+1}(x_{i+1}-x_i)\int_0^1 f(x(\xi))\,\xi\,d\xi \quad . \qquad \text{(A2.21)}$$

If one defines the following quantities:

$$k_{i,i} = \frac{1}{(x_{i+1}-x_i)} \qquad \text{(A2.22a)}$$

$$k_{i,i+1} = -\frac{1}{(x_{i+1}-x_i)} \qquad \text{(A2.22b)}$$

$$k_{i+1,i+1} = k_{i,i} \qquad \text{(A2.22c)}$$

$$F_i = (x_{i+1}-x_i)\int_0^1 (1-\xi)\,f(x(\xi))\,d\xi \qquad \text{(A2.22d)}$$

$$F_{i+1} = (x_{i+1}-x_i)\int_0^1 \xi\,f(x(\xi))\,d\xi \qquad \text{(A2.22e)}$$

then one may write eq.(A2.21) in a more convenient form as

$$I_j = \tfrac{1}{2}\{y_i, y_{i+1}\}\begin{bmatrix} k_{i,i} & k_{i,i+1} \\ k_{i+1,i} & k_{i+1,i+1} \end{bmatrix}\begin{Bmatrix} y_i \\ y_{i+1} \end{Bmatrix} - \{y_i, y_{i+1}\}\begin{Bmatrix} F_i \\ F_{i+1} \end{Bmatrix} \quad . \tag{A2.23}$$

Introducing operator or matrix notation eq.(A2.23) can be compacted to yield

$$I_j = \tfrac{1}{2} y_j^T k_j y_j - y_j^T F_j \quad \text{(no sum)} \tag{A2.24}$$

where superscript T represents the transpose of a matrix. To complete the exercise, it is necessary to sum the contributions from eq.(A2.24) and then carry out the minimization. Mathematically, this correponds to

$$\frac{d\Sigma I_j}{dy_j} = \frac{d}{dy_j} \sum_1^N (\tfrac{1}{2} y_j^T k_j y_j - y_j^T F_j) = 0 \quad . \tag{A2.25}$$

If it is true that the order of summation and differentiation may be interchanged then eq.(A2.25) provides a set of simultaneous equations that must be solved.

$$\sum_1^N \frac{d}{dy_j}(\tfrac{1}{2} y_j^T k_j y_j - y_j^T F_j) = 0 \tag{A2.26}$$

Eq.(A2.26) reduces to

$$\underset{n\times n}{[k]}\ \underset{n\times 1}{\{y\}} = \underset{n\times 1}{\{F\}} \tag{A2.27}$$

after carrying out the minimization.

Clearly, then, eq.(A2.27) is exactly the same as eq.(A2.2) and one concludes that the results of the variational approach are identical to the direct stiffness approach, as is always the case for a linear system.

A2.3 Choice of Elements

The finite element method centers around the ability to find an approximate solution within the solution domain. Typically, one divides the domain into smaller divisions of a simpler shape and works exclusively to approximate the solution within the element. Let us briefly investigate the notion of interpolation or shape functions to determine how one approximates the behavior of the unknown within an element.

Consider the two-dimensional triangular element shown in Figure A2.7. Its simplicity is rivaled only by the four node rectangular element, but it has the distinct advantage of being able to better approximate irregular boundaries. Therefore, only the triangular element will be considered in this discussion.

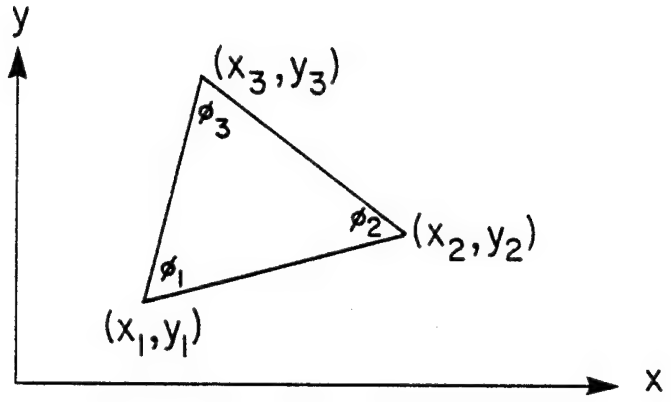

Figure A2.7 Linear triangular element in global coordinates

The interpolation functions are functions of the coordinates and possess the inherent property that $W_i(x_j) = \delta_{ij}$. This is to say that in eq.(A2.28) the function ϕ must equal the field variable at that node and may not have any contribution from other nodal values.

One seeks to approximate the unknown variation of the field variable ϕ throughout the triangular domain as

$$\phi = W_i \phi_i \qquad \text{(A2.28)}$$

where W_i are defined as the interpolation functions and ϕ_i are the nodal values of ϕ. This will be possible if

in the case of the triangular elements we use a two-dimensional polynomial to expand ϕ. One retains only

$$\phi = \alpha_1 + \alpha_2 x + \alpha_3 y \tag{A2.29}$$

the linear terms of the expansion which admit three unknown constants: α_1 , α_2 , and α_3. These constants may be exactly solved for since eq.(A2.29) applies to each of the three nodal values of the element, namely,

$$\begin{Bmatrix} \phi_1 \\ \phi_2 \\ \phi_3 \end{Bmatrix} = \begin{bmatrix} 1 & x_1 & y_1 \\ 1 & x_2 & y_2 \\ 1 & x_3 & y_3 \end{bmatrix} \begin{Bmatrix} \alpha_1 \\ \alpha_2 \\ \alpha_3 \end{Bmatrix} \tag{A2.30}$$

where

$$\begin{bmatrix} 1 & x_1 & y_1 \\ 1 & x_2 & y_2 \\ 1 & x_3 & y_3 \end{bmatrix} \equiv [C] \qquad (x_i, y_i) = \text{coordinate values}$$

Upon inversion of eq.(A2.30) we find

$$\{\alpha\} = [C]^{-1}\{\phi\} \tag{A2.31}$$

and one may rewrite eq.(A2.29) as

$$\phi = [1,x,y]\{\alpha\} = [1,x,y][C]^{-1}\{\phi\} \tag{A2.32}$$

If one compares eq.(A2.32) with eq.(A2.28) it is apparent

that the interpolation functions are

$$W_i = [1,x,y][C]^{-1} \tag{A2.33}$$

The method outlined above for obtaining the interpolation functions is straightforward in principle but may fail to yield meaningful information if $[C]^{-1}$ fails to exist. We endeavor to reveal a method that allows one to write down interpolation functions by inspection.

As one has seen from the previous section, it is beneficial to define a standard element whose normalized coordinate values range from 0 to 1. The standard triangular element is displayed in Figure A2.8 with the corresponding transformation equations given in determinental form by eqs.(A2.34).

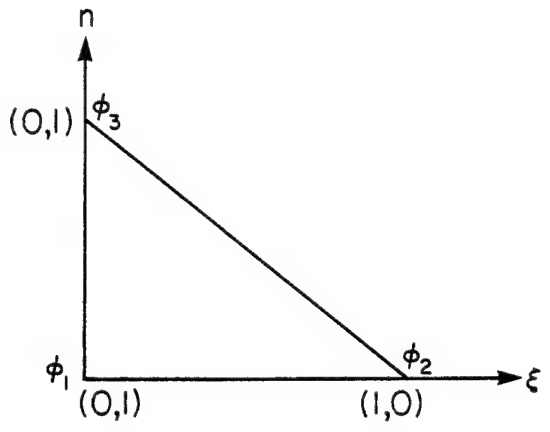

Figure A2.8 Standard triangular element

$$\xi = \frac{\begin{vmatrix} x-x_1 & x_3-x_1 \\ y-y_1 & y_3-y_1 \end{vmatrix}}{\begin{vmatrix} x_2-x_1 & x_3-x_1 \\ y_2-y_1 & y_3-y_1 \end{vmatrix}} \qquad \text{(A2.34a)}$$

$$\eta = \frac{\begin{vmatrix} x_2-x_1 & x-x_1 \\ y_2-y_1 & y-y_1 \end{vmatrix}}{|2\Delta|} \qquad \text{(A2.34b)}$$

The denominator of eq.(A2.34b) corresponds to twice the area of the triangular element.

In terms of these local coordinates, one seeks the interpolation functions that describe the variation of ϕ within the element. Consider W_1 and the figure below.

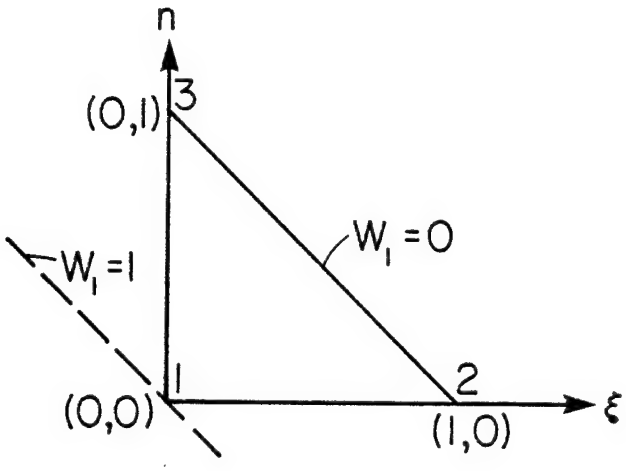

Figure A2.9 Determination of shape functions by inspection

By definition

$$W_1 = 1 \qquad (\xi=0,\ \eta=0) \tag{A2.35a}$$

and $W_1 = 0$ at points (0,1) and (1,0). The second criterion may be satisfied if one asks that $W_1 = 0$ along the line

$$f(\xi,\eta) = \xi + \eta - 1 = 0 \quad . \tag{A2.35b}$$

The interpolation function that satisfies eqs.(A2.35a) and (A2.35b) becomes

$$W_1 = 1 - \xi - \eta \quad . \tag{A2.36a}$$

The second interpolation function is simply

$$W_2 = \xi \tag{A2.36b}$$

and it can easily be verified that $W_2 = 0$ at nodes 1 and 3 and is unity at node 2. Also, it may be shown that

$$W_3 = \eta \quad . \tag{A2.36c}$$

Often these shape functions are called area coordinates which satisfy the relationships

$$W_1 = \frac{\Delta_1}{\Delta} = 1 - \xi - \eta \tag{A2.37a}$$

$$W_2 = \frac{\Delta_2}{\Delta} = \xi \tag{A2.37b}$$

$$W_3 = \frac{\Delta_3}{\Delta} = \eta \tag{A2.37c}$$

where Δ defines the area of a triangle. Clearly as a consequence of eqs.(A2.37) the shape functions must

satisfy the relationship

$$W_1 + W_2 + W_3 = 1 \quad .$$

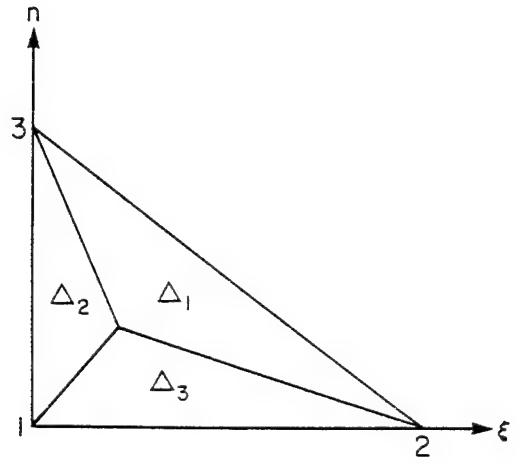

Figure A2.10 Area coordinates

The three-node triangle has been shown to model the linear variation of the field variable within the element. With this type of approximation the field variable is continuous at the element interfaces. One often refers to this type of behavior as C_o continuity.

It is possible to obtain quadratic interpolation for the triangular element if mid-side nodes are added to the existing nodes of Figure A2.11. The transformation equations to the standard element remain identical with those of eqs.(A2.34); however, one would expect the interpolation functions to be different.

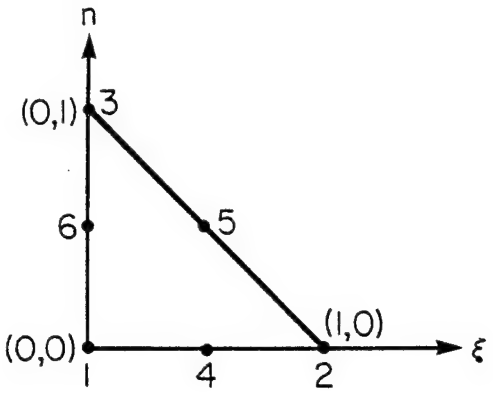

Figure A2.11 Six node (quadratic) triangular element in local coordinates

To see how one may construct interpolation functions by inspection, consider the development of ψ_1 for the six node triangle.

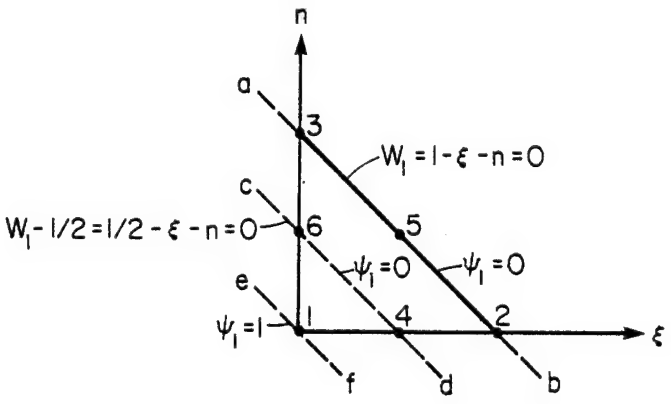

Figure A2.12 Determining ψ_1 by inspection

The shape function ψ_1 must vanish for nodes that lie along line ab and cd. To insure this fact one forms a product of these criteria, namely

$$\psi_1 \sim (1 - \xi - \eta)(\tfrac{1}{2} - \xi - \eta)$$
$$\sim (W_1)(W_1 - \tfrac{1}{2}) \qquad \text{(A2.38)}$$

Patching up the proportionality with a constant renders the shape function $\psi_1 = 1$ at $\xi = 0$, $\eta = 0$ resulting in the final expression

$$\psi_1 = 2W_1(W_1 - \tfrac{1}{2}) \qquad \text{(A2.39a)}$$

The derivation of the remaining shape functions follow similar arguments and are listed below.

$$\psi_2 = 2W_2(W_2 - \tfrac{1}{2}) \qquad \text{(A2.39b)}$$
$$\psi_3 = 2W_3(W_3 - \tfrac{1}{2}) \qquad \text{(A2.39c)}$$
$$\psi_4 = 4W_1W_2 \qquad \text{(A2.39d)}$$
$$\psi_5 = 4W_2W_3 \qquad \text{(A2.39e)}$$
$$\psi_6 = 4W_3W_1 \qquad \text{(A2.39f)}$$

It is logical to wonder what these shape functions look like that have been derived. The shape functions ψ_1 and ψ_4 for the six node triangle are shown in Figure A2.13.

One may be disillusioned at this point into thinking that placing more nodes along element boundaries will necessarily increase the degree of approximation.

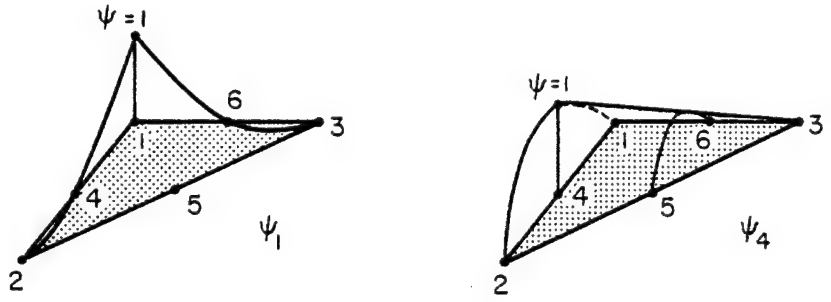

Figure A2.13 The shape functions ψ_1 and ψ_4 for the six node triangle

To explain why this need not be true we construct Pascal's triangle, shown in Figure A2.14.

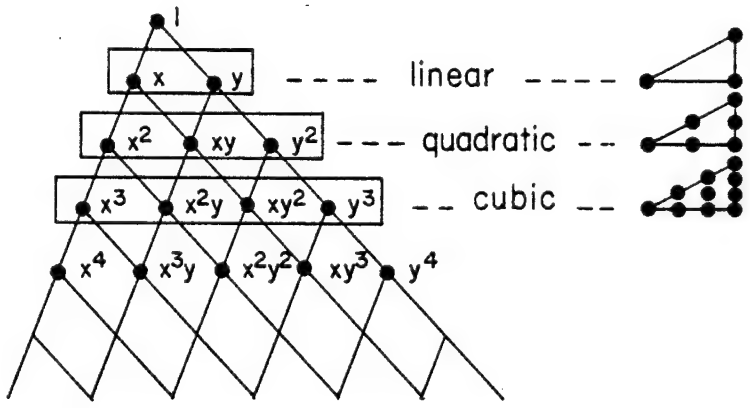

Figure A2.14 Pascal's triangle illustrating the degree of interpolation

The triangular array of variables lists the terms of a two-dimensional polynomial expansion. The most accurate results to the FEM are obtained when the interpolation functions contain the highest, complete order polynomials. Inclusion of a few terms of higher order in the interpolation functions tends not to increase the accuracy of the solution and often imparts noise into the system of equations. For example, suppose for certain problems it is advantageous to work on a four node quadrilateral element. The interpolation functions would contain the terms 1,x,y,xy. This type of representation for the field variable only admits linear variation along element sides. The inclusion of the xy term adds little in the form of increased accuracy to the solution approximation.

For the six-node triangular element Pascal's triangle reveals complete quadratic representation of the field variable throughout the element. This feature of quadratic interpolation functions as well as ease of boundary modeling make the six node triangle a desirable element to use. This element shall be employed when solving the fluid mechanics problem by finite element methods.

A2.4 Method of Weighted Residuals

We have made reference to alternate methods of solving a problem that is governed by a differential equation. In section A2.2.2, it was assumed that a variational principle existed for the phenomenon under consideration and that one could deal with the minimization of a functional. It was also pointed out that many problems are not amenable to a variational approach and one is forced to work directly with the differential equation. In this section, the method of weighted residuals is illustrated as it applies to the finite element method.

Consider the following equation

$$Lu(x) = f \tag{A2.40}$$

where L is an ordinary differential operator. The boundary conditions are such that

$$u(x) = \bar{u} \tag{A2.41}$$

for all x on the boundary. The possible functions u(x) under consideration must be square-integrable in the sense that

$$\int_a^b |u(x)|^2 dx < \infty \quad . \tag{A2.42}$$

Recall our discrete approximation to the continuous function

$$u^*(x) = \sum_{i=1}^{N} W_i u_i \qquad \text{(A2.43)}$$

In general, eq.(A2.43) will not satisfy the governing equation exactly. One may anticipate some error or residual to arise if the approximation is substituted into the governing differential equation. This may be shown by writing eq.(A2.40) with u(x) being replaced by $u^*(x)$,

$$Lu^*(x) - f = R$$

$$\sum_{i=1}^{N} u_i LW_i - f = R \qquad \text{(A2.44)}$$

Now, the method hinges on whether one can minimize the residual that is found in eq.(A2.44). To accomplish this a set of weighting functions v_i are introduced and it is required that the weighted integral of the residual vanish, namely

$$\langle v_i, R \rangle = \int_a^b v_i R dx \equiv 0 \quad . \qquad \text{(A2.45)}$$

If one imposes this condition on eq.(A2.44) the result becomes

$$\left\langle \sum_{i=1}^{N} u_i (LW_i, v_j) \right\rangle - \langle f, v_j \rangle = 0 \quad . \qquad \text{(A2.46)}$$

To this point the weighting functions v_j have been completely arbitrary and, in fact, to specify them will define a particular form of the method of weighted residuals. There are several possible choices each having their own merit, but the most useful seems to be the Galerkin method. Here, the weighting functions are designated to be the same shape or interpolation functions that are used to describe the unknown variation of the field variable within the element. Therefore eq.(A2.46) becomes

$$< \sum_{i=1}^{N} u_i (LW_i, W_j) > - <f, W_j> = 0 \quad . \tag{A2.47}$$

To understand why the Galerkin method works, one may investigate the underlying assumptions of eq.(A2.45). The weighting functions which were chosen as the interplation functions form a complete set of functions. That is to say that any given function may be expanded as a linear combination of the shape functions which is borne out by eq.(A2.43). Also the shape functions may be seen to be linearly independent if one recalls how they were derived. They assume a value of unity at the i-th node and equal zero at all other nodes. Thus, any function is capable of being represented by eq.(A2.43) provided

sufficient terms are utilized. Finally then, one may claim that the residual of eq.(A2.45) is forced to zero since it is a function that must be orthogonal to every member of the complete set of shape functions.

For a linear operator L, the Galerkin method will always lead to the same results as those obtained via the variational methods. Also, it is of interest that the Galerkin method satisfies the governing differential equation in the mean. This behavior contrasts that of other techniques which approximate the pointwise convergence of the solution.

A2.5 Derivation of Stoke's Problem

Thus far we have been concerned primarily with some preliminary ideas that are a part of all finite element problems. It seems appropriate, now, that one becomes specific and deals with a particular problem in an attempt to unify the ideas presented so far and at the same time draw on some important concepts discussed in Appendix A1. The governing element equations for two-dimensional Stoke's flow will be derived in a Cartesian (x,y) reference frame.

One may begin be recalling the governing equations of motion for fluid mechanics systems. For Stoke's approximation these equations simplify to

$$-\frac{\partial p}{\partial x} + \frac{\partial P_{xx}}{\partial x} + \frac{\partial P_{xy}}{\partial y} + f_x = 0 \qquad \text{(A2.48a)}$$

$$-\frac{\partial p}{\partial y} + \frac{\partial P_{xy}}{\partial x} + \frac{\partial P_{yy}}{\partial y} + f_y = 0 \qquad \text{(A2.48b)}$$

and the continuity equation may be written as

$$\frac{\partial u}{\partial x} + \frac{\partial v}{\partial y} = 0 \qquad \text{(A2.49)}$$

Three primitive variables are anticipated to enter into the formulation: two velocity components and the pressure. The stress components will not be considered as primitive since they are related directly to the velocity components via the Newtonian constitutive relations.

$$P_{xx} = 2\mu\frac{\partial u}{\partial x} \qquad \text{(A2.50a)}$$

$$P_{yy} = 2\mu\frac{\partial v}{\partial y} \qquad \text{(A2.50b)}$$

$$P_{xy} = \mu\left(\frac{\partial u}{\partial y} + \frac{\partial v}{\partial x}\right) \qquad \text{(A2.50c)}$$

It is natural to propose the following expressions to describe the variation of the primitive variables within the element.

$$u = \sum_{j=1}^{6} u_j \psi_j \qquad \text{(A2.51a)}$$

$$v = \sum_{j=1}^{6} v_j \psi_j \qquad \text{(A2.51b)}$$

$$p = \sum_{j=1}^{3} p_j \phi_j \qquad \text{(A2.51c)}$$

Apparent immediately is the fact that one may specify quadratic interpolation for the velocity components and linear interpolation for the pressure. This should be obvious from the order of derivatives that appear in eqs.(A2.48). The pressure is usually specified to be one order less than the velocity components so that over-constraints do not arise. A typical element showing the unknowns is shown in Figure A2.15; note that there are a total of 15 degrees of freedom per element.

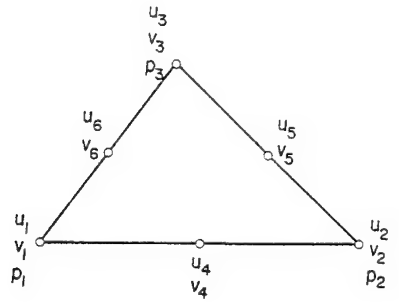

Figure A2.15 Typical element for the u,v,p formulation

If one applies the Galerkin method to eqs.(A2.48), the following expressions result.

$$\int_S \psi_i \left(\frac{\partial}{\partial x}(-p + P_{xx}) + \frac{\partial}{\partial y} P_{xy} + f_x \right) dS = 0 \qquad \text{(A2.52a)}$$

$$\int_S \psi_i \left(\frac{\partial}{\partial y}(-p + P_{yy}) + \frac{\partial}{\partial x} P_{xy} + f_y \right) dS = 0 \qquad \text{(A2.52b)}$$

$$\int_S \phi_i \left(\frac{\partial u}{\partial x} + \frac{\partial v}{\partial y} \right) dS = 0 \quad . \qquad \text{(A2.52c)}$$

These equations may be conveniently written as

$$\int_S \left(\frac{\partial}{\partial x}[\psi_i(-p + P_{xx})] + \frac{\partial}{\partial y}(\psi_i P_{xy}) - \frac{\partial \psi_i}{\partial x}(-p + P_{xx}) - \frac{\partial \psi_i}{\partial y} P_{xy} + \psi_i f_x \right) dS = 0 \qquad \text{(A2.53a)}$$

$$\int_S \left(\frac{\partial}{\partial y}[\psi_i(-p + P_{yy})] + \frac{\partial}{\partial x}(\psi_i P_{xy}) - \frac{\partial \psi_i}{\partial y}(-p + P_{yy}) - \frac{\partial \psi_i}{\partial x} P_{xy} + \psi_i f_y \right) dS = 0 \qquad \text{(A2.53b)}$$

$$\int_S \phi_i \left(\frac{\partial u}{\partial x} + \frac{\partial v}{\partial y} \right) dS = 0 \quad . \qquad \text{(A2.53c)}$$

If one concentrates on the first two terms of eqs.(A2.53a) and (A2.53b), it is apparent that they represent a divergence of the vector g defined as

$$g \equiv \psi_i((-p + P_{xx})\hat{i} + (P_{xy})\hat{j}) \quad . \tag{A2.54}$$

Recall from the two-dimensional form of the divergence theorem that

$$\int_S \nabla \cdot g \, dS = \int_C \hat{n} \cdot g \, dC \quad . \tag{A2.55}$$

Here $\hat{n}$ is defined as the unit outward normal vector.

If eq.(A2.55) is applied to eqs.(A2.53) the result is given by

$$<\frac{\partial \psi_i}{\partial x}, -p+P_{xx}> + <\frac{\partial \psi_i}{\partial y}, P_{xy}> = <f_x, \psi_i> + \int_C \psi_i t_x dC \tag{A2.56a}$$

$$<\frac{\partial \psi_i}{\partial x}, P_{xy}> + <\frac{\partial \psi_i}{\partial y}, -p+P_{yy}> = <f_y, \psi_i> + \int_C \psi_i t_y dC \tag{A2.56b}$$

$$<\phi_i, \frac{\partial u}{\partial x} + \frac{\partial v}{\partial y}> = 0 \tag{A2.56c}$$

The brackets indicate a scalar product of the quantities separated by commas. The notation t_x and t_y represents the x and y components of the surface traction vector, an idea borrowed from continuum mechanics. It is well known that any combination of surface stresses may be resolved into a single traction vector whose components shall be represented by t_x and t_y.

The result of the application of the divergence theorem to the momentum equations has been to remove the

derivatives from the primitive variables and onto the shape functions. Derivatives of the shape functions are trivial and may be easily accessed during numerical calculations.

The final step in the derivation of the governing element equations is to implement the constitutive relations of eqs.(A2.50), as well as the discretized representation of the primitive variables. These substitutions render the governing equations of the following form.

$$[<\frac{\partial\psi_i}{\partial x},2\mu\frac{\partial\psi_j}{\partial x}> + <\frac{\partial\psi_i}{\partial y},\mu\frac{\partial\psi_j}{\partial y}>]u_j + [<\frac{\partial\psi_i}{\partial y},\mu\frac{\partial\psi_j}{\partial x}>]v_j$$

$$- [<\frac{\partial\psi_i}{\partial x},\phi_j>]p_j = <f_x,\psi_i> + \int_C \psi_i t_x dC \qquad \text{(A2.57a)}$$

$$[<\frac{\partial\psi_i}{\partial x},\mu\frac{\partial\psi_j}{\partial y}>]u_j + [<\frac{\partial\psi_i}{\partial x},\mu\frac{\partial\psi_j}{\partial x}> + <\frac{\partial\psi_i}{\partial y},2\mu\frac{\partial\psi_j}{\partial y}>]v_j$$

$$- [<\frac{\partial\psi_i}{\partial y},\phi_j>]p_j = <f_y,\psi_i> + \int_C \psi_i t_y dC \qquad \text{(A2.57b)}$$

$$-[<\phi_i,\frac{\partial\psi_j}{\partial x}>]u_j - [<\phi_i,\frac{\partial\psi_j}{\partial y}>]v_j = 0 \qquad \text{(A2.57c)}$$

For convenience, the bracketed quantities are defined as

$$A_{ij} = <\frac{\partial\psi_i}{\partial x},2\mu\frac{\partial\psi_j}{\partial x}> + <\frac{\partial\psi_i}{\partial y},\mu\frac{\partial\psi_j}{\partial y}> \qquad \text{(A2.58a)}$$

$$B_{ij} = <\frac{\partial\psi_i}{\partial x},\mu\frac{\partial\psi_j}{\partial x}> + <\frac{\partial\psi_i}{\partial y},2\mu\frac{\partial\psi_j}{\partial y}> \qquad \text{(A2.58b)}$$

$$C_{ij} = \left\langle \frac{\partial \psi_i}{\partial y}, \frac{\partial \psi_j}{\partial x} \right\rangle \qquad \text{(A2.58c)}$$

$$D_{ij} = \left\langle \frac{\partial \psi_i}{\partial x}, \phi_j \right\rangle \qquad \text{(A2.58d)}$$

$$E_{ij} = \left\langle \frac{\partial \psi_i}{\partial y}, \phi_j \right\rangle \qquad \text{(A2.58e)}$$

Thus, the system of equations to be solved now becomes

$$\begin{pmatrix} A_{ij} & C_{ij} & -D_{ij} \\ C_{ji} & B_{ij} & -E_{ij} \\ -D_{ji} & -E_{ji} & 0 \end{pmatrix} \begin{pmatrix} u_j \\ v_j \\ p_j \end{pmatrix} = \begin{pmatrix} \langle f_x, \psi_i \rangle + \int_C \psi_i t_x dC \\ \langle f_y, \psi_i \rangle + \int_C \psi_i t_y dC \\ 0 \end{pmatrix} \qquad \text{(A2.59)}$$

Since the Stoke's equations are linear, the coefficient matrix of eq.(A2.59) is symmetric. In fact the same equation may be derived from the appropriate variational principle. The range of indices of eq.(A2.59) may be properly viewed in Figure A2.16 where the size of the submatrices are drawn to scale and labeled.

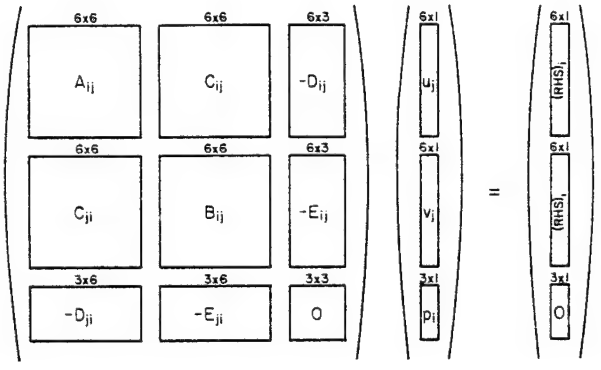

Figure A2.16 System of equations governing Stoke's flow

A2.6 Solution by Frontal Elimination

There are several possibilities that exist to solve the linear system of equations

$$[k]\ \{y\} = \{f\} \quad . \tag{A2.60}$$

Conceptually, the easiest way is to multiply eq.(A2.60) by $[k]^{-1}$ and obtain

$$\{y\} = [k]^{-1}\{f\}$$

Quite often the [k] matrix is so large that attempts to invert it are cumbersome if not impossible. An alternate method is that of Gauss elimination in which the [k] matrix is reduced to triangular form and then solved by back substitution. To assist in the solution of the eq.(A2.60) by Gauss elimination, one may make use of the following helpful ideas. The finite element method will inherently produce many zero components within the coefficient matrix. The positions of these zero elements will be off the main diagonal as dictated by the nodal numbering scheme. One may take advantage of this fact by retaining only a banded portion of the overall matrix which drastically reduces the storage requirement for the system of equations. Also if the matrix is symmetric, it is necessary to store only half of the members. These ideas are shown in Figure A2.17.

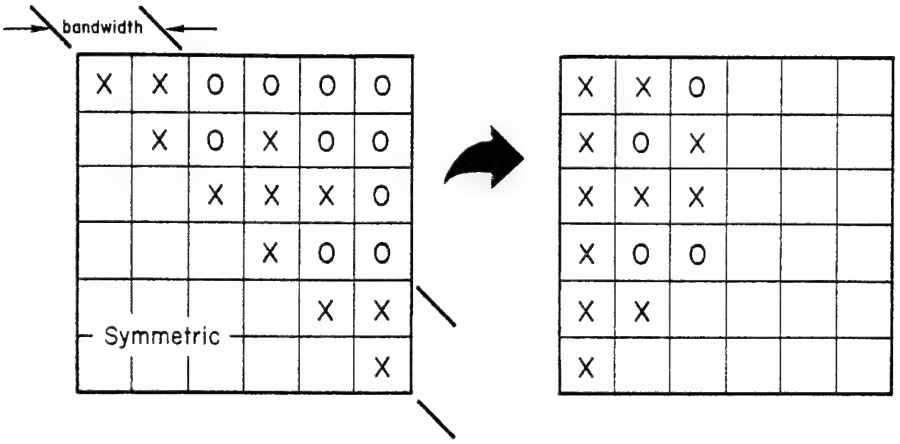

Figure A2.17 Storing a banded, symmetric matrix (x indicates a nonzero member)

The bandwidth is inherently dependent upon the numbering of the degrees of freedom, or more commonly, the global nodes. If nodes are numbered erratically, then large bandwidths may arise resulting in little reduction in the size of the coefficient matrix in core. Even when we utilize the banded matrix it may still prove too large for the existing computer. It is thus desirable for smaller computing facilities to further reduce the size of the [k] matrix. One may introduce a method of solution that depends not upon the node numbering, but upon the numbering of the elements. Invariably, this method will

reduce the number of equations in core by working on a very small active matrix.

The frontal elimination solution method was first introduced by Irons [23] in 1969 as an alternative way of solving large systems of equations, especially those of finite elements. The technique will be briefly outlined here since this was the method used in solving the fluid mechanics problem.

Consider the finite element representation of a very long domain as in Figure A2.18. We number the elements in such a manner so that their sequence indicates the direction of the front. The nodes are numbered so as to provide for conveninece say in plotting the mesh or some other criterion.

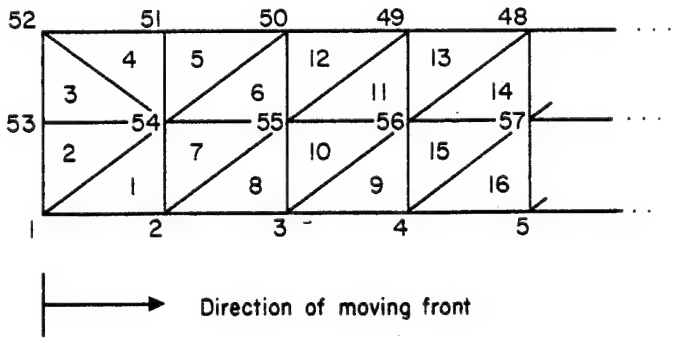

Figure A2.18 Element and nodal numbering scheme for frontal elimination

Suppose, for ease of illustration, that there corresponds only one degree of freedom with each node, then the local "stiffness" matrices of elements 1 and 2 are as follows:

$$\begin{array}{c} \\ 1 \\ 2 \\ 54 \end{array}\begin{array}{c} \begin{array}{ccc} 1 & 2 & 54 \end{array} \\ \begin{bmatrix} k^{(1)}_{1,1} & k^{(1)}_{1,2} & k^{(1)}_{1,54} \\ & k^{(1)}_{2,2} & k^{(1)}_{2,54} \\ \text{symmetric} & & k^{(1)}_{54,54} \end{bmatrix} \end{array} \qquad \text{Element 1}$$

$$\begin{array}{c} \\ 1 \\ 54 \\ 53 \end{array}\begin{array}{c} \begin{array}{ccc} 1 & 54 & 53 \end{array} \\ \begin{bmatrix} k^{(2)}_{1,1} & k^{(2)}_{1,54} & k^{(2)}_{1,53} \\ & k^{(2)}_{54,54} & k^{(2)}_{54,53} \\ \text{symmetric} & & k^{(2)}_{53,53} \end{bmatrix} \end{array} \qquad \text{Element 2}$$

If one assembles the contributions from elements 1 and 2 into the global stiffness matrix it becomes apparent that

$$k_{ij} = \begin{array}{c} \\ 1 \\ 2 \\ \\ 53 \\ 54 \end{array}\begin{array}{c} \begin{array}{cccc} 1 & 2 & 53 & 54 \end{array} \\ \begin{bmatrix} k^{(1)}_{1,1}+k^{(2)}_{1,1} & k^{(1)}_{1,2} & \cdots & k^{(2)}_{1,53} & k^{(1)}_{1,54}+k^{(2)}_{1,54} \\ & k^{(1)}_{2,2} & & & k^{(1)}_{2,54} \\ \vdots & & & & \vdots \\ & & & k^{(2)}_{53,53} & k^{(2)}_{54,53} \\ \text{symmetric} & & & & k^{(1)}_{54,54}+k^{(2)}_{54,54} \end{bmatrix} \end{array} \qquad \text{(A2.61)}$$

Next, a working or active matrix (K_{ACTIVE}) is defined to contain the assembled contributions to k_{ij}.

$$K_{ACTIVE} = \begin{array}{c} \\ 1 \\ 2 \\ 53 \\ 54 \end{array} \begin{array}{c} \begin{array}{cccc} 1 & 2 & 53 & 54 \end{array} \\ \begin{bmatrix} K11 & K12 & K13 & K14 \\ & K22 & K23 & K24 \\ & & K33 & K34 \\ \text{symmetric} & & & K44 \end{bmatrix} \end{array} \qquad \text{(A2.62)}$$

(The components KIJ (I,J=1-4) are defined by association with those of eq.(A2.61).)

The active matrix will contain only the equations associated with the variables on the front. The variables ahead of the front will not yet be assembled while those behind the front are eliminated. To see how this elimination occurs, refer to Figure A2.18. Upon assemblage of the first two elements, we note that no other elements contain node 1. The consequence of this is reflected in the fact that the first row of the global stiffness matrix is complete. That is to say, there are no more K_{1N} terms within the system of equations. Thus, one may eliminate the first row of eq.(A2.62) in the usual fashion, first dividing by the pivot and subtracting this equation from the remaining ones in the active matrix.

$$K_{ACTIVE} = \begin{array}{c} \\ 52 \\ 2 \\ 53 \\ 54 \end{array} \begin{array}{c} \begin{array}{cccc} 52 & 2 & 53 & 54 \end{array} \\ \begin{bmatrix} & K22 - \frac{K12}{K11} & K23 - \frac{K13}{K11} & K24 - \frac{K14}{K11} \\ & & K33 - \frac{K13}{K11} & K34 - \frac{K14}{K11} \\ \text{symmetric} & & & K44 - \frac{K14}{K11} \end{bmatrix} \end{array} \qquad \text{(A2.63)}$$

The eliminated equation may be written on disk to be recalled later during the back substitution process. Therefore the vacant first row of the active matrix is ready to receive an additional equation as we assemble element 3. Eq.(A2.63) becomes

$$K_{ACTIVE} = \begin{array}{c} \\ 52 \\ 2 \\ 53 \\ 54 \end{array} \begin{array}{c} \begin{array}{cccc} 52 & 2 & 53 & 54 \end{array} \\ \begin{bmatrix} k_{52,52} & & k_{52,53} & k_{52,54} \\ \hline & K22 - \frac{K12}{K11} & K23 - \frac{K13}{K11} & K24 - \frac{K14}{K11} \\ \hline & & k_{53,53} + K33 - \frac{K13}{K11} & k_{53,54} + K34 - \frac{K14}{K11} \\ \hline \text{symmetric} & & & k_{54,54} + K44 - \frac{K14}{K11} \end{bmatrix} \end{array} \qquad \text{(A2.64)}$$

The subscripted stiffness coefficients refer to the contributions from the local stiffness matrix of element 3. Upon assemblage of the first 3 elements, it is noted that

in addition to the variable at node 1, the variable at node 53 may also be eliminated. The procedures of assemblage and elimination continue simultaneously until the entire assembly of elements is complete. The profound advantage of this type of scheme is seen from the relatively small size of the active stiffness matrix needed to be solved after final assembly. For the problem at hand, and according to the particular numbering scheme, the largest that the active matrix will be is 5×5, irregardless of the length of the structure. It is seen then that the number of variables residing on the front determines the final size of the stiffness matrix that needs to be stored in core.

If there exists a drawback to the frontal elimination scheme, it would be in the extra work needed to devise an efficient algorithm for keeping track of the variable placement in the active matrix. With the placing of equations in and out of the active matrix it is essential that each variable is sent to the proper position during evaluation. With such a code, the overall method proves quite satisfactory for implementation on small or large computer systems.

A2.7 Calculating the Derived Quantities

A2.7.1 Stream Function

In the previous section, the primitive variables u, v and p were solved for by using the frontal elimination method. Now it is desirable to know the behavior of certain derived quantities. Derived quantities shall be defined as those variables which are not primitive and which require additional numerical methods to discern their behavior. In particular, the stream function and vorticity will be referred to as derived quantities since they may be calculated in terms of the primitive variables. We shall not consider the stresses as requiring further attention since their evaluation is seen directly through constitutive equations. What little assistence is needed in calculating the stresses will follow directly from the ensuing discussion. Recall from section A1.1.5 that the velocity components were related to the stream function through the equations

$$u = \frac{\partial \psi}{\partial y} \qquad \text{and} \qquad v = \frac{-\partial \psi}{\partial x} \tag{A2.65}$$

Since one has only a discretized representation of the velocity field, a method is sought that will yield the stream function if the nodal velocity components are

known. One such procedure utilizes the Galerkin method and is outlined below.

The starting point of the derivation is to note that the Laplacian of the stream function may be written as

$$\nabla^2\psi = -\frac{\partial v}{\partial x} + \frac{\partial u}{\partial y} \tag{A2.66}$$

In the usual manner, the approximations to the velocities and stream function are defined to be

$$u \equiv \sum_{i=1}^{6} u_i \phi_i \tag{A2.67a}$$

$$v \equiv \sum_{i=1}^{6} v_i \phi_i \tag{A2.67b}$$

$$\psi \equiv \sum_{i=1}^{6} \psi_i \phi_i \tag{A2.67c}$$

where, as before, ϕ_i are the quadratic interpolation functions given by eqs.(A2.39). Now, substituting eqs.(A2.67) and also applying the Galerkin criterion to eq.(A2.66), the resulting expression becomes

$$\langle \phi_i, \nabla^2 (\sum_{j=1}^{6} \psi_j \phi_j) \rangle = \langle \phi_i, \frac{-\partial}{\partial x} (\sum_{j=1}^{6} v_j \phi_j) + \frac{\partial}{\partial y} (\sum_{j=1}^{6} u_j \phi_j) \rangle \quad . \tag{A2.68}$$

The bracketed notation indicates the appropriate scalar

product between the quantities separated by commas (i.e. $<\phi_i,\phi_j> \equiv \sum_{i=1}^{6}\sum_{j=1}^{6}\phi_i\phi_j$). In view of the fact that one is dealing with discretized quantities this definition of the scalar product follows directly from the more familiar one of continuous quantities (i.e. $(\phi,\phi) \equiv \int\int\phi\phi dxdy$).

Removing the summation signs and resorting to the implied summation convention, the left-hand side of eq.(A2.68) yields

$$\psi_j<\phi_i,\nabla\cdot\nabla\phi_j> \tag{A2.69a}$$

which may be conveniently rewritten as

$$\psi_j<\nabla\cdot(\phi_i,\nabla\phi_j) - \nabla\phi_i,\nabla\phi_j>$$

or

$$-\psi_j<\nabla\phi_i,\nabla\phi_j> + <\nabla\cdot(\phi_i,\nabla\psi_j\phi_j)> \tag{A2.69b}$$

Employing the divergence theorem to eq.(A2.69b), the resulting equation becomes

$$-\psi_j<\nabla\phi_i,\nabla\phi_j> + \underline{<(\phi_i,\nabla\psi_j\phi_j)\cdot\hat{n}>}$$

or

$$-\psi_j<\nabla\phi_i,\nabla\phi_j> + \underline{<\phi_i,\frac{\partial\psi_j}{\partial n}\phi_j>}$$

or

$$-\psi_j<\nabla\phi_i,\nabla\phi_j> + \underline{\int_C \phi_i\frac{\partial\psi_j}{\partial n}\phi_j dC} \tag{A2.69c}$$

where the underlined quantities are taken to be over the domain boundary.

Upon substitution of eq.(A2.69c) for the left-hand side of eq.(A2.68), we arrive at the desired expression for calculating the stream function.

$$<\nabla\phi_i,\nabla\phi_j>\psi_j = <\phi_i,\frac{\partial\phi_j}{\partial x}>v_j - <\phi_i,\frac{\partial\phi_j}{\partial y}>u_j + \int_C \phi_i \frac{\partial\psi_j}{\partial n}\phi_j dC \qquad \text{(A2.70)}$$

Immediately, it is evident that the above expression is of the form

$$A_{ij}\psi_j = C_i \qquad \text{(A2.71)}$$

where

$$A_{ij} \equiv <\nabla\phi_i,\nabla\phi_j>$$

$$C_i \equiv <\phi_i,\frac{\partial\phi_j}{\partial x}>v_j - <\phi_i,\frac{\partial\phi_j}{\partial y}>u_j + \int_C \phi_i \frac{\partial\psi_j}{\partial n}\phi_j dC$$

and may be solved via the methods of section A2.6. From the above discussion it is clear that the stream function may only be calculated subsequent to the solution of the velocity field since a knowledge of the nodal velocity components is needed in the right-hand side of eq.(A2.71). As a final comment on the general solution of eq.(A2.71), the contour integration found in eq.(A2.70) is identified to be the natural boundary condition on the stream function and is zero if the streamlines intersect the boundaries

at right angles. On portions of the boundary where this is not the case, essential boundary conditions (ψ is specified) are usually prescribed.

A2.7.2 Vorticity

The vorticity vector has been previously defined according to

$$Z_k = e_{ijk}\omega_{ij} = \tfrac{1}{2}e_{ijk}\left(\frac{\partial v_i}{\partial x_j} - \frac{\partial v_j}{\partial x_i}\right)$$

$$= \tfrac{1}{2}\left(\frac{\partial u}{\partial y} - \frac{\partial v}{\partial x}\right) \quad . \tag{A2.72}$$

In the same manner as the previous section, one seeks a discretized representation for the vorticity in terms of the primitive variables. The approximating functions are introduced in eqs.(A2.73).

$$Z = \sum_1^3 Z_j \Psi_j \tag{A2.73a}$$

$$u = \sum_1^6 u_j \phi_j \tag{A2.73b}$$

$$v = \sum_1^6 v_j \phi_j \tag{A2.73c}$$

Note here that the representation of the vorticity vector is linear in nature while the usual quadratic interpolation

functions are employed to describe the velocity variations. This type of formulation will yield nodal values of the vorticity function at the vertices only. The derivatives of the velocity components in eq.(A2.72) suggest a lesser order of approximation to the vorticity function to insure a compatible field. This procedure is common practice in numerical approximation techniques.

Substituting eqs.(A2.73) into eq.(A2.72) and applying the Galerkin criterion, the following expression results for the vorticity representation.

$$\langle \Psi_i, \Psi_j \rangle Z_j = \tfrac{1}{2}\left(u_j \langle \Psi_i, \frac{\partial \phi_j}{\partial y} \rangle - v_j \langle \Psi_i, \frac{\partial \phi_j}{\partial x} \rangle\right) \qquad \text{(A2.74)}$$

If one defines the following quantites

$$A_{ij} \equiv \langle \Psi_i, \Psi_j \rangle \qquad \text{(A2.75a)}$$

$$C_i \equiv \tfrac{1}{2}\left(u_j \langle \Psi_i, \frac{\partial \phi_j}{\partial y} \rangle - v_j \langle \Psi_i, \frac{\partial \phi_j}{\partial x} \rangle\right) \qquad \text{(A2.75b)}$$

then eq.(A2.74) may be written compactly as

$$A_{ij} Z_j = C_i$$

and solved by the methods described previously. With the conclusion of this section, the reader now possesses the tools to interrogate the response of the primitive variables as well as the behavior of the derived quantities. In the final section, we will investigate the

solution to a problem using the aforementioned solution methods.

A2.8 Numerical Solution of 2-D Poiseuille Flow

Consider the shearing flow bounded by two stationary walls as shown in Figure A2.19a. The accompanying boundary conditions of the flow domain are also illustrated in the adjacent figure. Note that symmetry has been used to reduce the area that must be discretized.

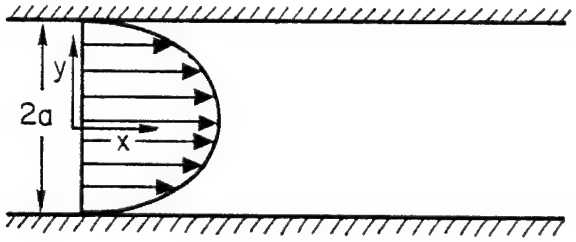

(a)

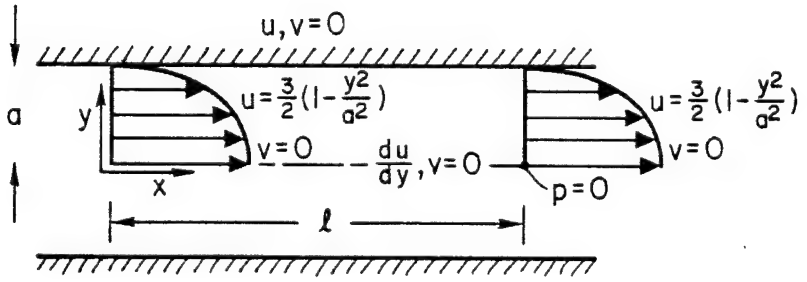

(b)

Figure A2.19 (a) 2-D Poiseuille flow
(b) Boundary conditions for 2-D Poiseuille flow

One possible discretization is shown in Figure A2.20a. The domain consists of 12 elements with quadratic interpolation for both velocity components and a linear interpolation for the pressure. As a result, the system to be solved contains 82 degrees of freedom, but using the frontal elimination method the largest active matrix is only 20×20. The numerical results of the velocity field agree exactly with those imposed on the boundary as they should since the problem is steady. The usual output form for finite-element programs is of a plotted nature, which provides a quick and easy way to investigate the behavior of the variable. Following this lead, contours of all the nonzero quantities of interest for this problem are illustrated in Figures A2.20b - f. As a standard, we shall plot 10 contours of the field variable, equally incremented between the maximum and minimum values. Having viewed the behavior of the individual field variables of Figures A2.20b - f, one will find them to be identical with those anticipated from the analytical expressions. This example provides the necessary confidence in the solution of the fluid mechanics problem by the finite-element method.

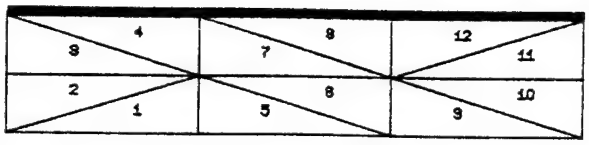

(a)

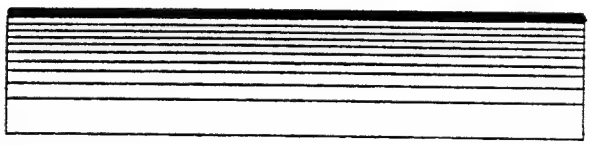

(b)

AXIAL VELOCITY

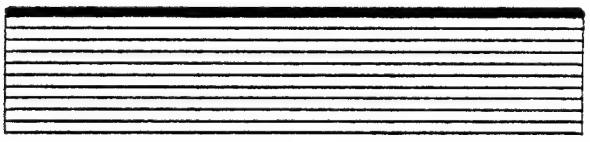

(c)

SHEAR STRESS

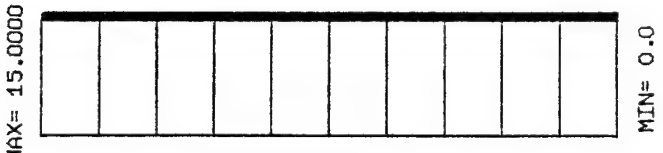

(d)

PRESSURE

Figure A2.20

NOTE: Contours are plotted in 10 equal increments spanning the range between maximum and minimum values.

(continued next page)

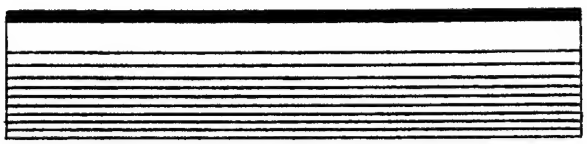

(e)

STREAM FUNCTION

(f)

VORTICITY

(Figure A2.20, continued)

APPENDIX 3

NUMERICAL CODE "COLINS"

```
C************************************************************
C************************************************************
C
C
C          PROGRAM "COLINS" PROVIDES A NUMERICAL SCHEME
C           THAT ALLOWS GRAFICAL REPRESENTATION OF THE
C           FIBER ORIENTATION WITHIN A 2-DIMENSIONAL
C           MOLDED SHORT-FIBER COMPOSITE.
C
C          A COMPLETE DESCRIPTION OF THE FLOW FIELD MUST
C           BE CONTAINED IN THE FILE "NEWSOL.RES" PRIOR
C           TO IMPLEMENTING THIS PROGRAM.  A FILE
C           "GRID.DAT" SUPPLIES THE FINITE ELEMENT MESH
C           PATTERN AND TOPOLGICAL INFORMATION.
C
C          ALL NECESSARY CHANGES TO THE PROGRAM ARE
C           DESIGNATED IN THE FOLLOWING MANNER:
C
C                   C $     ***(INSTRUCTION)***
C
C************************************************************
C************************************************************
C
C
C
C
C
C
C
C
      DIMENSION ICOUNT(20)
      DIMENSION LTRARR(10)
      DIMENSION INDEX(4,3)
      DIMENSION MENU(6)
      DIMENSION XX(3),YY(3),ZZ(3)
      DIMENSION SXX(3),SYY(3),SXY(3),U(3),V(3),VORT(3)
C************************************************************
C $     ***INTRODUCE THE NUMBER OF NODES(NNODE) 29 TIMES***
C************************************************************
      DIMENSION XP(99),YP(99),F(99)
      DIMENSION SXXP(99),SYYP(99),SXYP(99),STTP(99)
      DIMENSION UP(99),VP(99),VORTP(99)
      COMMON /A1/NNODE,NVAR,NELEM,NBD,NSO,NVEL
      COMMON /A2/X(99)
      COMMON /A3/Y(99)
      COMMON /A5/SXXR(20,99)
      COMMON /A6/SYYR(20,99)
      COMMON /A7/SXYR(20,99)
      COMMON /A8/STTR(20,99)
      COMMON /A9/UR(20,99)
      COMMON /A10/VR(20,99)
```

```
      COMMON /A11/VORTR(20,99)
      COMMON /A12/XR(20,99)
      COMMON /A13/YR(20,99)
      COMMON /A14/SXXAR(20,99)
      COMMON /A15/SYYAR(20,99)
      COMMON /A16/SXYAR(20,99)
      COMMON /A17/UAR(20,99)
      COMMON /A18/VAR(20,99)
      COMMON /A19/VORTAR(20,99)
      COMMON /A20/XAR(20,99)
      COMMON /A21/YAR(20,99)
      COMMON /A26/PHI(10,20,60)
C*****************************************************************
C $     ***INTRODUCE THE NUMBER OF NODES(NNODE) IN SUBROUTINE BOUNP
C*****************************************************************
      COMMON /ICOPY/ICOPY,IFIB
      COMMON /ITER/ITER,OCOUNT
      COMMON /IHERM/IHERM
C*****************************************************************
C $     ***INTRODUCE THE NUMBER OF ELEMENTS(NELEM) 1 TIME***
C*****************************************************************
      COMMON /A4/INOD(6,40)
C*****************************************************************
C $     ***INTRODUCE  NVAR+NNODE+NNODE  ***
C*****************************************************************
      COMMON /D3/Z(1851)
      COMMON /A23/BX,BY,MINX,MINY,XMIN,YMIN,SCALE,MENU
      COMMON /A30/HEIGHT
      DATA ((INDEX(I,J),I=1,4),J=1,3)/1,4,5,4,4,5,3,2,6,6,6,5/
      TYPE 1000
      ACCEPT 1010,SC
      TYPE 1020
      TYPE 1030
      ACCEPT 1040,BX,BY
      IF (BX.EQ.0) BX= 1.
      IF (BY.EQ.0) BY= 1.
      TYPE 1050
      ACCEPT 1060,ICOPY
      TYPE 1070
      ACCEPT 1060,IAX
      OPEN(UNIT=29,DEVICE='DSK',FILE='VARI.DAT')
      OPEN(UNIT=24,FILE='GRID.DAT')
      READ(24,1080) NSO,NNODE,NBD,NVAR,NELEM
      TYPE 1110
      ACCEPT 1160,IFIB
      TYPE 1120
      ACCEPT 1160,ITER
      TYPE 1130
      ACCEPT 1160,IHERM
      DO 10 I= 1,NELEM
10         READ(24,1080) (INOD(J,I),J=1,6)
```

```
      CONTINUE
      DO 20 I= 1,NNODE
20         READ(24,1090) X(I),Y(I)
      CONTINUE
      CLOSE(UNIT=24)
C
C
C        CALCULATING THE SCALED PLOTTER COORDINATES
C
C
      DO 30 I= 1,NNODE
         XP(I)= BX*X(I)
30       YP(I)= BY*Y(I)
      CONTINUE
      XMIN= XP(1)
      XMAX= XP(1)
      YMIN= YP(1)
      YMAX= YP(1)
      DO 40 I= 2,NSO
         XI= XP(I)
         YI= YP(I)
         IF (XI.LT.XMIN) XMIN= XI
         IF (XI.GT.XMAX) XMAX= XI
         IF (YI.LT.YMIN) YMIN= YI
         IF (YI.GT.YMAX) YMAX= YI
40    CONTINUE
      S1= 6.5/(XMAX-XMIN)
      S2= 8./(YMAX-YMIN)
      IF (S1.GT.S2) 50,60
50    SCALE= S2
      GO TO 70
60    SCALE= S1
70    WIDTH= SCALE*(XMAX-XMIN)
      HEIGHT= SCALE*(YMAX-YMIN)
      MINX= (8.5-WIDTH)/2.
      MINY= (10.-HEIGHT)/2.+1.
      DO 80 I= 1,NNODE
         XP(I)= MINX+(XP(I)-XMIN)*SCALE
80       YP(I)= MINY+(YP(I)-YMIN)*SCALE+1.
      CONTINUE
      OPEN(UNIT=17,DEVICE='DSK',FILE='NEWSOL.RES')
C*************************************************************
C $    ***FOR STOKES PROBLEM    NN=NVAR+5*NNODE
C        FOR MAXLIN PROBLEM    NN=NVAR+2*NNODE
C        FOR MAXWEL PROBLEM    NN=NVAR+2*NNODE
C*************************************************************
      NN= NVAR+5*NNODE
C
C
C     READ IN FLOW DATA GENERATED BY FINITE ELEMENT PROGRAM
C
```

```
C
      READ(17,1140) (Z(I),I=1,NN)
      CLOSE(UNIT=17)
90    TYPE 1150
C
C
C     DETERMINE THE FIELD VARIABLE FOR PLOTTING
C
C
      ACCEPT 1160,IFUNC
      IF (IFUNC.EQ.9) GO TO 140
      IF (IFUNC.LE.4) 100,110
100   I1= (IFUNC-1)*NNODE
      GO TO 150
110   IF (IFUNC.EQ.8) 130,120
120   I1= (IFUNC-2+IAX)*NNODE
      GO TO 150
130   I1= (5+IAX)*NNODE+NSO
      GO TO 150
140   I1= (6+IAX)*NNODE+NSO
150   II1= NNODE
      IF (IFUNC.EQ.7) II1= NSO
      DO 160 I= 1,II1
           K= I1+I
160        F(I)= Z(K)
      CONTINUE
C
C
C     ASSIGN ALL NODAL VARIABLES FOR LATER USE IN DETERMINING
C      INTERPOLATED VALUES ALONG STREAMLINS
C
C
      DO 170 I= 1,NNODE
           SXXP(I)= Z(I)
           J1= NNODE+I
           SYYP(I)= Z(J1)
           J2= 2*NNODE+I
           SXYP(I)= Z(J2)
           J3= 3*NNODE+I
           UP(I)= Z(J3)
           J4= 4*NNODE+I
           VP(I)= Z(J4)
           J5= 6*NNODE+NSO+I
           VORTP(I)= Z(J5)
170   CONTINUE
      TYPE 1170
      ACCEPT 1180,MENU
      TYPE 1190
      ACCEPT 1200,IDEN
      FMIN= F(1)
      FMAX= F(1)
```

```
        DO 180 I= 1,NNODE
             FF= F(I)
             IF (FF.LT.FMIN) FMIN= FF
180          IF (FF.GT.FMAX) FMAX= FF
        CONTINUE
        TYPE 1210,FMIN,FMAX
        TYPE 1220
        ACCEPT 1270,IFM
        TYPE 1230
        ACCEPT 1240,FIN,FINCR,NLIN
        TYPE 1250
        ACCEPT 1240,HIN,HINCR,NHLIN
        IF (ICOPY.EQ.1.AND.IFIB.EQ.1) GO TO 240
        IF (ICOPY.EQ.1) 190,200
190     CALL PLTSRT('JONES',30)
        GO TO 210
200     CALL PLTSRT('JONES',20)
210     CALL FACTOR(SC)
C
C
C    PLOT MARGIN AND BOARDERS
C
C
220     CALL PLOT(0.,0.,3)
        CALL PLOT(8.5,0.,2)
        CALL PLOT(8.5,11.5,2)
        CALL PLOT(0.,11.5,2)
        CALL PLOT(0.,0.,2)
        CALL PLOT(0.,1.,3)
        CALL PLOT(8.5,1.,2)
        CALL SYMBOL(0.5,0.375,0.225,MENU,0.,30)
C
C
C     PLOT OF THE FINITE ELEMENT BOUNDARY
C
C


        X1= XP(1)
        Y1= YP(1)
        CALL PLOT(X1,Y1,3)
        NBD2= NBD/2
        DO 230 I= 1,NBD2
             J= I+1
             IF (I.EQ.NBD2) J= 1
             XXX= XP(J)
             YYY= YP(J)
230          CALL PLOT(XXX,YYY,2)
        CONTINUE
C
C
C     IDENTIFICATION OF CONTOUR LINES
```

```
C
C
      IF (IFM.EQ.0) GO TO 240

      CALL SYMBOL(.5,1.25,0.15,'MIN=',0.,4)
      CALL NUMBER(1.25,1.25,0.15,FMIN,0.,4)
      CALL SYMBOL(2.75,1.25,0.15,'MAX=',0.,4)
      CALL NUMBER(3.5,1.25,0.15,FMAX,0.,4)
240   CONTINUE

C
C
C     SEARCH OF CONTOUR LINES BEGINS
C
C
      DO 300 IZZ= 1,NLIN
           JCOUNT= 1
           ZLINE= FIN+FINCR*(IZZ-1)
           DO 290 IELEM= 1,NELEM
                IF (IDEN.EQ.1) GO TO 270
                DO 260 I= 1,4
                     DO 250 J= 1,3
                          KK= INDEX(I,J)
                          L= INOD(KK,IELEM)
                          SXX(J)= SXXP(L)
                          SYY(J)= SYYP(L)
                          SXY(J)= SXYP(L)
                          U(J)= UP(L)
                          V(J)= VP(L)
                          VORT(J)= VORTP(L)
                          XX(J)= XP(L)
                          YY(J)= YP(L)
250                       ZZ(J)= F(L)
                     CONTINUE
                     IZ= IZZ
260                  CALL TRIANG(ZLINE,XX,YY,ZZ,SXX,SYY,SXY,U,V,
     1                       VORT,JCOUNT,IZ)
                CONTINUE
                GO TO 290
270             DO 280 I= 1,3
                     L= INOD(I,IELEM)
                     SXX(I)= SXXP(L)
                     SYY(I)= SYYP(L)
                     SXY(I)= SXYP(L)
                     U(I)= UP(L)
                     V(I)= VP(L)
                     VORT(I)= VORTP(L)
                     XX(I)= XP(L)
                     YY(I)= YP(L)
280                  ZZ(I)= F(L)
                CONTINUE
```

```
                IZ= IZZ
                CALL TRIANG(ZLINE,XX,YY,ZZ,SXX,SYY,SXY,U,V,VORT,
     1                      JCOUNT,IZ)
290          CONTINUE
             ICOUNT(IZ)= JCOUNT
300     CONTINUE


        IF (IRASE.EQ.0) GO TO 310
        CALL ERASE
        CALL HOME
310     CONTINUE
        CALL ERASE
        GO TO 320
320     CONTINUE
C
C
C     RESCALE TO THE ORIGINAL COORDINATES
C
C
        DO 330 J= 1,NLIN
             DO 330 I= 1,ICOUNT(J)-1
                  XR(J,I)= (((XR(J,I)-MINX)/SCALE)+XMIN)/BX
                  YR(J,I)= ((YR(J,I)-MINY-1.)/SCALE+YMIN)/BY
330          CONTINUE
        CONTINUE
        IF (ICOPY.EQ.1.OR.IFIB.EQ.1) GO TO 340
        DO 340 J= 1,NLIN
             WRITE(29,1290)
C
C
C     WRITE DATA CHECK IN FILE VARI.DAT
C
C
             DO 340 I= 1,ICOUNT(J)-1
                  WRITE(29,1280) XR(J,I),YR(J,I),SXXR(J,I),SYYR(J,I),
     1                           SXYR(J,I),UR(J,I),VR(J,I),VORTR(J,I)
340          CONTINUE
        CONTINUE
        IF (ICOPY.EQ.1) GO TO 350
        OPEN(UNIT=39,DEVICE='DSK',FILE='ORIENT.DAT')
        CLOSE(UNIT=29)
350     IF (IFIB.EQ.1) CALL ARRANG(ICOUNT,NLIN)
        IF (IFIB.EQ.1) CALL BOUNP(ICOPY,SC)
        IF (ITER.EQ.0) GO TO 360
        DO 360 OCOUNT= 1,ITER
             IF (IFIB.EQ.1) CALL INTEG(ICOUNT,NLIN)
360     CONTINUE
        CALL HOME
        IF (IFIB.EQ.0) GO TO 370
        CALL BOUNP(ICOPY,SC)
```

```
      CALL VALHER(ICOUNT,NLIN)
      IF (IHERM.EQ.0) GO TO 370
      CALL HERMP(NLIN,ICOUNT,HIN,HINCR,NHLIN)
      CALL HOME
      IF (ICOPY.EQ.1) GO TO 370
      CLOSE(UNIT=39)
370   STOP
1000  FORMAT(' INTRODUCE SCALING FACTOR')
1010  FORMAT(F3.1)
1020  FORMAT(' ENTER BLOW UP FACTOR IN X AND Y ')
1030  FORMAT(' **.* **.* ')
1040  FORMAT(2F5.2)
1050  FORMAT(' DO YOU WANT HARDCOPY?YES=1,NO=0')
1060  FORMAT(I1)
1070  FORMAT(' IS IT AN AXISYMMETRIC PROBLEM?Y=1,N=0')
1080  FORMAT(6I4)
1090  FORMAT(2F7.3)
1100  FORMAT(E10.3)
1110  FORMAT(' DO YOU WANT FIBER PLOTS? YES=1,NO=0')
1120  FORMAT(' NUMBER OF INITIAL FIBER ORIENTATIONS')
1130  FORMAT(' DO YOU WANT A HERMAN PLOT?YES=1,NO=0')
1140  FORMAT(E13.6)
1150  FORMAT(
     1' SELECT F :SXX=1,SYY=2,SXY=3,STT=4,U=5,V=6,P=7,PSI=8,VORT=9')
1160  FORMAT(I1)
1170  FORMAT(' INTRODUCE TITLE:30 CHARACTERS')
1180  FORMAT(6(A5))
1190  FORMAT(' DO YOU WANT LINEAR(1) OR QUADRATIC(2) INTERPOLATION?'
     1)
1200  FORMAT(I1)
1210  FORMAT(' FMIN=',E9.3,'   FMAX=',F9.3)
1220  FORMAT(' DO YOU WANT FMIN,FMAX ON YOUR DRAWING?Y=1,N=0')
1230  FORMAT(' +0.***E+**+0.***E+**NN=INITIAL VAL.,INCREM.,NO OF LINES
     1)
1240  FORMAT(2E10.3,I2)
1250  FORMAT(' +0.***E+**+0.***E+**NN=INITIAL VAL;,INCR;,NO H LINES'
     1)
1260  FORMAT(' CONTOUR=',E9.3)
1270  FORMAT(I1)
1280  FORMAT(1X,8E12.4)
1290  FORMAT(////////////////////)
      END
C
C
C
C*************************************************************
C*************************************************************
C
C
C         SUBROUTINES
C
```

```
C
C*****************************************************************
C*****************************************************************
C
C
C
C
        SUBROUTINE TRIANG(Z,XX,YY,ZZ,SXX,SYY,SXY,U,V,VORT,JCOUNT,IZ)
C
C
C
C
C**********
C**********
C     SCANS EACH TRIANGLE FOR THE PROPER CONTOUR VALUES OF
C      THE STREAMLINES.  ALSO, CALCULATES INTERPOLATED
C      VALUES OF ALL FIELD VARIABLES WHERE A STREAMLINE
C      INTERSECTS AN ELEMENT BOUNDARY.
C**********
C**********
C
        DIMENSION XX(3),YY(3),ZZ(3)
        DIMENSION SXX(3),SYY(3),SXY(3),U(3),V(3),VORT(3)
        COMMON /A5/SXXR(20,1)
        COMMON /A6/SYYR(20,1)
        COMMON /A7/SXYR(20,1)
        COMMON /A9/UR(20,1)
        COMMON /A10/VR(20,1)
        COMMON /A11/VORTR(20,1)
        COMMON /A12/XR(20,1)
        COMMON /A13/YR(20,1)
        COMMON /ICOPY/ICOPY,IFIB
        IP= 0
        DO 100 M= 1,3
             K1= M
             K2= M+1-3*(M/3)
             A= ZZ(K1)
             B= ZZ(K2)
             C= (Z-A)*(Z-B)
             IF (C.GT.0.) GO TO 100
             IF (Z.EQ.A.AND.Z.NE.B.OR.Z.EQ.B.AND.Z.NE.A) GO TO 100
             X1= XX(K1)
             X2= XX(K2)
             Y1= YY(K1)
             Y2= YY(K2)
             SXX1= SXX(K1)
             SXX2= SXX(K2)
             SYY1= SYY(K1)
             SYY2= SYY(K2)
             SXY1= SXY(K1)
             SXY2= SXY(K2)
```

```
            U1= U(K1)
            U2= U(K2)
            V1= V(K1)
            V2= V(K2)
            VORT1= VORT(K1)
            VORT2= VORT(K2)
            IF (A.EQ.B) GO TO 50
            X= X1+(Z-A)*(X2-X1)/(B-A)
            Y= Y1+(Z-A)*(Y2-Y1)/(B-A)
            SXXR(IZ,JCOUNT)= SXX1+(Z-A)*(SXX2-SXX1)/(B-A)
            SYYR(IZ,JCOUNT)= SYY1+(Z-A)*(SYY2-SYY1)/(B-A)
            SXYR(IZ,JCOUNT)= SXY1+(Z-A)*(SXY2-SXY1)/(B-A)
            UR(IZ,JCOUNT)= U1+(Z-A)*(U2-U1)/(B-A)
            VR(IZ,JCOUNT)= V1+(Z-A)*(V2-V1)/(B-A)
            VORTR(IZ,JCOUNT)= VORT1+(Z-A)*(VORT2-VORT1)/(B-A)
            XR(IZ,JCOUNT)= X
            YR(IZ,JCOUNT)= Y
            JCOUNT= JCOUNT+1
            IF (IP.EQ.0) 10,30
10          IF (IFIB.EQ.1) GO TO 20
            CALL PLOT(X,Y,3)
20          IP= 1
            GO TO 100
30          IF (IFIB.EQ.1) GO TO 40
            CALL PLOT(X,Y,2)
40          GO TO 100
50          XR(IZ,JCOUNT)= X1
            YR(IZ,JCOUNT)= Y1
            SXXR(IZ,JCOUNT)= SXX1
            SYYR(IZ,JCOUNT)= SYY1
            SXYR(IZ,JCOUNT)= SXY1
            UR(IZ,JCOUNT)= U1
            VR(IZ,JCOUNT)= V1
            VORTR(IZ,JCOUNT)= VORT1
            JCOUNT= JCOUNT+1
            XR(IZ,JCOUNT)= X2
            YR(IZ,JCOUNT)= Y2
            SXXR(IZ,JCOUNT)= SXX2
            SYYR(IZ,JCOUNT)= SYY2
            SXYR(IZ,JCOUNT)= SXY2
            UR(IZ,JCOUNT)= U2
            VR(IZ,COUNT)= V2
            VORTR(IZ,JCOUNT)= VORT2
            JCOUNT= JCOUNT+1
            IF (IP.EQ.0) 60,80
60          IF (IFIB.EQ.1) GO TO 70
            CALL PLOT(X1,Y1,3)
70          IP= 1
            GO TO 90
80          IF (IFIB.EQ.1) GO TO 90
            CALL PLOT(X1,Y1,2)
```

```
90          IF (IFIB.EQ.1) GO TO 100
            CALL PLOT(X2,Y2,2)
100     CONTINUE
        RETURN
        END
C*******************************************************************************
C
C
C
C
        SUBROUTINE ARRANG(ICOUNT,NLIN)
C
C
C
C
C**********
C**********
C     ARRANGES STREAMPOINTS IN ORDER TO FORM A UNIQUE STREAMLINE
C**********
C**********
        DIMENSION ICOUNT(20)
        COMMON /A5/SXXR(20,1)
        COMMON /A6/SYYR(20,1)
        COMMON /A7/SXYR(20,1)
        COMMON /A9/UR(20,1)
        COMMON /A10/VR(20,1)
        COMMON /A11/VORTR(20,1)
        COMMON /A12/XR(20,1)
        COMMON /A13/YR(20,1)
        COMMON /A14/SXXAR(20,1)
        COMMON /A15/SYYAR(20,1)
        COMMON /A16/SXYAR(20,1)
        COMMON /A17/UAR(20,1)
        COMMON /A18/VAR(20,1)
        COMMON /A19/VORTAR(20,1)
        COMMON /A20/XAR(20,1)
        COMMON /A21/YAR(20,1)
        COMMON /ICOPY/ICOPY,IFIB
C
C
C     FIND THE INITIAL POINT IN THE STREAMLINE
C
C
        DO 90 I= 1,NLIN
             DO 10 J= 1,ICOUNT(I)-1
                  IF (XR(I,J).NE.0) GO TO 10
                  XAR(I,1)= XR(I,J)
                  YAR(I,1)= YR(I,J)
                  SXXAR(I,1)= SXXR(I,J)
                  SYYAR(I,1)= SYYR(I,J)
                  SXYAR(I,1)= SXYR(I,J)
```

```
                UAR(I,1)= UR(I,J)
                VAR(I,1)= VR(I,J)
                VORTAR(I,1)= VORTR(I,J)
                GO TO 20
10          CONTINUE
C
C
C   DETERMINE THE NEIGHBOR OF THE INITIAL POINT
C
C
20          T= J
            IF (T/2..EQ.INT(T/2.)) GO TO 30
            XAR(I,2)= XR(I,J+1)
            YAR(I,2)= YR(I,J+1)
            SXXAR(I,2)= SXXR(I,J+1)
            SYYAR(I,2)= SYYR(I,J+1)
            SXYAR(I,2)= SXYR(I,J+1)
            UAR(I,2)= UR(I,J+1)
            VAR(I,2)= VR(I,J+1)
            VORTAR(I,2)= VORTR(I,J+1)
            XR(I,J)= 0.
            YR(I,J)= 0.
            XR(I,J+1)= 0.
            YR(I,J+1)= 0.
            GO TO 40
30          XAR(I,2)= XR(I,J-1)
            YAR(I,2)= YR(I,J-1)
            SXXAR(I,2)= SXXR(I,J-1)
            SYYAR(I,2)= SYYR(I,J-1)
            SXYAR(I,2)= SXYR(I,J-1)
            UAR(I,2)= UR(I,J-1)
            VAR(I,2)= VR(I,J-1)
            VORTAR(I,2)= VORTR(I,J-1)
            XR(I,J)= 0.
            YR(I,J)= 0.
            XR(I,J-1)= 0.
            YR(I,J-1)= 0.
40          CONTINUE
C
C
C
C    DETERMINE THE REMAINING STREAMLINE POINTS IN ORDER
C
C
C
            TOL= .00001
            DO 80 L= 3,(ICOUNT(I)-1)/2+1
                DO 50 M= 1,ICOUNT(I)-1
                    IF (XR(I,M)+TOL.GE.XAR(I,L-1).AND.XR(I,M)-TOL.
     1                  LE.XAR(I,L-1).AND.YR(I,M)+TOL.GE.YAR(I,L-1).
     1                  AND.YR(I,M)-TOL.LE.YAR(I,L-1)) GO TO 60
```

```
50              CONTINUE
                GO TO 80
C
C
C     DETERMINE THE NEIGHBORS
C
C
60              S= M
                IF (S/2..EQ.INT(S/2.)) GO TO 70
                XAR(I,L)= XR(I,M+1)
                YAR(I,L)= YR(I,M+1)
                SXXAR(I,L)= SXXR(I,M+1)
                SYYAR(I,L)= SYYR(I,M+1)
                SXYAR(I,L)= SXYR(I,M+1)
                UAR(I,L)= UR(I,M+1)
                VAR(I,L)= VR(I,M+1)
                VORTAR(I,L)= VORTR(I,M+1)
                XR(I,M)= 0.
                YR(I,J)= 0.
                XR(I,M+1)= 0.
                YR(I,M+1)= 0.
                GO TO 80
70              XAR(I,L)= XR(I,M-1)
                YAR(I,L)= YR(I,M-1)
                SXXAR(I,L)= SXXR(I,M-1)
                SYYAR(I,L)= SYYR(I,M-1)
                SXYAR(I,L)= SXYR(I,M-1)
                UAR(I,L)= UR(I,M-1)
                VAR(I,L)= VR(I,M-1)
                VORTAR(I,L)= VORTR(I,M-1)
                XR(I,M)= 0.
                YR(I,M)= 0.
                XR(I,M-1)= 0.
                YR(I,M-1)= 0.
C
C
80          CONTINUE
90      CONTINUE
        IF (ICOPY.EQ.1) GO TO 110
        OPEN(UNIT=31,DEVICE='DSK',FILE='STREAM.DAT')
        DO 100 J= 1,NLIN
             WRITE(31,1000)
             DO 100 I= 1,(ICOUNT(J)-1)/2+1
                  WRITE(31,1010) XAR(J,I),YAR(J,I),SXXAR(J,I),SYYAR(J,
        1                        I),SXYAR(J,I),UAR(J,I),VAR(J,I),
        1                        VORTAR(J,I)
100          CONTINUE
        CONTINUE
        CLOSE(UNIT=31)
110     RETURN
1000    FORMAT(//////////////////)
```

```
1010    FORMAT(1X,8E12.4)
        END
C*******************************************************************************
C
C
C
C
        SUBROUTINE INTEG(ICOUNT,NLIN)
C
C
C
C
C**********
C**********
C     INTEGRATES THE ORIENTATION ALONG A STREAMLINE
C**********
C**********
        DIMENSION ICOUNT(20)
        DIMENSION VAL(20)
        DIMENSION VAT(20)
        DIMENSION Y(1),C(24),W(1,9)
        COMMON /A14/SXXAR(20,1)
        COMMON /A15/SYYAR(20,1)
        COMMON /A16/SXYAR(20,1)
        COMMON /A17/UAR(20,1)
        COMMON /A18/VAR(20,1)
        COMMON /A19/VORTAR(20,1)
        COMMON /A20/XAR(20,1)
        COMMON /A21/YAR(20,1)
        COMMON /A22/I,J,B
        COMMON /A26/PHI(10,20,60)
        COMMON /ICOPY/ICOPY,IFIB
        COMMON /ITER/ITER,OCOUNT
        COMMON /IHERM/IHERM
        EXTERNAL FCN1
        DATA (VAL(I),I=1,20)/-1.50,-1.50,-1.50,-1.50,-1.50,-1.50,-1.50,
        1    -1.50,-1.50,-1.50,-1.5,-1.5,-1.5,-1.5,-1.5,-1.5,-1.5,-1.5,
        1    -1.5,-1.5/
        DO 10 I= 1,20
             VAT(I)= VAL(I)+(OCOUNT-1)/ITER*3.141592654
10      CONTINUE
        IF (ICOPY.EQ.1) GO TO 20
20      CONTINUE
        B= 1.0
        DO 60 I= 1,NLIN
             IND= 1
             TOL= .0001
             NW= 1
             N= 1
             Y(1)= VAT(I)
             XEND= 0.0
```

```
              X= 0.0
              DO 50 J= 1,(ICOUNT(I)-1)/2+1
                   IF (J.EQ.1) GO TO 30
                   TOP= (((XAR(I,J)-XAR(I,J-1))**2.+(YAR(I,J)-YAR(I,J-
         1              1))**2.)**.5)
                   BOTTOM= ((UAR(I,J-1)**2+VAR(I,J-1)**2)**.5)
                   TINC= TOP/BOTTOM
                   XEND= XEND+TINC
                   CALL DVERK(N,FCN1,X,Y,XEND,TOL,IND,C,NW,W,IER)
30                 IF (IHERM.EQ.1) GO TO 40
                   CALL FPLOT(I,J,Y)
40                 CONTINUE
                   PHI(OCOUNT,I,J)= Y(1)
                   IF (ICOPY.EQ.1) GO TO 50
                   WRITE(39,1010) Y(1),XEND,XAR(I,J),YAR(I,J),UAR(I,J),
         1                        VAR(I,J),TINC,TOP,BOTTOM
50            CONTINUE
              IF (ICOPY.EQ.1) GO TO 60
              WRITE(39,1020)
60       CONTINUE
         IF (ICOPY.EQ.1) GO TO 70
70       RETURN
1000     FORMAT(5X,I1)
1010     FORMAT(1X,9E10.3)
1020     FORMAT(///////////////)
         END
C*******************************************************************************
C
C
C
C
         SUBROUTINE FCN1(N,X,Y,YPRIME)
C
C
C
C
C**********
C**********
C     EXTERNAL SUBROUTINE FOR INTEG
C**********
C**********
         DIMENSION Y(1),YPRIME(1)
         COMMON /A14/SXXAR(20,1)
         COMMON /A15/SYYAR(20,1)
         COMMON /A16/SXYAR(20,1)
         COMMON /A17/UAR(20,1)
         COMMON /A18/VAR(20,1)
         COMMON /A19/VORTAR(20,1)
         COMMON /A20/XAR(20,1)
         COMMON /A21/YAR(20,1)
         COMMON /A22/I,J,B
```

```
      COMMON /ICOPY/ICOPY,IFIB
      YPRIME(1)= VORTAR(I,J)+B*(SXYAR(I,J)/2.DC*COS(2*Y(1))-0.5*
     1          (SYYAR(I,J)/2.DC-SXXAR(I,J)/2.DC)*SIN(2*Y(1)))
      IF (ICOPY.EQ.1) GO TO 10
10    RETURN
1000  FORMAT(20X,4E10.3)
      END
C*********************************************************************
C
C
C
C
      SUBROUTINE BOUNP(ICOPY,SC)
C
C
C
C
C**********
C**********
C     SUBROUTINE TO PLOT THE BOUNDARY
C**********
C**********
      COMMON /A1/NNODE,NVAR,NELEM,NBD,NSO,NVEL
      COMMON /A2/X(1)
      COMMON /A3/Y(1)
      COMMON /A23/BX,BY,MINX,MINY,XMIN,YMIN,SCALE,MENU
C*****************************************************************
C $   ***INTRODUCE NNODE TWICE***
C*****************************************************************
      DIMENSION XP(254),YP(254)
      DO 10 I= 1,NNODE
           XP(I)= BX*X(I)
           YP(I)= BY*Y(I)
10    CONTINUE
      DO 20 I= 1,NNODE
           XP(I)= MINX+(XP(I)-XMIN)*SCALE
           YP(I)= MINY+(YP(I)-YMIN)*SCALE+1.
20    CONTINUE
      IF (ICOPY.EQ.1) 30,40
30    CALL PLTSRT('JONES',30)
      GO TO 50
40    CALL PLTSRT('JONES',20)
50    CALL FACTOR(SC)
60    CALL PLOT(0.,0.,3)
      CALL PLOT(8.5,0.,2)
      CALL PLOT(8.5,11.5,2)
      CALL PLOT(0.,11.5,2)
      CALL PLOT(0.,0.,2)
      CALL PLOT(0.,1.,3)
      CALL PLOT(8.5,1.,2)
      CALL SYMBOL(0.5,0.375,0.225,MENU,0.,30)
```

```
C
C
C      PLOT OF THE BOUNDARY
C
C

         X1= XP(1)
         Y1= YP(1)
         CALL PLOT(X1,Y1,3)
         NBD2= NBD/2
         DO 70 I= 1,NBD2
              J= I+1
              IF (I.EQ.NBD2) J= 1
              XXX= XP(J)
              YYY= YP(J)
70            CALL PLOT(XXX,YYY,2)
         CONTINUE
         RETURN
         END
C*******************************************************************************
C
C
C
C
         SUBROUTINE FPLOT(I,J,Y)
C
C
C
C
C**********
C**********
C      PLOTS INDIVIDUAL FIBER ORIENTATIONS
C**********
C**********
         DIMENSION XART(20,100),YART(20,100)
         DIMENSION Y(1)
         COMMON /A23/BX,BY,MINX,MINY,XMIN,YMIN,SCALE
         COMMON /A20/XAR(20,1)
         COMMON /A21/YAR(20,1)
         COMMON /A30/HEIGHT
         COMMON /IHERM/IHERM
         IF (IHERM.EQ.1) GO TO 10
         PI= 3.141592654
         FLENG= 0.025*HEIGHT
         XART(I,J)= XAR(I,J)
         YART(I,J)= YAR(I,J)
C
C
C      RESCALE TO PLOTTING COORDINATES
C
C
```

```
      XART(I,J)= MINX+(XART(I,J)*BX-XMIN)*SCALE
      YART(I,J)= MINY+(YART(I,J)*BY-YMIN)*SCALE+1.
      XF= XART(I,J)-FLENG*COS(PI/2.-Y(1))
      YF= YART(I,J)-FLENG*SIN(PI/2.-Y(1))
      CALL PLOT(XF,YF,3)
      XL= XART(I,J)+FLENG*COS(PI/2.-Y(1))
      YL= YART(I,J)+FLENG*SIN(PI/2.-Y(1))
      CALL PLOT(XL,YL,2)
10    RETURN
      END
C*******************************************************************************
C
C
C
C
      SUBROUTINE VALHER(ICOUNT,NLIN)
C
C
C
C
C**********
C**********
C     CALCULATES VALUES OF HERMANS ORIENTATION PARAMETER
C**********
C**********
      DIMENSION ICOUNT(20)
      COMMON /A26/PHI(10,20,60)
      COMMON /ICOPY/ICOPY,IFIB
      COMMON /A27/PHILOC(20,60)
      COMMON /ITER/ITER,OCOUNT
      COMMON /A28/HERM(20,60)
      COMMON /A20/XAR(20,1)
      COMMON /A21/YAR(20,1)
      IF (ICOPY.EQ.1) GO TO 10
      OPEN(UNIT=47,DEVICE='DSK',FILE='HERM.DAT')
10    DO 50 N= 1,NLIN
        DO 40 J= 1,(ICOUNT(N)-1)/2+1
          PHIM= 0.0
          DO 20 I= I,ITER
            PHIM= PHIM+PHI(I,N,J)
20        CONTINUE
          PHIM= PHIM/ITER
          PHSQ= 0.0
          DO 30 I= 1,ITER
            PHSQ= PHSQ+(PHI(I,N,J)-PHIM)**2.
30        CONTINUE
          PHIRMS= (PHSQ/ITER)**.5
          PHILOC(N,J)= 3.141592654/2-PHIM
          HERM(N,J)= 2*((COS(PHIRMS))**2)-1.
          IF (HERM(N,J).LT.0) PHILOC(N,J)= 3.141592654/2.
     1                                    -PHILOC(N,J)
```

```
                IF (HERM(N,J).LT.0) HERM(N,J)= -HERM(N,J)
                IF (ICOPY.EQ.1) GO TO 40
                WRITE(47,1000) XAR(N,J),YAR(N,J),HERM(N,J),PHILOC(N.
     1                         J),PHIRMS,PHIM,PHSQ
40           CONTINUE
50      CONTINUE
        IF (ICOPY.EQ.1) GO TO 60
        CLOSE(UNIT=47)
60      RETURN
1000    FORMAT(7E14.6)
        END
C*******************************************************************************
C
C
C
C
        SUBROUTINE HERMP(NLIN,ICOUNT,HIN,HINCR,NHLIN)
C
C
C
C
C**********
C**********
C     SCANS INDIVIDUAL TRIANGLES FOR CONTOURS OF HERMANS
C      ORIENTATION PARAMETER
C**********
C**********
        DIMENSION ICOUNT(20)
        DIMENSION XXXX(3),YYYY(3),HHH(3)
        COMMON /A20/XAR(20,1)
        COMMON /A21/YAR(20,1)
        COMMON /A28/HERM(20,60)
        COMMON /ICOPY/ICOPY,IFIB
        DO 70 HIZ= 1,NHLIN
             HLIN= HIN+HINCR*(HIZ-1)
             IF (ICOPY.EQ.1) GO TO 10
             WRITE(5,1000) HLIN
10           CONTINUE
             DO 60 I= 1,NLIN-1
                  MIN= (ICOUNT(I)-1)/2+1
                  IF (ICOUNT(I+1).LE.ICOUNT(I)) MIN= (ICOUNT(I+1)-1)/2+
     1                                              1
                  DO 20 J= 1,MIN-1
                       XXXX(1)= XAR(I,J)
                       YYYY(1)= YAR(I,J)
                       HHH(1)= HERM(I,J)
                       XXXX(2)= XAR(I+1,J)
                       YYYY(2)= YAR(I+1,J)
                       HHH(2)= HERM(I+1,J)
                       XXXX(3)= XAR(I,J+1)
                       YYYY(3)= YAR(I,J+1)
```

```
                    HHH(3)= HERM(I,J+1)
                    CALL TRIANH(HLIN,XXXX,YYYY,HHH)

                    XXXX(1)= XAR(I+1,J)
                    YYYY(1)= YAR(I+1,J)
                    HHH(1)= HERM(I+1,J)
                    XXXX(2)= XAR(I+1,J+1)
                    YYYY(2)= YAR(I+1,J+1)
                    HHH(2)= HERM(I+1,J+1)
                    XXXX(3)= XAR(I,J+1)
                    YYYY(3)= YAR(I,J+1)
                    HHH(3)= HERM(I,J+1)
                    CALL TRIANH(HLIN,XXXX,YYYY,HHH)
20                CONTINUE
                  IF (ICOUNT(I+1).EQ.ICOUNT(I)) GO TO 60
                  IF (ICOUNT(I+1).LT.ICOUNT(I)) GO TO 40
                  DO 30 M= J,(ICOUNT(I+1)-1)/2
                    XXXX(1)= XAR(I,J)
                    YYYY(1)= YAR(I,J)
                    HHH(1)= HERM(I,J)
                    XXXX(2)= XAR(I+1,M+1)
                    YYYY(2)= YAR(I+1,M+1)
                    HHH(2)= HERM(I+1,M+1)
                    XXXX(3)= XAR(I+1,M)
                    YYYY(3)= YAR(I+1,M)
                    HHH(3)= HERM(I+1,M)
                    CALL TRIANH(HLIN,XXXX,YYYY,HHH)
30                CONTINUE
                  GO TO 60
40                DO 50 M= J,(ICOUNT(I)-1)/2
                    XXXX(1)= XAR(I,M)
                    YYYY(1)= YAR(I,M)
                    HHH(1)= HERM(I,M)
                    XXXX(2)= XAR(I,M+1)
                    YYYY(2)= YAR(I,M+1)
                    HHH(2)= HERM(I,M+1)
                    XXXX(3)= XAR(I+1,J)
                    YYYY(3)= YAR(I+1,J)
                    HHH(3)= HERM(I+1,J)
                    CALL TRIANH(HLIN,XXXX,YYYY,HHH)
50                CONTINUE
60              CONTINUE
70        CONTINUE
          RETURN
1000      FORMAT(' CONTOUR=',E9.3)
          END
C*******************************************************************************
C
C
C
C
```

```
      SUBROUTINE TRIANH(HLIN,XXXX,YYYY,HHH)
C
C
C
C
C**********
C**********
C     PLOTS CONTOURS OF HERMANS ORIENTATION PARAMETER
C**********
C**********
      DIMENSION XXXX(3),YYYY(3),HHH(3)
      COMMON /A23/BX,BY,MINX,MINY,XMIN,YMIN,SCALE,MENU
      IP= 0
      DO 10 I= 1,3
C
C
C     RESCALE TO PLOTTING COORDINATES
C
C
          XXXX(I)= MINX+(XXXX(I)*BX-XMIN)*SCALE
          YYYY(I)= MINY+(YYYY(I)*BY-YMIN)*SCALE+1.
10    CONTINUE
      DO 80 M= 1,3
          K1= M
          K2= M+1-3*(M/3)
          A= HHH(K1)
          B= HHH(K2)
          C= (HLIN-A)*(HLIN-B)
          IF (C.GT.0) GO TO 80
          X1= XXXX(K1)
          X2= XXXX(K2)
          Y1= YYYY(K1)
          Y2= YYYY(K2)
          IF (A.EQ.B) GO TO 40
          X= X1+(HLIN-A)*(X2-X1)/(B-A)
          Y= Y1+(HLIN-A)*(Y2-Y1)/(B-A)
          IF (IP.EQ.0) 20,30
20        CALL PLOT(X,Y,3)
          IP= 1
          GO TO 80
30        CALL PLOT(X,Y,2)
          GO TO 80
40        IF (IP.EQ.0) 50,60
50        CALL PLOT(X1,Y1,3)
          IP= 1
          GO TO 70
60        CALL PLOT(X1,Y1,2)
70        CALL PLOT(X2,Y2,2)
80    CONTINUE
      RETURN
      END
```